A Dissertation on

DUAL MODE LUMINESCENCE IN RARE EARTH ION DOPED ZnO NANOPARTICLES

Submitted in partial fulfillment of the requirement
for the award of degree of

MASTER OF TECHNOLOGY
in
NANOSCIENCE & TECHNOLOGY

Submitted by

NAVEEN KHICHAR
(Roll No. 2K11/NST/08)

Under the Supervision of

Dr. M. S. MEHATA
DTU-DELHI

Dr. SANTA CHAWLA
CSIR-NPL

Department of Applied Physics

Delhi Technological University

(Formerly Delhi College of Engineering)

Bawana Road, Delhi- 110042

(2011-2013)

A Dissertation on

DUAL MODE LUMINESCENCE IN RARE EARTH ION DOPED ZnO NANOPARTICLES

Submitted in partial fulfillment of the requirement
for the award of degree of

MASTER OF TECHNOLOGY
in
NANOSCIENCE & TECHNOLOGY

Submitted by
NAVEEN KHICHAR
(Roll No. 2K11/NST/08)

Under the Supervision of

Dr. M. S. MEHATA
DTU-DELHI

Dr. SANTA CHAWLA
CSIR-NPL

Department of Applied Physics

Delhi Technological University

(Formerly Delhi College of Engineering)

Bawana Road, Delhi- 110042

(2011-2013)

DECLARATION

*This is to certify that this work entitled "**Dual mode luminescence in Rare Earth ion doped ZnO nanoparticles**", which is submitted by me in partial fulfillment of the requirement for the completion of **M. Tech. Degree** in **Nano Science & Technology** to D**elhi Technological University (DTU) .** This dissertation comprises only my original work and it has not been published anywhere by anybody.*

NAVEEN KHICHAR

(2K11/NST/08)

CERTIFICATE

*This is to certify that the thesis entitled "**Dual mode luminescence in Rare Earth ion doped ZnO nanoparticles**" is submitted in partial fulfillment of the requirements for the award of degree of **Master of Technology** in **Nano Science & Technology** at **Delhi Technological University.***

*It is a faithful record of bonafide research work carried out by **Mr. Naveen Khichar** under my supervision and guidance at CSIR-NPL. It is further certified that no part of thesis has been submitted to any other University or Institute for the award of any other Degree or Diploma to the best of my knowledge.*

The work has been carried out from 1st January 2013 to 15th July 2013.

Dr. SANTA CHAWLA
Senior Principal Scientist
Luminescent Materials and Devices Group
Material Physics Engineering Division
CSIR-National Physical Laboratory
New Delhi –100 012

Dr. RAJEEV CHOPRA
Scientist
Head, HRD
CSIR-National Physical Laboratory
New Delhi – 110 012

CERTIFICATE

This is to certify that the dissertation title ***"Dual mode luminescence in Rare Earth ion doped ZnO nanoparticles"*** *is the authentic work of* ***Mr. Naveen Khichar*** *under supervision and guidance of Dr. Santa Chawla at CSIR-NPL and Dr. M. S. Mehata at DTU. This work is in the partial fulfilment of requirement towards the degree of* ***Master of Technology*** *run by the Department of Applied Physics in* ***Delhi Technological University.***

Dr. M. S. MEHATA
Assistant Professor
Department of Applied Physics
Delhi Technological University
New Delhi – 110 042

Prof. S. C. SHARMA
Head of Department
Department of Applied Physics
Delhi Technological University
New Delhi – 110 042

ACKNOWLEDGEMENTS

The task of acknowledging the incalculable debt of appreciation, which is owed to many, is a very pleasant facet of dissertation. It gives an utmost joy in thanking those who were associated with me in completion of this work.

"Acknowledging the good that you already have in your life is the foundation for all abundance."

With deep regard and profound respect, I take this opportunity to express my deep sense of gratitude and indebtedness to ***Dr. Santa Chawla****, Senior Principal Scientist, National Physical Laboratory, New Delhi. No words can possibly convey my deep sense of gratitude to my worthy supervisor for her learned counsel and dynamic guidance, constructive criticism and valuable suggestion throughout this research work.*

I would like to thank my HOD, ***Dr. S.C. Sharma*** *and internal supervisor* ***Dr. M.S. Mehata,*** *Department of Applied Physics, Delhi Technological University, Delhi, for allowing me to carry out my project work in this esteemed research laboratory, and for rendering great help & co-operation.*

I am extremely thankful to ***Dr. Virendra Shanker****, Head of LMD group; NPL, New Delhi, his constant but silent and sincere inspiration and his liberal co-operation in all respect are really unforgettable experience for me.*

I express my thanks to Mr. Sandeep Mishra Sir, Mr. Vineet Dhuan, and Mrs. Vanjula for their helping nature, kind co-operation & discussions.

I am also thankful to Dr. Sukhbir Singh, Dr. Vidyanand Singh, Dr. N. Vijayan, and Dr. Awana Sir for characterization of my samples.

I express my thanks to ***Prof. R.C. Budhani****, Director, NPL and I would like to convey my regards to* ***Dr. Rajeev Chopra,*** *Head, HRD Group and Mr. P. Joshi, Technical officer, HRD Group, NPL, for allowing me to do my M.Tech. Research Project at National Physical Laboratory, New Delhi.*

I am also grateful to all the faculties of Department of Applied Physics, whose vast knowledge in the field of nanomaterials has enlightened me in different areas of this

research work. It is my pleasure to give my sincere thanks to ***Dr. Pawan Kr. Tyagi*** *for their valuable guidance. I am also thankful to Ms. Lucky and Mr. Vinay yadav, Ph.D. scholar in Department of Applied Physics, for providing the joyful environments in the Department and helping me. It was a nice and memorable experience with all the things of my department. I wish to give them my heartfelt thanks for their constant help and support.*

I could not have reached so far in life without the blessings and wishes of my family members. Words cannot describe my deep feelings and thankfulness towards all near and dear ones. I express my deep sense of gratitude to my parents ***Mr. Sultan Singh, Mrs. Santosh choudhary****; my sister* ***Dr. Neha Choudhary*** *and my brother-in-law* ***Dr. Mukesh Meel.*** *Above all, I thank the Almighty God for giving me all these people to help and encourage me, and for the skills and opportunity to complete this report.*

The financial assistance rendered by ***MHRD, New Delhi*** *is gratefully acknowledged.*

Place: New Delhi ***Naveen Khichar***

Date: ***(2K11/NST/08)***

ABSTRACT

Zinc oxide (ZnO) is multifunctional wide band gap (3.37eV) semiconductor and exhibit fluorescence when excited by ultraviolet (UV) light. The aim of the present work is to make ZnO nanoparticles with dual mode luminescence properties by selective doping with rare earth elements. Towards this goal, nanoparticles of undoped zinc oxide (ZnO) and ZnO doped with different rare earth elements like Erbium (Er), ytterbium (Yb), Holmium (Ho) have been synthesized and characterized. The nanoparticles were synthesized by two methods namely (1) room temperature co-precipitation method from acetate precursor in highly alkaline environment and (2) solid state reaction at relatively low temperature (500^0C).

The synthesized white powder of ZnO, ZnO:Er, ZnO:ErYb, ZnO:Ho, ZnO:HoYb, ZnO:ErLi nanoparticles were characterized by X-Ray diffraction, SEM, TEM, Photoluminescence (PL) spectroscopy and time resolved luminescence decay. X-Ray diffraction SEM and TEM analysis confirmed the formation of monophasic hexagonal wutzite ZnO nanoparticles with average particle size in the range of 5 to 40 nm. Flower like structure composed of nanoparticles of doped ZnO has been revealed by SEM and TEM measurements. PL measurements show that synthesized undoped ZnO and ZnO doped with different rare earth elements emit broadband white light under UV (370nm) excitation. Under Infrared (980nm) excitation, doped ZnO (Er/Ho,Yb) exhibit red and green upconversion fluorescence. Hence dual excitation i.e., both down and up conversion fluorescence could be introduced in ZnO nanoparticles by doping with rare earth elements Er and Ho.

CONTENTS

LIST OF FIGURES

List of Figures Page no.

LIST OF TABLES

CHAPTER-1

INTRODUCTION

Abstract:

The chapter includes general introduction on phosphor materials and the various phenomena associated with these materials. A review of the up and down convertor phenomena and its application in solar cell is also discussed.

1.1 Introduction:-

Nanotechnology is defined as the study of manipulating matter on the atomic and molecular scale. In General, nanotechnology deals with structures whose sizes vary between 1 to 100 nm in one dimension at least, and involves developing materials having at least one dimension within that size range. It covers various areas ranging from conventional device physics to completely new approaches based on molecular self-assembly, from developing materials having dimensions of the nanoscale to finding out whether we can control matter on the atomic scale. It is able to create many new materials with a vast range of applications, such as in medicine, biomaterials, electronics, and production of energy. However, nanotechnology raises many concerns about toxicity and impact of nanomaterials on environment, and their effects on global economics.

Nanoparticles are particles that have one dimension that is 100 nanometres or less in size. The properties of many conventional materials change when formed from nanoparticles. This is typically because Nanoparticles have a greater surface area per weight than larger particles; this causes them to be more reactive to certain other molecules. Nanoparticles are used, or being evaluated for use, in many fields.

Nanoparticles are of great scientific interest as they are effectively a bridge between bulk materials and atomic or molecular structures. A bulk material should have constant physical properties regardless of its size, but at the nano-scale size-dependent properties are often observed.

Thus, the properties of materials generally change as their size approaches the nanoscale and as the percentage of atoms at the surface of a material starts to become significant. For bulk materials larger than one micrometer (or micron), the percentage of

atoms at the surface is insignificant in comparison to the number of atoms in the bulk of the material. The interesting and sometimes unexpected properties of nanoparticles are therefore largely due to the large surface area of the material, which dominates the contributions made by the small bulk of the material. Nanoparticles often possess unexpected optical properties as they are small enough to confine their electrons and produce quantum effects. Other size-dependent property changes in the nanoparticles include quantum confinement in semiconductor particles, surface resonance in some metal particles and paramagnetism in magnetic materials.

1.1.1 Properties of Nanoparticles:

- A bulk material should have constant physical properties regardless of its size, but at the nano-scale size-dependent properties are often observed. Thus, the properties of materials change as their size approaches the nanoscale and as the percentage of atoms at the surface of a material becomes significant.
- For bulk materials larger than one micrometer (or micron), the percentage of atoms at the surface is insignificant in relation to the number of atoms in the bulk of the material. The interesting and sometimes unexpected properties of nanoparticles are therefore largely due to the large surface area of the material, which dominates the contributions made by the small bulk of the material.
- Nanoparticles of usually yellow gold and gray silicon are red in colour; gold nanoparticles melt at much lower temperatures (nearly 300 C for 2.5 nm size) than the gold slabs (1064 C); and absorption of solar radiation in photovoltaic cells is much higher in materials composed of nano-particles than it is in thin films of continuous sheets of material, the smaller the particles, the grater the solar absorption.
- Suspensions of nanoparticles are possible since the interaction of the particle surface with the solvent is strong enough to overcome density differences, which otherwise usually result in a material either sinking or floating in a liquid.
- Nanoparticles also often possess unexpected optical properties as they are small enough to confine their electrons and produce quantum effects. For example gold nanoparticles appear deep red to black in solution.
- The high surface area to volume ratio of nanoparticles provides a tremendous driving force for diffusion, especially at elevated temperatures.

- Moreover, nanoparticles have been found to impart some extra properties to various day today products. For example the presence of titanium dioxide nanoparticles imparts what we call the self-cleaning effect, and the size being nano range, the particles cannot be observed. Zinc oxide particles have been found to have superior UV blocking properties compared to its bulk substitute. This is one of the reasons why it is often used in the preparation of sunscreen lotions, and is completely photo stable.

1.1.2 Advantages of Nanoparticles:

The advantages of using nanoparticles include the following:

- Particle size and surface characteristics of nanoparticles can be easily changed to achieve both passive and active drug targeting after parenteral administration.
- They control and sustain release of the drug during the transportation and at the site of localization, altering organ distribution of the drug and subsequent clearance of the drug so as to achieve increase in drug therapeutic efficacy and reduction in side effects.
- Site-specific targeting can be achieved by attaching targeting ligands to surface of particles or use of magnetic guidance.
- The system can be used for various routes of administration including oral, nasal, parenteral, intermolecular etc.

1.1.3 Limitations of Nanoparticles:

In spite of these advantages, nanoparticles do have limitations.

- For example, their small size and large surface area can lead to particle-particle aggregation, making physical handling of nanoparticles difficult in liquid and dry forms.
- In addition, small particles size and large surface area readily result in limited drug loading and burst release.

These practical problems have to be overcome before nanoparticles can be made commercially available. The present review details the latest development of nanoparticulate drug delivery systems, surface modification issues, drug loading strategies, release control and potential applications of nanoparticles.

1.2 Luminescence:-

Light is a form of energy. To create light, another form of energy must be supplied. There are two common ways for this to occur, incandescence and luminescence.

Incandescence is light from heat energy. If you heat something to a high enough temperature, it will begin to glow. When an electric stove's heater or metal in a flame begin to glow "red hot", that is incandescence. When the tungsten filament of an ordinary incandescent light bulb is heated still hotter, it glows brightly "white hot" by the same means. The sun and stars glow by incandescence.

Luminescence is the process of emission of electromagnetic radiation from substances when excited by some form of energy which is different from incandescence. When certain materials absorb energy in some form or other, a fraction of absorbed energy may be re-emitted as electromagnetic radiation. Such cold emission of light is known as luminescence. Luminescence is at least two step processes, the excitation of the electronic system of the substance and the subsequent radiative recombination giving rise to emission of photons. Luminescence is "cold light" that can be emitted at normal and lower temperatures. In luminescence, some energy source kicks an electron of an atom out of its lowest energy "ground" state into a higher energy "excited" state; then the electron returns the energy in the form of light so it can fall back to its "ground" state. With few exceptions, the excitation energy is always greater than the energy (wavelength, colour) of the emitted light.

There are several varieties of luminescence, each named according to the source of energy, or the trigger for the luminescence:

Photoluminescence is luminescence where the energy is supplied by electromagnetic radiation (rays such as light, which will be discussed later). Photoluminescence is generally taken to mean "luminescence from any electromagnetic radiation", while fluorescence is often used only for luminescence caused by ultraviolet, although it may also be used for other photoluminescence's. Fluorescence is seen in fluorescent lights, amusement park & movie special effects and the redness of rubies in

sunlight, "day-glow" or "neon" colours, and in emission nebulae seen with telescopes in the night sky. Bleaches enhance their whitening power with a white fluorescent material.

Photoluminescence should not be confused with reflection, refraction, or scattering of light, which cause most of the colours you see in daylight or bright artificial lighting. Photoluminescence is distinguished in that the light is absorbed for a significant time, and generally produces light of a frequency that is lower than, but otherwise independent of, the frequency of the absorbed light.

Phosphorescence is delayed luminescence or "afterglow". When an electron is kicked into a high-energy state, it may get trapped there for some time (as if you lifted that rock, then set it on a table). In some cases, the electrons escape the trap in time; in other cases they remain trapped until some trigger gets them unstuck (like the rock will remain on the table until something bumps it). Many glow-in-the-dark products, especially toys for children, involve substances that receive energy from light, and emit the energy again as light later.

1.3 Phosphors:-

Materials that convert absorbed energy to visible light without going to high temperatures i.e. incandescence are known as luminescent materials and also referred as phosphors. Such materials find applications in displays like television i.e. cathode ray tubes (CRT), plasma display panels (PDP), Electroluminescence (EL) based displays and field emission displays; in light sources like fluorescent tubes, compact fluorescent lamps and cold cathode lamps; as detectors for x-rays, temperature and pressure.

A phosphor, most generally, is a substance that exhibits the phenomenon of luminescence. Somewhat confusingly, this includes both phosphorescent materials, which show a slow decay in brightness (>1ms), and fluorescent materials, where the emission decay takes place over tens of nanoseconds. Phosphorescent materials are known for their use in radar screens and glow-in-the-dark toys, whereas fluorescent materials are common in CRT and plasma video display screens, sensors, and white LEDs.

Phosphors are often transition metal compounds or rare earth compounds of various types. The most common uses of phosphors are in CRT displays and fluorescent lights. CRT phosphors were standardized beginning around World War II and designated by the letter "P" followed by a number. Phosphorus, the chemical element named for its light-emitting behaviour, emits light due to chemiluminescence, not phosphorescence. [1][2]

Dopant plays different roles in different host lattices depending upon their electronic configuration, solubility and structures of the host lattices. Furthermore, dopants have been classified into various categories on the basis of their function in host lattices.

Activator: In phosphors the activator is the element added as dopant to the crystal of the material to create desired type of non-homogeneities. In luminescence, only a small fraction of atoms, called emission centres or luminescence centres, emit light. In inorganic phosphors, these in homogeneities in the crystal structure are created usually by addition of a trace amount of dopants, impurities called activators. The wavelength emitted by the emission centre is dependent on the atom itself, its electronic configuration, and on the surrounding crystal structure.

Sensitizer: - It is a chemical substance added into the crystal lattice as a one of the dopants. It absorbs most of the energy and transfers it to the activator for the process of emission.

Co-activators: The dopant ion that does not show luminescence but help in the process of luminescence by acting as charge compensator or by creating hole/electron traps is known as co-activator. For example Al^{3+}, Cl^{-}, F^{-}

Quencher or killer: The dopant ion that is responsible for decrease or complete disappearance of luminescence is known as quencher. When energy is transferred from an emitting centre in a nonradioactive manner with evolution of heat it causes quenching of luminescence. For example Fe, Co and Ni in ZnS act as nonradioactive centre, thus called quenchers.

1.4 Nanophosphor:-

Phosphors are generally crystalline and in powder form with particle size ranging from 1-100 μm. Phosphors with one dimension <100 nm are called nano-phosphors, possess strikingly different absorption and emission characteristics with improved efficiency and life time's [3]. As band gap energy is varied with particle size in nanometre range, immense possibilities of designing phosphors and related devices are predicted. Synthesis of nano-phosphors has been attempted by several methods and their properties have been compared to bulk phosphors by many workers [4]. Work on devices and applications are going on but much of it is in regime of industrial secrecy. Nano-phosphors synthesized with a view to different new applications employing cathode-luminescence are reported. Nanosized luminescent phosphors synthesized inside the voids and different templates have been employed for different situations with increased resolution. This class of materials processed with inorganic capping such as ZnO capped ZnS:Mn, ZnS capped CdS have not only increased efficiency but also much better operational resistance in devices. Up-converting and down converting phosphors in nanosizes have great promise in increasing efficiency of Si solar cells. Laser action in Ce^{3+} and Pr^{3+} ions doped δ-Al_2O_3 nano-phosphors under cathode rays is likely to open new vistas of applications. Electroluminescent (EL) displays based on nano-phosphors have shown higher resolution, lower power requirement and low voltage operation (~10 V). Use of nano-phosphors in generation of white light employing blue/UV emitting LEDs is likely to change the energy demand for lighting.

Nano-phosphors of ZnO and TiO_2 in cosmetics do have increased absorption of ultraviolet rays from sun but also add special tinge due to dopants. Demir Akin [5] et al reported bacteria-mediated delivery of nano-phosphors and cargo into cells of live animals. Hongguang Liu[6] et al have reviewed use of nano-phosphors as new contrast agents for tumor imaging. A novel homogeneous up-conversion fret-based assay technology utilizing a particulate up-converting rare earth phosphor as a donor and a fluorescent protein as an acceptor is described. The sensitized emission of the acceptor is measured free of auto fluorescence and scattered light. The interferences of matrix absorption are almost completely eliminated as the donor is excited at near-infrared and the sensitized emission is measured at red or at far-red above the major absorption of both the oxy- and the deoxyhemoglobin as well as most of the other compounds present

in any biological samples. No temporal resolution in detection is required, because the auto fluorescence is completely absent and neither the acceptor generates any direct emission under near-infrared excitation. Nanophosphor has so many applications that are known and new potentials are becoming distinct every day. Future is going to be very different because of nano-phosphors.

1.5 Why ZnO?

Recently, much research attention has been paid to the field of rare earth materials since they have many potential applications based on their novel electronic and optical properties resulting from their 4f electrons. Among the various rare earth element doped materials doped ZnO has many wonderful characteristics including excellent thermal, mechanical, and optical properties; especially they play an important role in many optical devices, catalysts, and laser host materials.

We choose ZnO because it is biocompatible semiconducting material and find potential application in electronics, optoelectronics, spintronics, biosensors, fluorescent labels in biology etc. ZnO has been commonly used in its polycrystalline form for over a hundred years in a wide range of applications: facial powders, ointments, sunscreen, catalysts, lubricant, additives, paint pigmentation, piezoelectric, transducers varistors and as transparent conducting electrodes.

ZnO has exhibited better radiation resistance than GaN for possible devices used in space and nuclear applications. ZnO can be grown on inexpensive substrate, such as glass, at relatively low temperatures. Its research interest has waxed and waned as new prospective applications revive interest in the material, but the applications have been limited by the technology available at the time.

The research on rare earth (RE) doped with luminescent materials is always the most active field owing to the large in the field of illumination and display, such as fluorescent lamps, cathode ray tube, field emission displays, and the developing white light emitting diodes. ZnO is an important oxide material in material science and technology. ZnO is a good host for rare earth, is synthesized by different method i.e. solid state reaction method and co-precipitation method. It is known that different material preparation methods have some important effects on material micro structure

and physical properties. It has been well documented that grain size, morphology, homogeneity, and/or surface modification have been an impact on the chemical and/or physical properties of materials.

We have prepared ZnO by co-precipitation method, these are ideal for detection application due to its large surface area to volume ratio.

One device that has great commercial potential is a UV light-emitting diode (LED), which could be combined with phosphors to produce solid-state white lighting. Another is a transparent field-effect transistor, which could serve as an active element in large-area displays.

A first principle investigation by van de walle [7] suggests that the simultaneous incorporation of nitrogen and hydrogen may be beneficial for achieving p-type doping in ZnO. Rare-earth (RE) doped semiconductors are since long being investigated due to their applications. Among the metal oxide semiconductors one that is attracting considerably attention for its new potential applications is ZnO. This is due to its wide direct band gap, transparency in the visible part of the spectrum, and specially, because of its possible room temperature (RT) ferromagnetism when doped with transition metals.

ZnO has a relatively large direct band gap of ~3.37 eV at room temperature. Advantages associated with a large band gap include higher breakdown voltages, ability to sustain large electric fields, lower electronic noise, and high-temperature and high-power operation. The band gap of ZnO can further be tuned to ~3–4 eV by its alloying with magnesium oxide or cadmium oxide.[8] Most ZnO has *n*-type character, even in the absence of intentional doping. Nonstoichiometry is typically the origin of n-type character, but the subject remains controversial.[9] An alternative explanation has been proposed, based on theoretical calculations, that unintentional substitutional hydrogen impurities are responsible.[10] Controllable n-type doping is easily achieved by substituting Zn with group-III elements such as Al, Ga, In or by substituting oxygen with group-VII elements chlorine or iodine.[11]

Reliable p-type doping of ZnO remains difficult. This problem originates from low solubility of p-type dopants and their compensation by abundant n-type impurities.

This problem is observed with GaN and ZnSe. Measurement of p-type in "intrinsically" n-type material is complicated by the inhomogeneity of samples.[12]

Current limitations to p-doping do not limit electronic and optoelectronic applications of ZnO, which usually require junctions of n-type and p-type material. Known p-type dopants include group-I elements Li, Na, K; group-V elements N, P and As; as well as copper and silver. However, many of these form deep acceptors and do not produce significant p-type conduction at room temperature.[13]

Electron mobility of ZnO strongly varies with temperature and has a maximum of ~2000 $cm^2/(V \cdot s)$ at 80 K. Data on hole mobility are scarce with values in the range 5–30 $cm^2/(V \cdot s)$.[14]

Nanostructures of ZnO can be synthesized into a variety of morphologies including nanowires, nanorods, tetrapods, nanobelts, nanoflowers, nanoparticles etc. Nanostructures can be obtained with most above-mentioned techniques, at certain conditions, and also with the vapor-liquid-solid method.[15][16]

Rod like nanostructures of ZnO can be produced via aqueous methods, which are attractive for the following reasons: They are low cost, less hazardous and thus capable of easy scaling up; the growth occurs at a relatively low temperature, compatible with flexible organic substrates; there is no need for the use of metal catalysts, and thus it can be integrated with well-developed silicon technologies. In addition, there are a variety of parameters that can be tuned to effectively control the morphology and properties of the final product. Wet chemical methods have been demonstrated as a very powerful and versatile technique for growing one dimensional ZnO nanostructures.[17] The synthesis is typically carried out at temperatures of about 90 °C, in an equimolar aqueous solution of zinc nitrate and hexamine, the latter providing the basic environment. Certain additives, such as polyethylene glycol or polyethylenimine, can improve the aspect ratio of the ZnO nanowires.[18] Doping of the ZnO nanowires has been achieved by adding other metal nitrates to the growth solution.[19] The morphology of the resulting nanostructures can be tuned by changing the parameters relating to the precursor composition (such as the zinc concentration and pH) or to the thermal treatment (such as the temperature and heating rate).[20]

Aligned ZnO nanowires on pre-seeded silicon, glass and gallium nitride substrates have been grown in aqueous solutions using aqueous zinc salts such

as Zinc nitrate and Zinc acetate in basic environments.[21] Pre-seeding substrates with ZnO creates sites for homogeneous nucleation of ZnO crystal during the synthesis. Common pre-seeding methods include in-situ thermal decomposition of zinc acetate crystallites, spin coating of ZnO nanoparticles and the use of physical vapor deposition methods to deposit ZnO thin films.[22][23] Pre-seeding can be performed in conjunction with top down patterning methods such as electron beam lithography and nanosphere lithography to designate nucleation sites prior to growth. Aligned ZnO nanowires can be used in dye-sensitized solar cells and field emission devices.[24][25]

1.6 ZnO Structure:-

Zinc oxide crystallizes in two main forms, **hexagonal wurtzite**[26] and **cubic zincblende**. The wurtzite structure is most stable at ambient conditions and thus most common. The zincblende form can be stabilized by growing ZnO on substrates with cubic lattice structure. In both cases, the zinc and oxide centers are tetrahedral, the most characteristic geometry for Zn (II). In addition to the wurtzite and zincblende polymorphs, ZnO can be crystallized in the rocksalt motif at relatively high pressures about 10 GPa.[27]

Hexagonal and zincblende polymorphs have no inversion symmetry (reflection of a crystal relative to any given point does not transform it into itself). This and other lattice symmetry properties result in piezoelectricity of the hexagonal and zincblende ZnO, and pyroelectricity of hexagonal ZnO.

The hexagonal structure has a point group 6 mm (Hermann-Mauguin notation) or C_{6v} (Schoenflies notation), and the space group is $P6_3mc$ or C_{6v}[28]. The lattice constants are ***a* = 3.25 Å** and ***c* = 5.2 Å**; their ratio ***c/a* ~ 1.60** is close to the ideal value for hexagonal cell ***c/a* = 1.633**[29]**.** As in most group materials, the bonding in ZnO is largely ionic (Zn^{2+}–O^{2-}) with the corresponding radii of 0.074 nm for Zn^{2+} and 0.140 nm for O^{2-}. This property accounts for the preferential formation of wurtzite rather than zincblende structure,[30] as well as the strong piezoelectricity of ZnO. Because of the polar Zn-O bonds, zinc and oxygen planes are electrically charged. To maintain electrical neutrality, those planes reconstruct at atomic level in most relative materials, but not in ZnO – its surfaces are atomically flat, stable and exhibit no reconstruction. This anomaly of ZnO is not fully explained yet.[31]

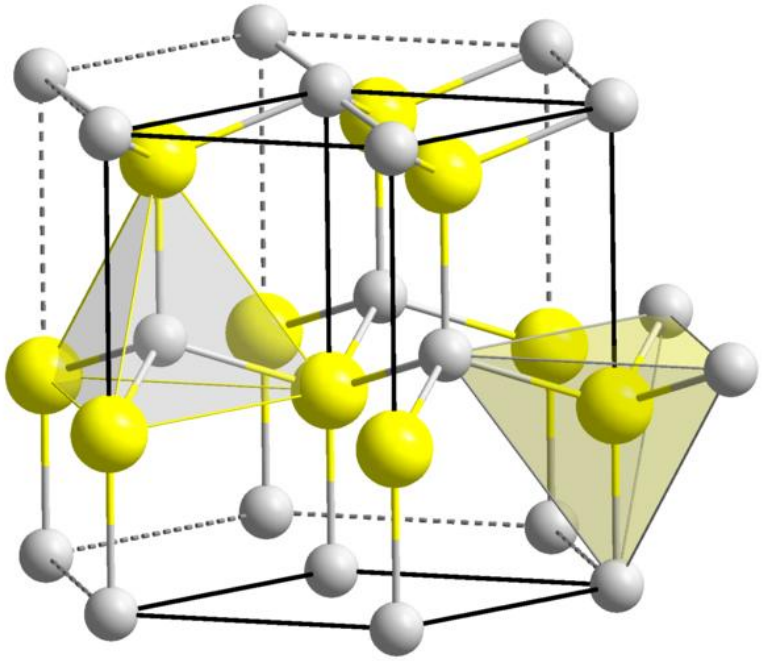

Fig 1.1: Wurtzite structure

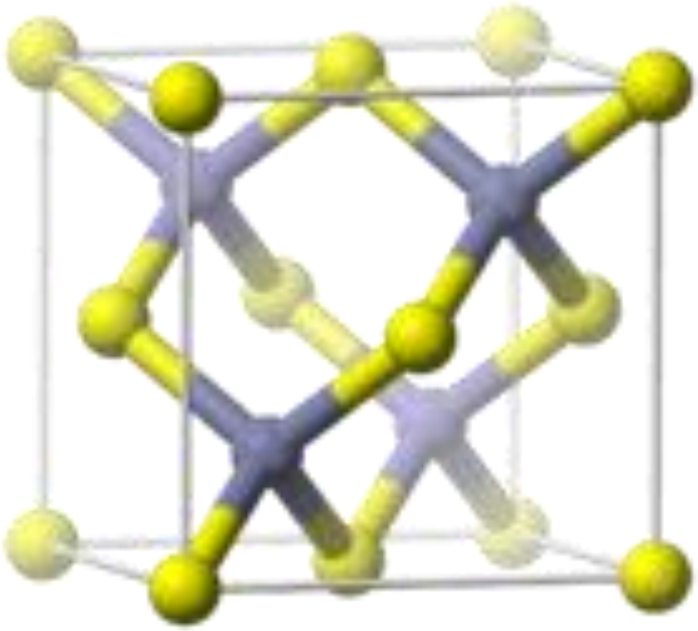

Fig 1.2: A zincblende unit cell

Table 1.1

Properties	
Molecular formula	ZnO
Molar mass	81.408 g/mol
Appearance	White solid
Odour	odourless
Density	5.606 g/cm^3
Melting point	1975 °C (decomposes)[n]
Boiling point	1975 °C (decomposes)
Band gap	3.3 eV (direct)
Refractive index(n_D)	2.0041

1.7 Rare earth elements:-

The rare earth elements (REEs), which include the 15 lanthanide elements (Z = 57 through 71) are called so because most of them were originally isolated in the 18th and 19th centuries as oxides from rare minerals. Because of their reactivity, the REEs were found to be difficult to refine to pure metal. Furthermore, efficient separation processes were not developed until the 20th century because of REEs' chemical similarity. A statement attributed to Sir William Crookes, a noted English scientist, betrays the frustrations of late 19th-century chemists with this group of elements (Emsley 2001) "The rare earth elements perplex us in our researches, baffle us in our speculations, and haunt us in our very dreams. They stretch like an unknown sea before us, mocking, mystifying and murmuring strange revelations and possibilities."

All of the REEs were finally identified in the 20th century. Promethium, the rarest, was not identified until 1945, and pure lutetium metal was not refined until 1953 (Emsley 2001). Commercial markets for most of the REEs have arisen in only the past 50 years. Most REEs are not as uncommon in nature as the name implies. Cerium, the most abundant REE (Table 1.2), comprises more of the earth's crust than copper or lead. Many REEs are more common than tin and molybdenum, and all but promethium are more common than silver or mercury (Taylor and McLennan 1985).[15] Promethium, best known as an artificial element, occurs in very minute quantities in natural materials because it has no stable or long-lived isotopes. Lanthanide elements with low atomic numbers are generally more abundant in the earth's crust than those with high atomic numbers. Those with even atomic numbers are two to seven times more abundant than adjacent lanthanides with odd atomic lanthanides or heavy lanthanides plus yttrium. The relative abundance of individual lanthanide elements has been found useful in the understanding of magmatic processes and natural aqueous systems. Comparisons are generally made using a logarithmic plot of lanthanide abundances normalized to abundances in chondritic (stony) meteorites.

Table 1.2 [15]

Table 1. REEs, atomic numbers, and abundances

Element	Symbol	Atomic Number	Upper Crust Abundance, *ppm**	Chondrite Abundance, *ppm*†
Yttrium	Y	39	22	na‡
Lanthanum	La	57	30	0.34
Cerium	Ce	58	64	0.91
Praseodymium	Pr	59	7.1	0.121
Neodymium	Nd	60	26	0.64
Promethium	Pm	61	na	na
Samarium	Sm	62	4.5	0.195
Europium	Eu	63	0.88	0.073
Gadolinium	Gd	64	3.8	0.26
Terbium	Tb	65	0.64	0.047
Dysprosium	Dy	66	3.5	0.30
Holmium	Ho	67	0.80	0.078
Erbium	Er	68	2.3	0.20
Thulium	Tm	69	0.33	0.032
Ytterbium	Yb	70	2.2	0.22
Lutetium	Lu	71	0.32	0.034

The use of this method eliminates the abundance variation between lanthanides of odd and even atomic number, and allows de termination of the extent of fractionation between the lanthanides, because such fractionation is not considered to have taken place during chondrite formation. The method also is useful because chondrites are thought to be compositionally similar to the original earth's mantle. Europium (Eu) anomalies (positive or negative departures of europium from chondrite-normalized plots) have been found to be particularly effective for petro genetic modelling. In addition, RE E isotopes, particularly of neodymium and samarium, have found use in petro genetic modelling and geochronology. The lanthanide elements traditionally have been divided into two groups: the light rare earth elements (LREEs)—lanthanum through europium (Z = 57 through 63); and the heavy rare earth elements (HREEs)—gadolinium through lutetium (Z = 64 through 71). Although yttrium is the lightest REE, it is usually grouped with the HREEs to which it is chemically and physically similar. The REEs are lithophile elements (elements enriched in the earth's crust) that invariably

occur together naturally because all are trivalent (except for Ce^{+4} and Eu^{+2} in some environments) and have similar ionic radii. An increase in atomic number in the lanthanide group is not accompanied by change in valence, and the lanthanide elements all inhabit the same cell in most versions of the periodic table. The similar radii and oxidation states of the REEs allow for liberal substitution of the REEs for each other into various crystal lattices. This substitution accounts for their wide dispersion in the earth's crust and the characteristic multiple occurrences of REEs within a single mineral. The chemical and physical differences that exist within the REEs group are caused by small differences in ionic radius and generally result in segregation of REEs into deposits enriched in either light

Common Properties of the Rare Earths:-

These common properties apply to both the lanthanides and actinides.

- The rare earths are silver, silvery-white, or gray metals.
- The metals have a high luster, but tarnish readily in air.
- The metals have high electrical conductivity.
- The rare earths share many common properties. This makes them difficult to separate or even distinguish from each other.
- There are *very* small differences in solubility and complex formation between the rare earths.
- The rare earth metals naturally occur together in minerals (e.g., monazite is a mixed rare earth phosphate).
- Rare earths are found with non-metals, usually in the 3+ oxidation state. There is little tendency to vary the valance. (Europium also has a valence of 2+ and cerium also a valence of 4+.)

1.8 Erbium:-

Erbium is a chemical element in the lanthanide series, with the symbol **Er** and atomic number 68. A silvery-white solid metal when artificially isolated, natural erbium is always found in chemical combination with other elements on Earth. As such, it is a rare earth element which is associated with several other rare elements in the mineral gadolinite from Ytterby in Sweden.

Erbium's principal uses involve its pink-colored Er^{3+} ions, which have optical fluorescent properties particularly useful in certain laser applications. Erbium-doped glasses or crystals can be used as optical amplification media, where erbium (III) ions are optically pumped at around 980 nm or 1480 nm and then radiate light at 1530 nm in stimulated emission. This process results in an unusually mechanically simple laser optical amplifier for signals transmitted by fiber optics. The 1550 nm wavelength is especially important for optical because standard single mode optical fibers have minimal loss at this particular wavelength. In addition to optical fiber lasers, a large variety of medical applications (i.e. dermatology, dentistry) utilize the erbium ion's 2940 nm emission (Er:YAG laser), which is highly absorbed in water in tissues, making its effect very superficial. Such shallow tissue deposition of laser energy is helpful in laser surgery, and for the efficient production of steam for laser enamel ablation in certain types of laser dentistry. Erbium is slightly toxic if ingested, but erbium compounds are not toxic.[32] Metallic erbium in dust form presents a fire and explosion hazard.

Table 1.3

Properties	
Phase	solid
Density (near r.t.)	9.066 g·cm^{-3}
Melting point	1802 K2784 °F 1529 °C,
Boiling point	5194 °F 2868 °C,3141 K,
Oxidation states	3, 2, 1(basic oxide)
Atomic radius	176 pm
Covalent radius	189±6 pm
Crystal structure	hexagonal close-packed

1.9 Ytterbium:-

Ytterbium is a chemical element with symbol **Yb** and atomic number 70. It is the fourteenth and penultimate element in the lanthanide series, or last element in the f-block, which is the basis of the relative stability of the +2 oxidation state. However, like the other lanthanides, the most common oxidation state is +3, seen in its oxide, halides and other compounds. In aqueous solution, like compounds of other late lanthanides, soluble ytterbium compounds form complexes with nine water molecules. Because of its closed-shell electron configuration, its density and melting and boiling points differ from those of the other lanthanides.

Natural ytterbium is a mixture of seven stable isotopes, which altogether are present at concentrations of 3 parts per million. This element is mined in China, the United States, Brazil, and India in form of the minerals monazite, euxenite, and xenotime. The ytterbium concentration is low, because the element is found among many other rare earth elements; moreover, it is among the least abundant ones. Once extracted and prepared; ytterbium is somewhat hazardous as an eye and skin irritant. The metal is a fire and explosion hazard.

Table 1.4

Properties	
Phase	solid
Density (near r.t.)	6.90 g·cm^{-3}
Liquid density atm.p.	6.21 g·cm^{-3}
Melting point	1097 K1515 °F 824 °C, ,
Boiling point	2185 °F 1196 °C,1469 K,
Oxidation states	**3**, 2, 1 (basic oxide)
Ionization energies	1st: 603.4 kJ·mol^{-1}

	2nd: 1174.8 kJ·mol^{-1}
	3rd: 2417 kJ·mol^{-1}
Atomic radius	176 pm
Covalent radius	187±8 pm
Crystal structure	face-centered cubic
Magnetic ordering	paramagnetic

1.10 Holmium:

Holmium is a chemical element with the symbol **Ho** and atomic number 67. Part of the lanthanide series, holmium is a rare earth element. Holmium was discovered by Swedish chemist Per Theodor Cleve. Its oxide was first isolated from rare earth ores in 1878 and the element was named after the city of Stockholm. Elemental holmium is a relatively soft and malleable silvery-white metal. It is too reactive to be found uncombined in nature, but when isolated, is relatively stable in dry air at room temperature. However, it reacts with water and rusts readily, and will also burn in air when heated.

Holmium is found in the minerals monazite and gadolinite, and is usually commercially extracted from monazite using ion exchange techniques. Its compounds in nature, and in nearly all of its laboratory chemistry, are trivalent oxidized, containing Ho(III) ions. Trivalent holmium ions have fluorescent properties similar to many other rare earth ions (while yielding their own set of unique emission light lines), and holmium ions are thus used in the same way as some other rare earths in certain laser and glass colorant applications. Holmium has the highest magnetic strength of any element and therefore is used for the pole pieces of the strongest static magnets. Because holmium strongly absorbs neutrons, it is also used in nuclear control rods.

Table 1.5

Properties	
Phase	solid
Density (near r.t.)	8.79 g·cm^{-3}
Liquid density atm.p.	8.34 g·cm^{-3}
Melting point	1734 K2662 °F 1461 °C,
Oxidation states	3, 2, 1 (basic oxide)
Atomic radius	176 pm
Covalent radius	192±7 pm
Crystal structure	hexagonal close-packed
Magnetic ordering	paramagnetic

1.11 Lanthanides ions as spectral converters for solar cells:-

The use of lanthanide ions to convert photons to different, more useful, wavelengths is well-known from a wide range of applications (e.g. fluorescent tubes, lasers, white light LEDs). Recently, a new potential application has emerged: the use of lanthanide ions for spectral conversion in solar cells. The main energy loss in the conversion of solar energy to electricity is related to the so-called spectral mismatch: low energy photons are not absorbed by a solar cell while high energy photons are not used efficiently. To reduce the spectral mismatch losses, both up conversion and down conversion of solar photons are viable options.

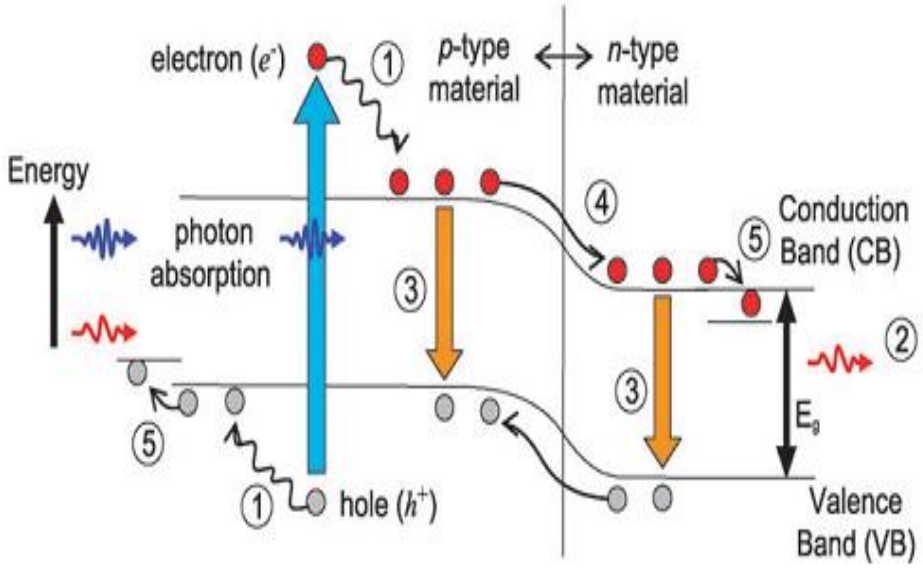

Fig 1.3: *Primary loss mechanism within a standard photovoltaic structure {1} lattice loss; {2} transparency loss; {3} recombination loss; {4} junction loss {5} contact loss (Adapted from Richards*)]

1.12 Up Conversion (UC):-

In the case of up conversion, two or more low energy infrared photons that cannot be utilized by the solar cell, are absorbed by a material to give one high energy visible photon that can be absorbed. Here when a material is excited by two or more photons of longer wavelength resulting in photoluminescence at a shorter wavelength, It is also referred as anti-stokes emission since Stokes law states that the wavelength of the emitted light should be greater than the wavelength of the exciting radiation.

The process of photon up conversion (UC) is to convert photons from low to high frequencies i.e. absorption of two or more low energy photons may result in the emission of a high energy photon. By up conversion process, long wave length invisible IR photon can be converted in to the shorter wave length visible photon. The term up conversion refers to the process of converting low energy incident radiation into higher energy output radiation. Up conversion is a non linear optical process that requires two or more metastable energy states to store the energy of absorbed pump photons. The combined energies of pump photons can lead to the emission of a higher energy photon. Much work has been done to study the precise energy transfer processes that occur

during an up conversion event. Our fundamental energy transfer process is given in fig 1.4.

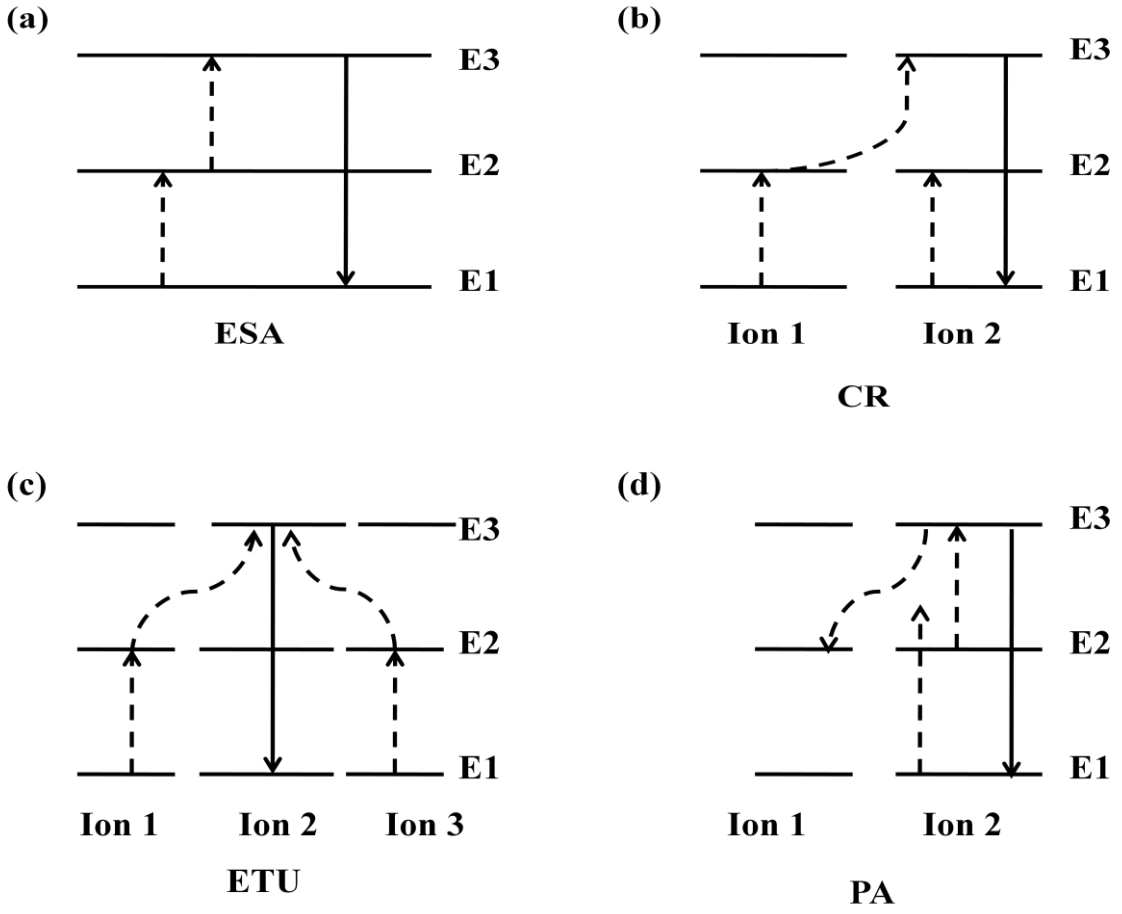

Fig 1.4: Four basic energy transfer mechanisms: (a) excited state absorption (b) cross relaxation (c) energy transfer up conversion. (d) Photonic avalanche

In the first process, excited state absorption (ESA), an ion absorbs a near-infrared pump photon, which excites the ion then returns to the ground state, E1 and gives off radiation with energy (E3-E1). The second process, cross relaxation (CR), involves two ions, each of which is initially excited by a pump photon to E2. One ion transfers energy to the other, resulting in one ground state ion and one ion excited to E3. The excited ion then releases the energy in the form of a photon. Ions that donate energy are generally referred to as sensitizers, and ions that receive energy and emit radiations are called activators. The third mechanism, energy transfer up conversion (ETU), involves three ions (two sensitizers and one activator). Two sensitizer ions absorb pump photons to each reach E2. Both ions transfer energy to a third ion, exciting it to E3. The activator then gives off a photon and returns to the ground state. It is worth noting that

ETU is the most efficient up-conversion mechanism offering more than an order of magnitude advantage over ESA. ETU is efficient because it favours resonant absorption, which leads to long excitation lifetimes and increases the probability of up conversion.

So far a variety of applications have been exploited based on infrared up-conversion, including lasing and three-dimensional (3D) display and up-conversion enhanced solar cells and up-conversion based weak infrared photon detection and infrared imaging.

1.13 Down conversion (DC):-

In the case of down conversion, one high energy photon can give rise to two lower energy photons that can both be absorbed by the solar cell. It occurs when a materials is excited by a very high energy photon resulting in emission of two low energy photon at longer wavelength. Since quantum efficiency of such phosphors can be more than unity, they are also called quantum cutters.

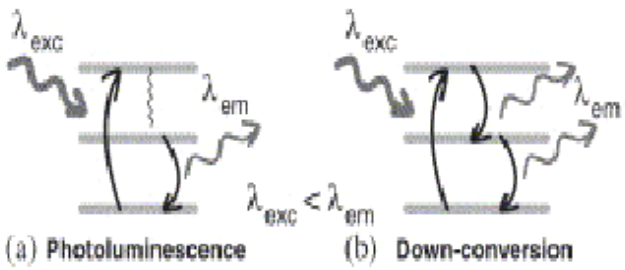

Fig 1.5: mechanism of Photoluminescence and down-conversion

1.14 Photoluminescence (PL)/ Down shifting:-

PL/DS is a single photon process in which one high energy photon is absorbed by a luminescent material and then re-emitted at a longer wavelength. This is normally Stokes shifted luminescence and most phosphor material falls in this category.

1.15 References:

1. Emsley, John (2000). The Shocking History of Phosphorus. London: Macmillan.ISBN 0330390058.
2. T. Justel , H. Nikol, C. Ronda, New development in the field of luminescent materials for lighting and display. Angew Chem int. Ed.37(1998)3084-3103.
3. A. Huignard, T.Gacoin ,J.P.Bioilot,Chem.Mater.12(2000)1090.
4. Peter W. Hawkes (1 October 1990). Advances in electronics and electron physics. Academic Press. pp. 350–. ISBN 978-0-12-014679-6. Retrieved 9 January 2012.
5. Akin, Demir; Ragheb, Kathy; Sturgis, Jennifer; Sherman, Debby; Burkholder, Kristen; Robinson, J. Paul; Bhunia, Arun K.; Mohammed, Sulma; and Bashir, Rashid, "Bacteria-mediated delivery of nanoparticles and cargo into cells" (2007).
6. Molecular Imaging Program at Stanford (MIPS), Department of Radiology and Bio-X Program, Canary Center at Stanford for Cancer Early Detection, Stanford University, Stanford, California.Journal of Nuclear Medicine (impact factor: 6.38). 08/2012; 53(10):1579-84.
7. C. G. Van de Walle, Phys. Rev. Lett. 85, 1012 2000.
8. Ohgaki, Takeshi; Ohashi, Naoki; Sugimura, Shigeaki; Ryoken, Haruki; Sakaguchi, Isao; Adachi, Yutaka; Haneda, Hajime (2008). "Positive Hall coefficients obtained from contact misplacement on evident *n*-type ZnO films and crystals". *Journal of Materials Research* **23** (9): 2293.
9. Wagner, P; Helbig, R (1974). "Halleffekt und anisotropie der beweglichkeit der elektronen in ZnO". *Journal of Physics and Chemistry of Solids* **35** (3): 327.
10. Ryu, Y. R.; Lee, T. S.; White, H. W. (2003). "Properties of arsenic-doped p-type ZnO grown by hybrid beam deposition". *Applied Physics Letters* **83**: 87.
11. Takahashi, Kiyoshi; Yoshikawa, Akihiko; Sandhu, Adarsh (2007). *Wide bandgap semiconductors: fundamental properties and modern photonic and electronic devices*. Springer. p. 357.
12. Ohgaki, Takeshi; Ohashi, Naoki; Sugimura, Shigeaki; Ryoken, Haruki; Sakaguchi, Isao; Adachi, Yutaka; Haneda, Hajime (2008). "Positive Hall coefficients obtained from contact misplacement on evident *n*-type ZnO films and crystals". *Journal of Materials Research* 23 (9): 2293. Bibcode:2008JMatR..23.2293O.doi:10.1557/JMR.2008.0300

13. Wagner, P; Helbig, R (1974). "Halleffekt und anisotropie der beweglichkeit der elektronen in ZnO". *Journal of Physics and Chemistry of Solids* **35** (3): 327.Bibcode:1974JPCS...35..327W. doi:10.1016/S0022-3697(74)80026-0.
14. Ryu, Y. R.; Lee, T. S.; White, H. W. (2003). "Properties of arsenic-doped p-type ZnO grown by hybrid beam deposition". *Applied Physics Letters* **83**: 87.Bibcode:2003ApPhL..83...87R. doi:10.1063/1.1590423.
15. Baruah, S. and Dutta, J. (2009). "Hydrothermal growth of ZnO nanostructures". *Sci. Technol. Adv. Mater.* (Free download pdf) 10: 013001. Bibcode: 2009STAdM. 10a3001B. doi:10.1088/1468-6996/10/1/013001.
16. Miao, L.; Ieda, Y.; Tanemura, S.; Cao, Y.G.; Tanemura, M.; Hayashi, Y.; Toh, S.; Kaneko, K. (2007). "Synthesis, microstructure and photoluminescence of well-aligned ZnO nanorods on Si substrate". *Science and Technology of Advanced Materials* (free downloadpdf) **8** (6):443. Bibcode:2007STAdM...8..443M.doi:10.1016/j.stam.2007.02.012
17. Xu, S.; Wang, ZL. (2011). "One-dimensional ZnO nanostructures: Solution growth and functional properties". *Nano Res.* **4** (11): 1013–1098. doi:10.1007/s12274-011-0160-7.
18. Ying Zhou *et al.* (2008). "Hydrothermal synthesis of ZnO nanorod arrays with the addition of polyethyleneimine". *Materials Research Bulletin* **43** (8–9): 2113–2118.doi:10.1016/j.materresbull.2007.09.024.
19. Cui, Jingbiao *et al.* (2006). "Synthesis and magnetic properties of Co-doped ZnO nanowires". *Journal of Applied Physics* **99** (8): 08M113.Bibcode:2006JAP....99hM113C. doi:10.1063/1.2169411.
20. Elen, K. *et al.* (2009). "Hydrothermal synthesis of ZnO nanorods: a statistical determination of the significant parameters in view of reducing the diameter".*Nanotechnology* **20** (5): 055608. Bibcode:2009Nanot..20e5608E. doi:10.1088/0957-4484/20/5/055608. PMID 19417355.
21. Greene, L. E. *et al.* (2003). "Low-Temperature Wafer-Scale Production of ZnO Nanowire Arrays". *Angew. Chem. Int. Ed* **42** (26): 3031–3032.doi:10.1002/anie.200351461. PMID 12851963.

22. Wu, Wan-Yu *et al.* (2009). "Effects of Seed Layer Characteristics on the Synthesis of ZnO Nanowires". *Journal of the American Ceramic Society* **92** (11): 2718–2723.doi:10.1111/j.1551-2916.2009.03022.x.
23. Greene, L. E.; Law, M; Tan, DH; Montano, M; Goldberger, J; Somorjai, G; Yang, P (2005). "General Route to Vertical ZnO Nanowire Arrays Using Textured ZnO Seeds".*NanoLetters* **5** (7):1231–1236. Bibcode:2005NanoL...5.1231G.doi: 10.1021/nl050788p. PMID 16178216.
24. Hua, Guomin *et al.* (2008). "Fabrication of ZnO nanowire arrays by cycle growth in surfactantless aqueous solution and their applications on dye-sensitized solar cells".*Materials Letters* **62** (25): 4109–4111. doi:10.1016/j.matlet.2008.06.018.
25. Lee, J.-H. *et al.* (2009). "Density-controlled growth and field emission property of aligned ZnO nanorod arrays". *Appl Phys A* **97** (2): 403–408.Bibcode:2009ApPhA..97..403L. doi:10.1007/s00339-009-5226-y.
26. Fierro, J. L. G (2006). *Metal Oxides: Chemistry & Applications*. 6000 Broken Sound Parkway NW, Suite 300: Taylor & Francis Group. p. 182. ISBN 0-8247-237-6 .
27. Özgür, Ü.; Alivov, Ya. I.; Liu, C.; Teke, A.; Reshchikov, M. A.; Doğan, S.; Avrutin, V.; Cho, S.-J. et al. (2005). "A comprehensive review of ZnO materials and devices".*Journal ofApplie Physics* **98** (4): 041301. Bibcode:2005JAP....98d1301O.doi:10.1063/1.1992666.
28. Klingshirn, C., C (2007). "ZnO: Material, Physics and Applications". *ChemPhysChem* **8** (6):782-803. doi:10.1002/cphc.200700002. PMID 17429819
29. Rossler, U., ed. (1999). *Landolt-Bornstein, New Series, Group III*. Vol. 17B, 22, 41B. Springer, Heidelberg.
30. Claus Franz Klingshirn; Bruno K. Meyer; Andreas Waag; Axel Hoffmann, Johannes M. M. Geurts (1 August 2010). *Zinc Oxide: From Fundamental Properties Towards Novel Applications*. Springer. pp. 9–10. ISBN 978-3-642-10576-0. Retrieved 9 December 2011.
31. Composition of the Continental Crust: *R. L. Rudnick University of Maryland, College Park, MD, USA And S. Gao: China University of Geosciences, Wuhan, People's Republic of China and Northwest University, Xi'an, People's Republic of China.*
32. Emsley, John (2011). *Nature's Building Blocks*.

CHAPTER-2

INSTRUMENTATION

Abstract:-

In this chapter various instruments that were used for characterization are discussed briefly. The basic working principle and instrument specifications were described. The various characterization techniques which were used i.e. XRD, PL spectroscopy, SEM, TEM, AFM.

2.1 X-ray Powder Diffraction (XRD):-

What is X-ray Powder Diffraction (XRD)

X-ray powder diffraction (XRD) is a rapid analytical technique primarily used for phase identification of a crystalline material and can provide information on unit cell dimensions. The analyzed material is finely ground, homogenized, and average bulk composition is determined.

Fundamental Principles of X-ray Powder Diffraction (XRD)

Max von Laue, in 1912, discovered that crystalline substances act as three-dimensional diffraction gratings for X-ray wavelengths similar to the spacing of planes in a crystal lattice. X-ray diffraction is now a common technique for the study of crystal structures and atomic spacing. X-ray diffraction is based on constructive interference of monochromatic X-rays and a crystalline sample. These X-rays are generated by a cathode ray tube, filtered to produce monochromatic radiation, collimated to concentrate, and directed toward the sample. The interaction of the incident rays with the sample produces constructive interference (and a diffracted ray) when conditions satisfy Bragg's Law ($n\lambda=2d \sin \theta$). This law relates the wavelength of electromagnetic radiation to the diffraction angle and the lattice spacing in a crystalline sample. These diffracted X-rays are then detected, processed and counted.

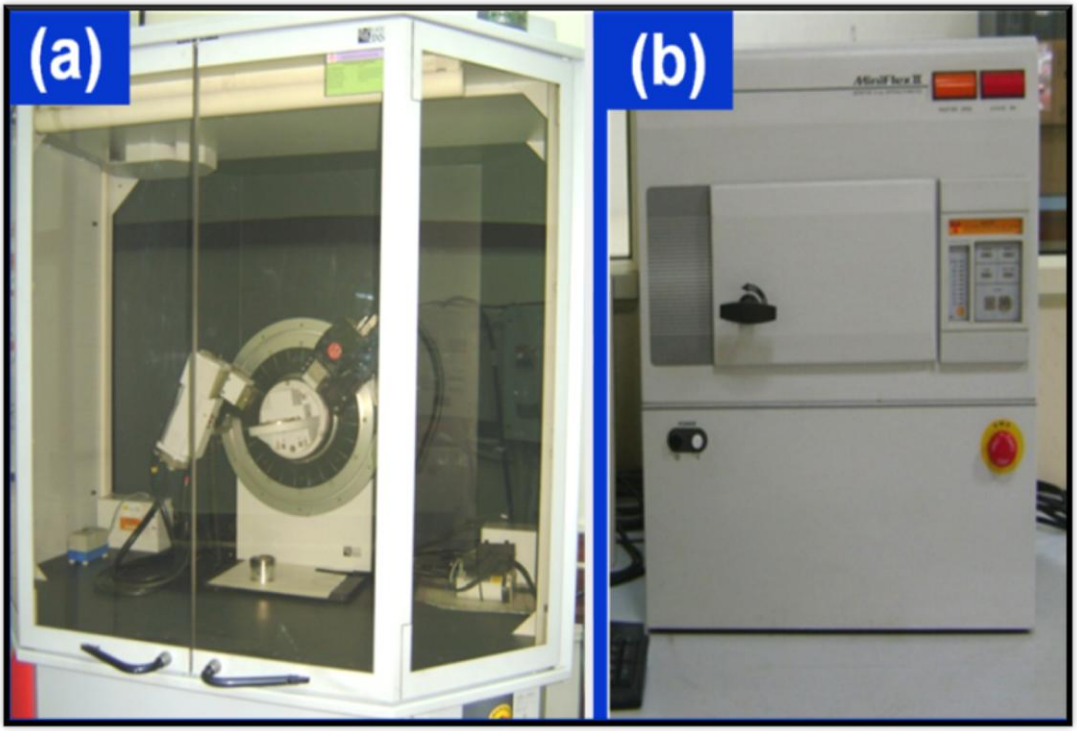

Fig.2.1: Actual photograph of X-Ray Diffractometer

By scanning the sample through a range of 2θangles, all possible diffraction directions of the lattice should be attained due to the random orientation of the powdered material. Conversion of the diffraction peaks to d-spacing allows identification of the mineral because each mineral has a set of unique d-spacing. Typically, this is achieved by comparison of d-spacing with standard reference patterns. All diffraction methods are based on generation of X-rays in an X-ray tube. These X-rays are directed at the sample, and the diffracted rays are collected. A key component of all diffraction is the angle between the incident and diffracted rays. Powder and single crystal diffraction vary in instrumentation beyond this.

X-ray Powder Diffraction (XRD) Instrumentation - How Does It Work?

X-ray diffractometer consist of three basic elements: an X-ray tube, a sample holder, and an X-ray detector. X-rays are generated in a cathode ray tube by heating a filament to produce electrons, accelerating the electrons toward a target by applying a voltage, and bombarding the target material with electrons. When electrons have sufficient energy to dislodge inner shell electrons of the target material, characteristic

X-ray spectra are produced. These spectra consist of several components, the most common being Kα and Kβ. Kα consists, in part, of Kα1 and Kα2. Kα1 has a slightly shorter wavelength and twice the intensity as Kα2. The specific wavelengths are characteristic of the target material (Cu, Fe, Mo, Cr). Filtering, by foils or crystal monochrometers, is required to produce monochromatic X-rays needed for diffraction. Kα1and Kα2 is sufficiently close in wavelength such that a weighted average of the two is used. Copper is the most common target material for single-crystal diffraction, with CuKα radiation = 1.5418Å. These X-rays are collimated and directed onto the sample. As the sample and detector are rotated, the intensity of the reflected X-rays is recorded. When the geometry of the incident X-rays impinging the sample satisfies the Bragg Equation, constructive interference occurs and a peak in intensity occurs. A detector records and processes this X-ray signal and converts the signal to a count rate which is then output to a device such as a printer or computer monitor. The geometry of an X-ray diffractometer is such that the sample rotates in the path of the collimated X-ray beam at an angle θ while the X-ray detector is mounted on an arm to collect the diffracted X-rays and rotates at an angle of 2θ. The instrument used to maintain the angle and rotate the sample is termed a goniometer. For typical powder patterns, data is collected at 2θfrom ~5° to 70°, angles that are preset in the X-ray scan.

Applications:-

X-ray powder diffraction is most widely used for the identification of unknown crystalline materials (e.g. minerals, inorganic compounds). Determination of unknown solids is critical to studies in geology, environmental science, material science, engineering and biology.

Other applications include:

- Characterization of crystalline materials
- Identification of fine-grained minerals such as clays and mixed layer clays, that are difficult to determine optically
- Determination of unit cell dimensions
- Measurement of sample purity

With specialized techniques, XRD can be used to:

- determine crystal structures using Rietveld refinement
- determine of modal amounts of minerals (quantitative analysis)
- Characterize thin films samples by:
  - Determining lattice mismatch between film and substrate and to inferring stress and strain
  - Determining dislocation density and quality of the film by rocking curve measurements
  - Measuring superlattices in multilayered epitaxial structures
  - Determining the thickness, roughness and density of the film using glancing incidence X-ray reflectivity measurements
- Make textural measurements, such as the orientation of grains, in a polycrystalline sample.

Strengths and Limitations of X-ray Powder Diffraction (XRD)

Strengths:-

- Powerful and rapid (< 20 min) technique for identification of an unknown mineral
- In most cases, it provides an unambiguous mineral determination
- Minimal sample preparation is required
- XRD units are widely available
- Data interpretation is relatively straight forward

Limitations:-

- Homogeneous and single phase material is best for identification of an unknown
- Must have access to a standard reference file of inorganic compounds (d-spacing, hkl)
- Requires tenths of a gram of material which must be ground into a powder
- For mixed materials, detection limit is ~ 2% of sample
- For unit cell determinations, indexing of patterns for non-isometric crystal systems is complicated
- Peak overlay may occur and worsens for high angle 'reflections'

2.2 Scanning Electron Microscopy (SEM):-

What is Scanning Electron Microscopy (SEM)

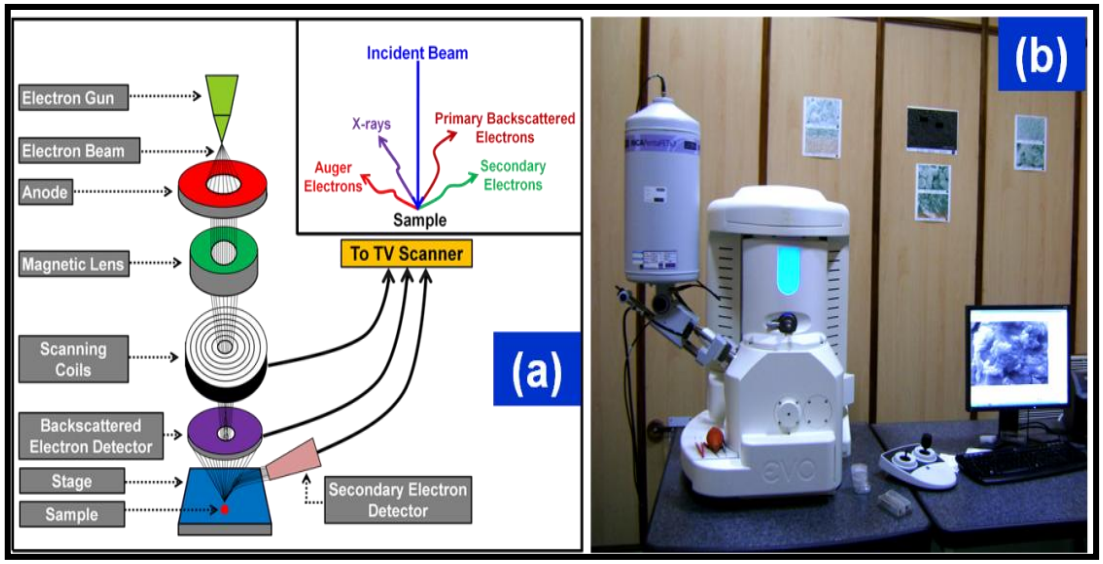

Fig 2.2: Schematic Diagram of SEM & its Image

A typical SEM instrument, showing the electron column, sample chamber, EDS detector, electronics console, and visual display monitors.

The scanning electron microscope (SEM) uses a focused beam of high-energy electrons to generate a variety of signals at the surface of solid specimens. The signals that derive from electron-sample interactions reveal information about the sample including external morphology (texture), chemical composition, and crystalline structure and orientation of materials making up the sample. In most applications, data are collected over a selected area of the surface of the sample, and a 2-dimensional image is generated that displays spatial variations in these properties. Areas ranging from approximately 1 cm to 5 microns in width can be imaged in a scanning mode using conventional SEM techniques (magnification ranging from 20X to approximately 30,000X, spatial resolution of 50 to 100 nm). The SEM is also capable of performing analyses of selected point locations on the sample; this approach is especially useful in qualitatively or semi-quantitatively determining chemical compositions (using EDS), crystalline structure, and crystal orientations (using EBSD). The design and function of

the SEM is very similar to the EPMA and considerable overlap in capabilities exists between the two instruments.

Fundamental Principles of Scanning Electron Microscopy (SEM):-

Accelerated electrons in an SEM carry significant amounts of kinetic energy, and this energy is dissipated as a variety of signals produced by electron-sample interactions when the incident electrons are decelerated in the solid sample. These signals include secondary electrons (that produce SEM images), backscattered electrons (BSE), diffracted backscattered electrons (EBSD that are used to determine crystal structures and orientations of minerals), photons (characteristic X-rays that are used for elemental analysis and continuum X-rays), visible light (cathodoluminescence--CL), and heat. Secondary electrons and backscattered electrons are commonly used for imaging samples: secondary electrons are most valuable for showing morphology and topography on samples and backscattered electrons are most valuable for illustrating contrasts in composition in multiphase samples (i.e. for rapid phase discrimination). X-ray generation is produced by inelastic collisions of the incident electrons with electrons in discrete orbital (shells) of atoms in the sample. As the excited electrons return to lower energy states, they yield X-rays that are of a fixed wavelength (that is related to the difference in energy levels of electrons in different shells for a given element). Thus, characteristic X-rays are produced for each element in a mineral that is "excited" by the electron beam. SEM analysis is considered to be "non-destructive"; that is, x-rays generated by electron interactions do not lead to volume loss of the sample, so it is possible to analyze the same materials repeatedly.[1][2]

Scanning Electron Microscopy (SEM) Instrumentation - How Does It Work?

Components of all SEMs include the following:

- Electron Source ("Gun")
- Electron Lenses
- Sample Stage
- Detectors for all signals of interest
- Display / Data output devices

Infrastructure Requirements:

- Power Supply
- Vacuum System
- Cooling system
- Vibration-free floor
- Room free of ambient magnetic and electric fields

SEMs always have at least one detector (usually a secondary electron detector), and most have additional detectors. The specific capabilities of a particular instrument are critically dependent on which detectors it accommodates.

Applications:-

The SEM is routinely used to generate high-resolution images of shapes of objects (SEI) and to show spatial variations in chemical compositions: 1) acquiring elemental maps or spot chemical analyses using EDS, 2) discrimination of phases based on mean atomic number (commonly related to relative density) using BSE, and 3) compositional maps based on differences in trace element "activators" (typically transition metal and Rare Earth elements) using CL. The SEM is also widely used to identify phases based on qualitative chemical analysis and/or crystalline structure. Precise measurement of very small features and objects down to 50 nm in size is also accomplished using the SEM. Backscattered electron images (BSE) can be used for rapid discrimination of phases in multiphase samples. SEMs equipped with diffracted backscattered electron detectors (EBSD) can be used to examine micro-fabric and crystallographic orientation in many materials.

2.3 Transmission electron microscopy (TEM):-

It is another electron microscopy used for analyzing morphology (shape, size arrangement of particles), crystallographic information (arrangement of atoms), compositional information, etc.

Working principle:-

As opposed to a light microscope, the wavelength of illumination that is produced by an energized beam of electrons in TEM increases greatly the resolving capabilities.

So, the main use of this technique is to examine the specimen structure, composition or properties in sub microscopic details so that this microscopy technique is significantly involved in numerous fields such as biological components, chemistry, materials science or electronics.

Using an electron microscope offers the advantage of increasing both the magnification of an object and the resolution over other imaging tools. Resolution is defined as the ability to distinguish two separate items from one another. In a light microscope, to magnify the image, the deflection of the illumination from its path is accomplished through the use of glass lenses where the properties are determined by its shape and index of refraction. So, as the light travels into the lens, refraction occurs when it is travelling through a medium with a different refractive index. The situation in a TEM differs as there is no change in the refractive index of the medium when the illumination beam is deflected; the vacuum in the lens is the same as the vacuum in the column. Deflection is in this case only due to the electromagnetic properties of the lens which are defined by electromagnetic plates that are only able to influence the path direction of the electrons, since all of the electrons carry a negative charge. Then, they have similar function to glass lenses in that they do produce a deviation in the trajectory of the electrons from a point source which causes them to converge at a single focal point. By this way, the electron beam is influenced in order to focus it precisely.

There are essentially three types of lenses used to form the final image in the TEM. These are the condenser, objective, and projector lenses. The mean function of the condenser lens is to concentrate and focus the beam of electrons coming off of the filament onto the sample to give a uniformly illuminated sample. The objective lens and its associated pole pieces is the heart of the TEM and the most critical of all the lenses. It forms the initial enlarged image of the illuminated portion of the specimen in a plane that is suitable for further enlargement by the projector lens.

Also, the TEM builds an image by way of differential contrast. Those electrons that pass through the sample go on to column form the image while those that are stopped or deflected by dense atoms in the specimen are subtracted from the image. In this way a black and white image is formed. Some electrons pass close to a heavy atom and are thus only slightly deflected. Thus many of these "scattered" electrons eventually make their way down the column and contribute to the image. In order to eliminate these

scattered electrons from the image we can place an aperture in the objective lens that will stop all those electrons that have deviated from the optical path. The smaller the aperture we use the more of these scattered electrons we will stop and the greater will be our image contrast.

Finally, one uses the projector lens to project the final magnified image onto the phosphor screen or photographic emulsion. It is in the projector lens that the majority of the magnification occurs. Thus total magnification is a product of the objective and projector magnifications. For higher magnifications an intermediate lens is often added between the objective and projector lenses. This lens serves to further magnify the image. The image is then projected onto either the fluorescent screen or onto the photographic film. Remember that the image is focused up at the objective lens. It is the focused image that is projected so the plane in which the final image appears is not critical and the image remains in focus regardless. What does change is the relative size of the projected image and thus the magnification on the screen and that on the photographic film will differ. Another important element of the TEM is the vacuum system. There are three main reasons why the microscope column must be operated under very high vacuum. The first of these is to avoid collisions between electrons of the beam and stray molecules. Such collisions can result in a spreading or diffusing of the beam or more seriously can result in volatilization event if the molecule is organic in nature. Such volatilizations can severely contaminate the microscope column especially in finely machined regions such as apertures and pole pieces that will serve to degrade the image. When examination of a specimen has to be performed, the extreme conditions that exist inside the TEM have to be considered, as for example high vacuum or intense heat generated by the beam of electrons. For a conventional TEM analysis, a specimen has to be reasonably dried and thin for ensuring electron transparency. In general, a sample has to follow certain conditions including a complete lack of water (as high vacuum conditions are used), an ability to remain stable when exposed to e-beam damage and the presence of both electron transparency and electron opacity zones. For that, specific specimen preparation steps are usually employed, including the use of fixatives, embedding resins and ultra-micro tomes for shaving off electron transparent slices of material. As part of this, it is important to try and keep the sample in as near a natural state as is possible.

Fig.2.3: Actual photograph of Transmission Electron Microscope.

2.4 Photoluminescence spectroscopy:-

What is photoluminescence?

Photoluminescence spectroscopy is a contactless, non-destructive method of probing the electronic structure of materials. Light is directed onto a sample, where it is absorbed and imparts excess energy into the material in a process called photo-excitation. One way this excess energy can be dissipated by the sample is through the emission of light, or luminescence. In the case of photo-excitation, this luminescence is called photoluminescence. Photo-excitation causes electrons within a material to move into permissible excited states. When these electrons return to their equilibrium states, the excess energy is released and may include the emission of light (a radiative process) or may not (a nonradiative process). The energy of the emitted light (photoluminescence) relates to the difference in energy levels between the two electron states involved in the transition between the excited state and the equilibrium state.

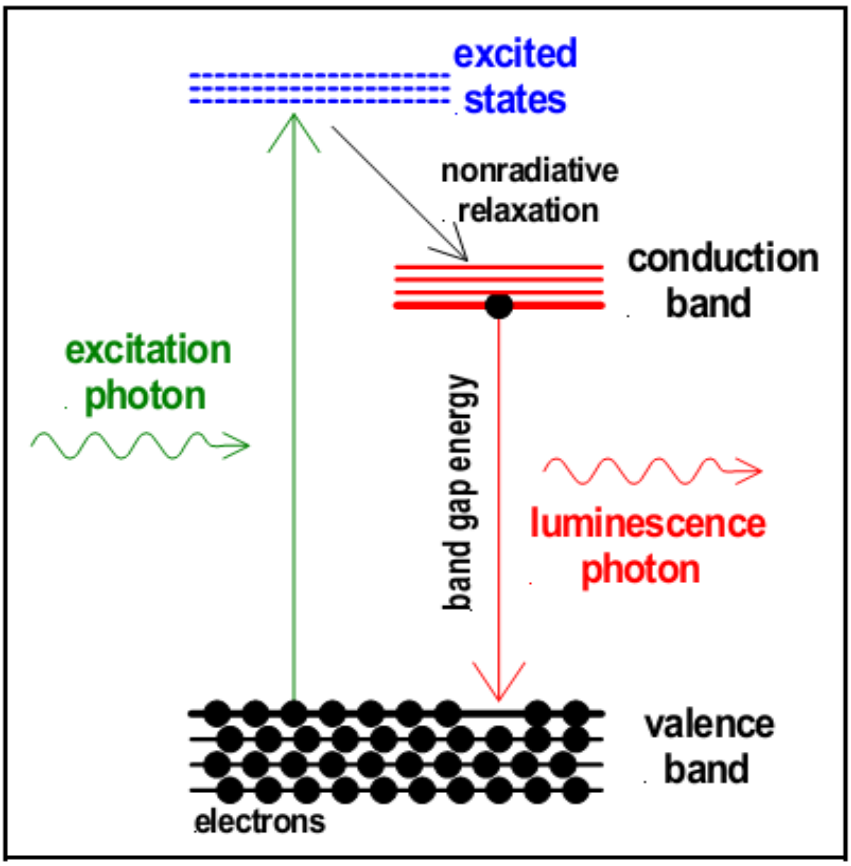

Fig 2.4: Relation between absorption and emission spectra

Fluorescence and phosphorescence come at lower energy than absorption (the excitation energy). As shown in Figure 2.4, in absorption, wavelength λ_0 corresponds to a transition from the ground vibrational level of S_0 to the lowest vibrational level of S1. After absorption, the vibrationally excited S_1 molecule relaxes back to the lowest vibrational level of S1 prior to emitting any radiation. The highest energy transition comes at wavelength λ_0, with a series of peaks following at longer wavelength. The absorption and emission spectra will have an approximate mirror image relation if the spacing's between vibrational levels are roughly equal and if the transition probabilities are similar. The λ_0 transitions in Figure 2.4 do not exactly overlap. As shown in Figure 2.6, a molecule absorbing radiation is initially in its electronic ground state, S0. This molecule possesses a certain geometry and solvation. As the electronic transition is faster than the vibrational motion of atoms or the translational motion of solvent molecules, when radiation is first absorbed, the excited S1 molecule still possesses its S_0 geometry and solvation. Shortly after excitation, the geometry and solvation change to their most favourable values for S_1 state. This rearrangement lowers the energy of

excited molecule. When an S_1 molecule fluoresces, it returns to the S_0 state with S_1 geometry and solvation. This unstable configuration must have a higher energy than that of an S_0 molecule with S_0 geometry and solvation. Net effect in Fig 2.6 is that the λ_0 emission energy is less than the λ_0 excitation energy.

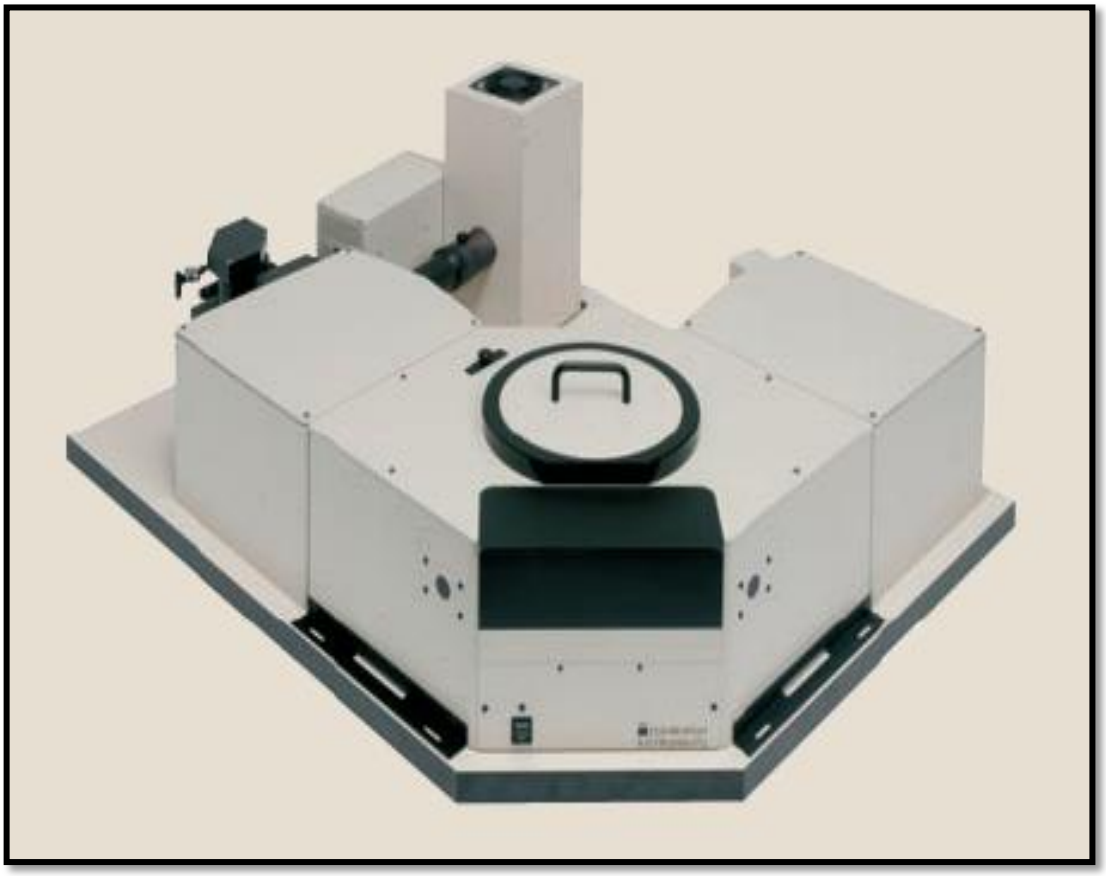

Fig.2.5:Combined steady state fluorescence and phosphorescence life time spectrometer (Edinburgh Instruments)

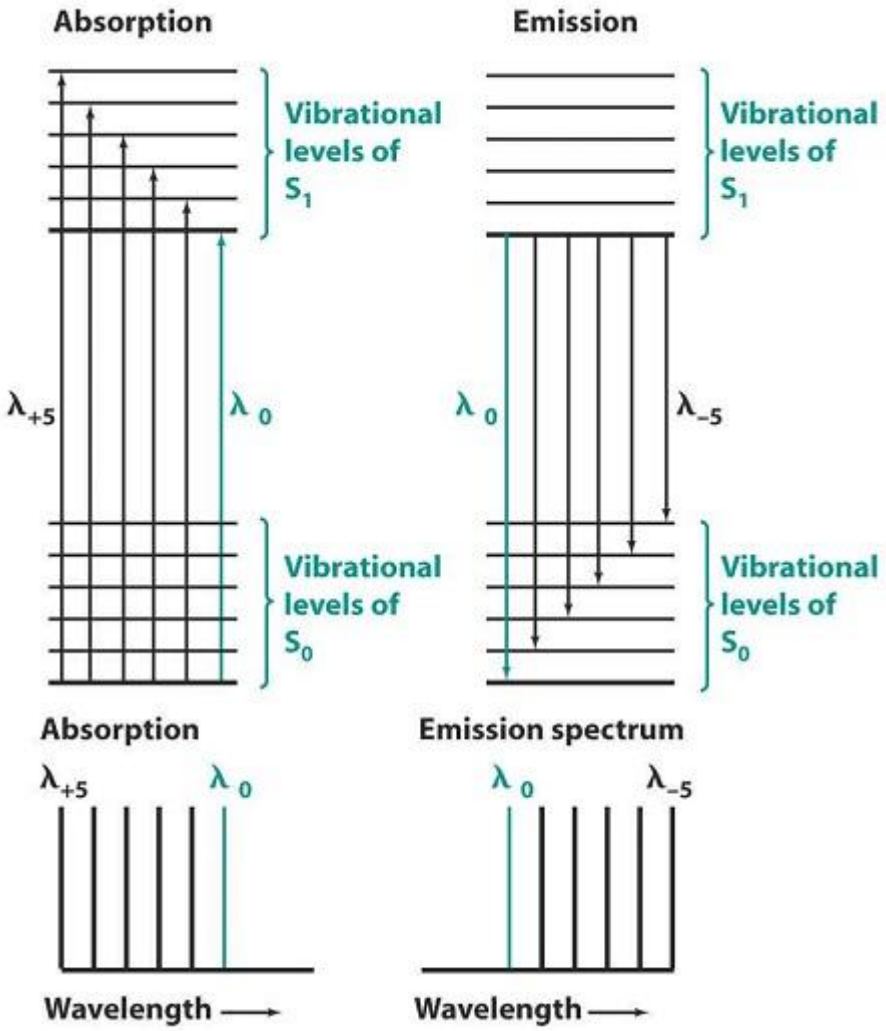

Fig 2.6: Energy-level diagram showing why structure is seen in the absorption and emission spectra and why the spectra are roughly mirror images of each other. Adapted from D. C. Harris, Quantitative Chemical Analysis, 7th Ed, W. H. Freeman and Company, New York (2006).

Instrumentation

A schematic of the excitation and emission process in photoluminescence experiment is shown schematically in Figure 2.6. A particular excitation wavelength from a white light source (e.g., Xe lamp) is selected by the grating in the excitation monochromator and falls on the sample which emits a spectrum of wavelengths which is scanned by a second monochromator, usually positioned at 90° to the incident light to minimize the intensity of scattered light reaching the detector. If the excitation wavelength is fixed and the emitted radiation is scanned, an emission spectrum is produced. When the

emission wavelength is fixed and excitation wavelength is scanned in a particular range, an excitation spectra is obtained.[3][4]

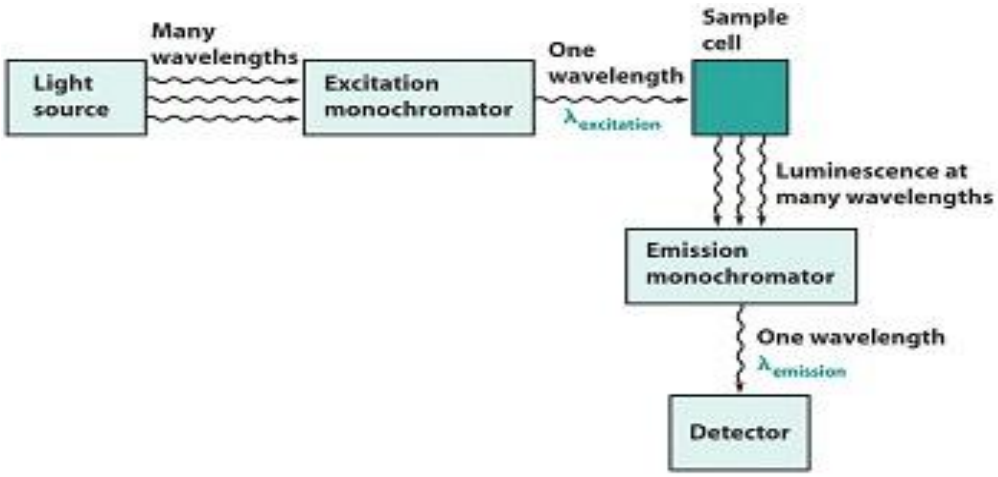

Fig 2.7: Essentials of a luminescence experiment. The sample is irradiated at one wavelength and emission is observed over a range of wavelengths. The excitation monochromator selects the excitation wavelength and the emission monochromator selects one wavelength at a time to observe.[Adapted from D. C. Harris, Quantitative Chemical Analysis, 7th Edition, W. H. Freeman and Company, New York, (2006)].

Applications:-

Apart from the detection of light emission patterns, photoluminescence spectroscopy is of great significance in other fields of analysis, especially semiconductors.

Band gap determination

Band gap is the energy difference between states in the conduction and valence bands, of the radioactive transition in semiconductors. The spectral distribution of PL from a semiconductor can be analyzed to non-destructively determine the electronic band gap. This provides a means to quantify the elemental composition of compound semiconductor and is vitally important material parameter influencing solar cell device efficiency.

Impurity levels and defect detection

Radiative transitions in semiconductors involve localized defect levels. The photoluminescence energy associated with these levels can be used to identify specific defects, and the amount of photoluminescence can be used to determine their concentration. The PL spectrum at low sample temperatures often reveals spectral peaks associated with impurities contained within the host material. Fourier transform photoluminescence micro spectroscopy, which is of high sensitivity, provides the potential to identify extremely low concentrations of intentional and unintentional impurities that can strongly affect material quality and device performance.

Recombination mechanisms

The return to equilibrium, known as "recombination", can involve both radiative and nonradiative processes. The quantity of PL emitted from a material is directly related to the relative amount of radiative and nonradiative recombination rates. Nonradiative rates are typically associated with impurities and the amount of photoluminescence and its dependence on the level of photo-excitation and temperature are directly related to the dominant recombination process. Thus, analysis of photoluminescence can qualitatively monitor changes in material quality as a function of growth and processing conditions and help understand the underlying physics of the recombination mechanism.

2.5 Time resolved spectroscopy

Luminescence decay time of the prepared nanophosphor were measured using *Edinburg Instrument model FLSP920 time resolved spectrometer* with micro second pulsed light sources (Xe flash lamp).

Principle:-

Time resolved spectroscopy is an important tool for studying energy and charge transfer processes, coupling of electronic and vibrational degree of freedom, vibrational and conformation relaxation, isomerization etc. The decay characterization of phosphors could suggest the process of excitation and return to ground state and their time scale. It employs excitation by very short pulses of radiation like flash lamps, laser, etc, which

can be spectrally tuned to the electronics transition of the material. Our fluorescence lifetime spectrometer is based on the Time Correlated Single Photon Counting Technique (TCSPC).

Instrument detail

TCSPC technique is the detection of single photon and the measurement of their arrival times in reference single, usually the light source. Fig 2.5 shows the photograph of *Edinburg Instrument model FLSP920* combined steady state fluorescence and phosphorescence life time spectrometer.

2.6 References:

1. Y. Hong, J. W. Y. Lam, and B. Z. Tang, Chem. Commun., 2009, 4332.
2. M. Anpo, M. Kondo, S. Coluccia, C. Louis, and M. Che, J. Am. Chem. Soc., 1989, 111, 8791.
3. N. S. Sariciftci, Primary Photoexcitations In Conjugated Polymers Molecular Exciton Versus Semiconductor Band Model, World Scientific Publishing Company.
4. D. C. Harris, Quantitative Chemical Analysis, 7th Ed, W. H. Freeman and Company, New York (2006).G. Davies, Phys. Rep., 1989, 176, 83.

CHAPTER-3

EXPERIMENTAL DETAILS

Synthesis Methods:

Two different techniques have been used in the present study to synthesize phosphor in bulk/nano form

- Solid state reaction (SSR)
- Co-precipitation method (CPP)

I. Solid state reaction (SSR)

SSR is a solvent less reaction method. It is most widely used for preparation of crystalline solid form a mixture of solid starting materials. Solids do not react together at room temperature over normal time scale and it is necessary to heat them to much higher temperatures, often to 800^0C to 1500^0C in order for the reaction to occur at an appreciable rate. The factors on which the feasibility and rate of a solid state reaction depend include, reaction conditions, structural properties of the reactants, surface area of the solids, their reactivity and the thermodynamic free energy change associated with the reaction.

II. Co-precipitation method (CPP)

Co-precipitation is a process in which a solid is precipitated from a solution containing other ions. These ions are incorporated into the solid by adsorption on the surface of the growing particles, physical entrapment in the pore spaces, or substitution in the crystal lattice. Adsorption is one of the principle mechanisms of co-precipitation. It is a process in which the solid species, or adsorbent, is added to a solution containing other ions, called adsorbents. In this case, the adsorbents are bound to the solid's surface by physical or chemical interactions between one adsorbate and the adsorbent.

CPP technique is often used for the synthesizing nanoparticles from solution. CPP technique used to prepare nano-sized powder usually with high sinterability and improved chemically homogeneity. There are many advantage of CPP; simple and rapid

preparation at room temperature, easy to control of particle size, easy to precipitate to get the powder, large quantity of final product compare to other chemical process.

3.1 Synthesis of ZnO Nanoparticles:

- **Precursors used:-**

  Zinc Acetate

  Molecular formula: - $Zn[(CH)_3(COOH)]_2.2H_2O$

  Company used: - Loba Chemie

  Percentage Purity: - 99.5%

  Melting Point: - 1975°C

- **Calculations:**

  Preparation of zinc acetate solution

  Mol. Weight of Zinc acetate =219.49 gm

  219.49 gm in 1000cc of water=1M

  We needed 0.027M

  219.49×0.027M in 1000cc of water=0.027M

  5.9262gm in 1000cc of water=0.027M

  5.9262÷10=0.59262 gm

  0.59262 gm in 100cc of water=0.027M

1. Co Precipitation method

- 0.59262 gm of zinc Acetate was dissolved in 100cc of distilled water (0.027M).
- 100cc of the prepared solution of zinc acetate solution is then mixed under magnetic stirring.

- Double diluted ammonia is prepared
  - 25cc of ammonia is mixed with D.I. water making up to 250cc-single diluted ammonia.
  - 25cc of single diluted ammonia is mixed in D.I. water making up to 250cc-double diluted ammonia.
- pH of Zinc acetate solution was neutral
- Double diluted ammonia is then added to 100cc of zinc acetate solution for making the above solution of pH 10 and the solution was kept for 1 hour.
- After 1 hour, pH was checked (it was 10pH)
- Solution was kept in preheated oven at 90°c for 24 hours.
- Upper solution was decanted; ethanol was added and ultrasonicated.
- This process was repeated 3-4 times
- The resulting material was then kept in oven.
- The powder material is then transferred in Petridis.

2. Solid State Reaction Method:

Stoichiometric molar compositions of host and dopant materials were taken according to the formula:

ZnO

Molecular weight = 219.49 g/mol

(Precursor amount can be reduced by dividing all the quantity by same constant i.e. 25 is used here)

Above mentioned chemical was taken according to Stoichiometric and mixed thoroughly in pestle-mortar and then packed in highly pure Quartz boat. The material was fired at 800^{o}C for 2 hours in air atmosphere. The thermal processing parameters such as heating rate were 5^{o}C min^{-1} till 800^{0}C. The total time taken to reach the desired temperature varied between 2-3 hrs. Time of constant temperature was fixed at 2 hrs and then the sintered material is allowed to cool naturally. Slow cooling rate is maintained to allow uniform temperature distribution throughout the reacting mixture,

which enables better luminescence intensity in the product. Finally a white sintered piece is obtained after cooling which is made into powder form by grinding.

3.2 Synthesis of ZnO doped with Er (2%) Nanoparticles:

- **Precursors used:-**

Host material

Zinc Acetate

Dopant

Erbium Oxide

Molecular formula: - Er_2O_3

Company used: - Aldrich

Percentage Purity: - 99.9

Melting Point: - 2344°C

- **Calculations**

a) Preparation of zinc acetate solution

Same as section 3.1.

b) Preparation of Erbium Oxide solution

Mol. Weight of Erbium oxide =353.27 gm

353.27 gm in 1000cc of water=1M

We needed 0.027M

353.27×0.027M in 1000cc of water=0.027M

10.32129gm in 1000cc of water=0.027M

10.32129÷(100×2)=0.05015 gm

0.05015 gm in 10cc of water=0.027M

This solution was dissolved in minimum amount of HNO_3, the solution turns transparent after dissolve. Continuous stirring and heating is done by using a hot plate & magnetic stirrer.

1. Co Precipitation method

- 0.59262 gm of zinc Acetate was dissolved in 100cc of distilled water (0.027M).
- 100cc of the prepared solution of zinc acetate solution is then mixed under magnetic stirring.
- Double diluted ammonia is prepared
    - 25cc of ammonia is mixed with D.I. water making up to 250cc-single diluted ammonia.
    - 25cc of single diluted ammonia is mixed in D.I. water making up to 250cc-double diluted ammonia.
- pH of Zinc acetate solution was neutral
- 2% of Er was added to 98% Zinc acetate solution.
- Double diluted ammonia is then added to 100cc of (zinc acetate + Er) solution for making the above solution of pH 10 and the solution was kept for 1 hour.
- After 1 hour, pH was checked (it was 10pH)
- Solution was kept in preheated oven at 90°c for 24 hours.
- Upper solution was decanted; ethanol was added and ultrasonicated.
- This process was repeated 3-4 times
- The resulting material was then kept in oven.
- The powder material is then transferred in Petridis.

2. Solid State Reaction Method:

Stoichiometric molar compositions of host and dopant materials were taken according to the formula:

ZnO

Molecular weight = 219.49 g/mol

0.98 mol of ZnO = 0.98×219.49 g/mol = 215.1002 gm

Er_2O_3

Molecular weight = 382.517 g/mol

0.02 mol of Er = 382.517×0.02÷2 g/mol = 3.82517 gm

(Precursor amount can be reduced by dividing all the quantity by same constant i.e. 25 is used here)

All the above mentioned chemicals were taken according to Stoichiometric and mixed thoroughly in pestle-mortar and then packed in highly pure Quartz boat. The material was fired at 800^{o}C for 2 hours in air atmosphere. The thermal processing parameters such as heating rate were 5^{o}C min^{-1} till 800^{0}C. The total time taken to reach the desired temperature varied between 2-3 hrs. Time of constant temperature was fixed at 2 hrs and then the sintered material is allowed to cool naturally. Slow cooling rate is maintained to allow uniform temperature distribution throughout the reacting mixture, which enables better luminescence intensity in the product. Finally a white sintered piece is obtained after cooling which is made into powder form by grinding.

3.3 Synthesis of ZnO doped with Er (2%) and Yb(10%) Nanoparticles:

- **Precursors used:-**

Host material

Zinc Acetate

Dopant

Erbium Oxide

Ytterbium oxide

Molecular formula: - Yb_2O_3

Company used: - Aldrich

Percentage Purity: - 99.9

- **Calculations**

a) Preparation of zinc acetate solution

Same as section 3.1.

b) Preparation of Erbium Oxide solution

Same as section 3.2.

c) Preparation of Ytterbium Oxide solution

Mol. Weight of Ytterbium oxide =394.077 gm

394.077 gm in 1000cc of water=1M

We needed 0.027M

394.077 ×0.027M in 1000cc of water=0.027M

10.64008gm in 1000cc of water=0.027M

10.64008÷ (100×2) =0.053200gm

0.053200 gm in 10cc of water=0.027M

This solution was dissolved in minimum amount of HNO_3, the solution turns transparent after dissolve. Continuous stirring and heating is done by using a hot plate & magnetic stirrer.

1. Co Precipitation method

- 0.59262 of zinc Acetate was dissolved in 100cc of distilled water (0.027M).
- 100cc of the prepared solution of zinc acetate solution is then mixed under magnetic stirring.
- Double diluted ammonia is prepared
  - 25cc of ammonia is mixed with D.I. water making upto 250cc-single diluted ammonia.
  - 25cc of single diluted ammonia is mixed in D.I. water making upto 250cc-double diluted ammonia.
- pH of Zinc acetate solution was neutral

- 2% of Er and 10% of Yb were added to 88% Zinc acetate solution.
- Double diluted ammonia is then added to 100cc of (zinc acetate + Er + Yb) solution for making the above solution of pH 10 and the solution was kept for 1 hour.
- After 1 hour, pH was checked (it was 10pH)
- Solution was kept in preheated oven at 90°c for 24 hours.
- Upper solution was decanted; ethanol was added and ultrasonicated.
- This process was repeated 3-4 times
- The resulting material was then kept in oven.
- The powder material is then transferred in Petridis.

2. Solid State Reaction Method:

Stoichiometric molar compositions of host and dopant materials were taken according to the formula:

ZnO

Molecular weight = 219.49 g/mol

0.88 mol of ZnO = 0.88×219.49 g/mol = 193.1512 gm

Er_2O_3

Molecular weight = 382.517 g/mol

0.02 mol of Er = 382.517×0.02÷2 g/mol = 3.82517 gm

Yb_2O_3

Molecular weight = 394.077 g/mol

0.10 mol of Yb = 394.077×0.10÷2 g/mol = 19.70385 gm

(Precursor amount can be reduced by dividing all the quantity by same constant i.e. 50 is used here)

All the above mentioned chemicals were taken according to Stoichiometric and mixed thoroughly in pestle-mortar and then packed in highly pure Quartz boat. The material was fired at 800^{o}C for 2 hours in air atmosphere. The thermal processing parameters such as heating rate were 5^{o}C min^{-1} till 800^{0}C. The total time taken to reach the desired temperature varied between 2-3 hrs. Time of constant temperature was fixed at 2 hrs and then the sintered material is allowed to cool naturally. Slow cooling rate is maintained to allow uniform temperature distribution throughout the reacting mixture, which enables better luminescence intensity in the product. Finally a white sintered piece is obtained after cooling which is made into powder form by grinding.

3.4 Synthesis of ZnO doped with Ho(2%) Nanoparticles:

- **Precursors used:-**

Host material

Zinc Acetate

Dopant

Holmium oxide

Molecular formula: - Ho_2O_3

Company used: - Aldrich

Percentage Purity: - 99.99

Melting Point: - 2415°C

- **Calculations**

a) Preparation of zinc acetate solution

Same as section 3.1.

b) Preparation of Holmium Oxide solution

Mol. Weight of holmium oxide =377.85 gm

377.85 gm in 1000cc of water=1M

We needed 0.027M

377.85×0.027M in 1000cc of water=0.027M

10.20195gm in 1000cc of water=0.027M

10.20195÷ (100×2) =0.05100975 gm

0.05100975 gm in 10cc of water=0.027M

This solution was dissolved in minimum amount of HNO_3, the solution turns transparent after dissolve. Continuous stirring and heating is done by using a hot plate & magnetic stirrer.

1. Co Precipitation method

- 0.59262 of zinc Acetate was dissolved in 100cc of distilled water (0.027M).
- 100cc of the prepared solution of zinc acetate solution is then mixed under magnetic stirring.
- Double diluted ammonia is prepared
  - 25cc of ammonia is mixed with D.I. water making up to 250cc-single diluted ammonia.
  - 25cc of single diluted ammonia is mixed in D.I. water making up to 250cc-double diluted ammonia.
- pH of Zinc acetate solution was neutral
- 2% of Ho was added to 98% Zinc acetate solution.
- Double diluted ammonia is then added to 100cc of (zinc acetate + Ho) solution for making the above solution of pH 10 and the solution was kept for 1 hour.
- After 1 hour, pH was checked (it was 10pH)
- Solution was kept in preheated oven at 90°c for 24 hours.
- Upper solution was decanted; ethanol was added and ultrasonicated.
- This process was repeated 3-4 times
- The resulting material was then kept in oven.
- The powder material is then transferred in Petridis.

2. Solid State Reaction Method:

Stoichiometric molar compositions of host and dopant materials were taken according to the formula:

ZnO

Molecular weight = 219.49 g/mol

0.98 mol of ZnO = 0.98×219.49 g/mol = 215.1002 gm

Ho_2O_3

Molecular weight = 377.85 g/mol

0.02 mol of Ho = 377.85×0.02÷2 g/mol = 3.7785 gm

(Precursor amount can be reduced by dividing all the quantity by same constant i.e. 25 is used here)

All the above mentioned chemicals were taken according to Stoichiometric and mixed thoroughly in pestle-mortar and then packed in highly pure Quartz boat. The material was fired at 800^oC for 2 hours in air atmosphere. The thermal processing parameters such as heating rate were $5^oC\ min^{-1}$ till 800^0C. The total time taken to reach the desired temperature varied between 2-3 hrs. Time of constant temperature was fixed at 2 hrs and then the sintered material is allowed to cool naturally. Slow cooling rate is maintained to allow uniform temperature distribution throughout the reacting mixture, which enables better luminescence intensity in the product. Finally a white sintered piece is obtained after cooling which is made into powder form by grinding.

3.5 Synthesis of ZnO doped with Ho (2%) Yb(10%) Nanoparticles:

- **Precursors used:-**

Host material

Zinc Acetate

Dopant

Holmium oxide

Ytterbium oxide

1. Solid State Reaction Method:

Stoichiometric molar compositions of host and dopant materials were taken according to the formula:

ZnO

Molecular weight = 219.49 g/mol

0.88 mol of ZnO = 0.88×219.49 g/mol = 193.1512 gm

Ho_2O_3

Molecular weight = 377.85 g/mol

0.02 mol of Ho = 377.85×0.02÷2 g/mol = 3.7785 gm

Yb_2O_3

Molecular weight = 394.077 g/mol

0.10 mol of Yb = 394.077×0.10÷2 g/mol = 19.70385 gm

(Precursor amount can be reduced by dividing all the quantity by same constant i.e. 25 is used here)

All the above mentioned chemicals were taken according to Stoichiometric and mixed thoroughly in pestle-mortar and then packed in highly pure Quartz boat. The material was fired at 800^{o}C for 2 hours in air atmosphere. The thermal processing parameters such as heating rate were 5^{o}C min^{-1} till 800^{0}C. The total time taken to reach the desired temperature varied between 2-3 hrs. Time of constant temperature was fixed at 2 hrs and then the sintered material is allowed to cool naturally. Slow cooling rate is maintained to allow uniform temperature distribution throughout the reacting mixture, which enables better luminescence intensity in the product. Finally a white sintered piece is obtained after cooling which is made into powder form by grinding.

3.6 Synthesis of ZnO doped with Li (2%) Er(2%) Nanoparticles:

- **Precursors used:-**

Host material

Zinc Acetate

Dopant

Holmium oxide

Ytterbium oxide

Solid State Reaction Method:

Stoichiometric molar compositions of host and dopant materials were taken according to the formula:

ZnO

Molecular weight = 219.49 g/mol

0.96 mol of ZnO = 0.96×219.49 g/mol = 210.7104 gm

Er_2O_3

Molecular weight = 382.517 g/mol

0.02 mol of Er = 382.517×0.02÷2 g/mol = 3.82517 gm

$LiOH.2H_2O$

Molecular weight = 41.96 g/mol

0.02 mol of Li = 41.96×0.02 g/mol = 0.8392 gm

(Precursor amount can be reduced by dividing all the quantity by same constant i.e. 50 is used here)

All the above mentioned chemicals were taken according to Stoichiometric and mixed thoroughly in pestle-mortar and then packed in highly pure Quartz boat. The material was fired at 500^oC for 1 hour in air atmosphere. The thermal processing parameters such as heating rate were $5^oC\ min^{-1}$ till 500^0C. The total time taken to reach the desired temperature varied between 1-2 hrs. Time of constant temperature was fixed at 1 hrs and then the sintered material is allowed to cool naturally. Slow cooling rate is maintained to allow uniform temperature distribution throughout the reacting mixture, which enables better luminescence intensity in the product. Finally a white sintered piece is obtained after cooling which is made into powder form by grinding.

CHAPTER 4

RESULT & DISCUSSION

This chapter describes the experimental results of all the synthesized undoped and rare earth doped ZnO samples.

4.1 Structural characterization by XRD

The X-ray powder diffraction (XRD) of the synthesized samples was examined on a Rigaku miniflex x-ray diffractometer using the principle of Bragg Brentano Geometry, with Cu-Kα radiation (1.54A°). Diffractograms were recorded in grazing incidence geometry. The diffraction angle 2θ was scanned in the range 20 to 80°. Figures show the intensities of x-ray at various deflection angles (2 θ) for all synthesized samples.

1) ZnO by CPP:

Powder XRD spectra of undoped ZnO synthesized by CPP is shown in Fig.4.1

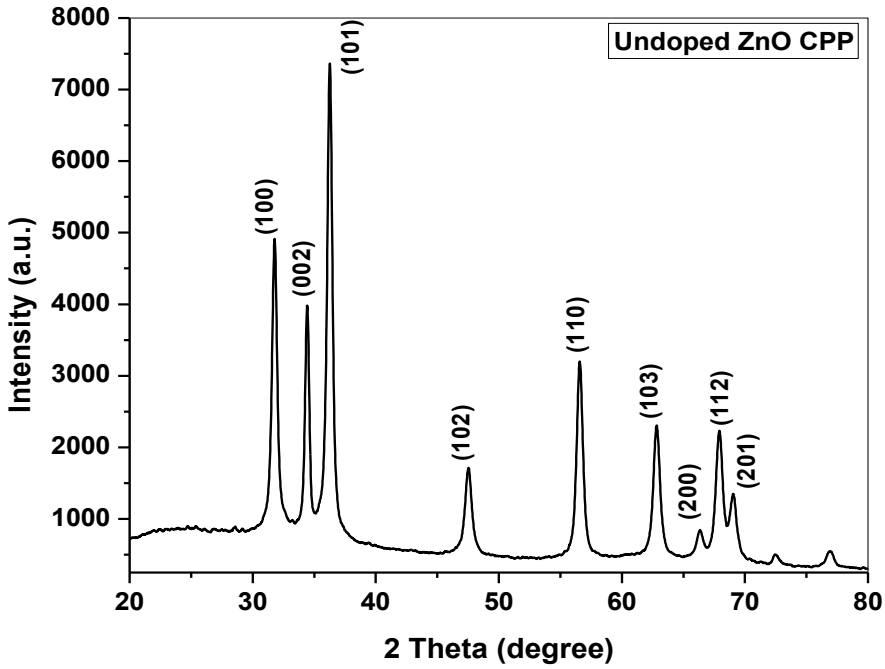

Fig. 4.1: XRD pattern of Undoped ZnO by CPP method at pH=10

The XRD pattern matches well to the hexagonal wurtzite phase of ZnO according to JCPDS card no. 36-1451. Table 4.1 give a comparison between the standard and observed values of phase for undoped ZnO preparing by co-precipitation (CPP) method.

Table 4.1: comparison between standard and observed values of phase for ZnO by CPP

Hkl	**2θ(std.)**	**2θ(observed)**	**hkl**	**2θ(std.)**	**2θ(observed)**
100	31.770	31.780	**103**	62.864	62.820
002	34.422	34.440	**200**	66.380	66.340
101	36.253	36.280	**112**	67.939	67.940
102	47.539	47.540	**201**	69.100	69.060
110	56.603	56.580			

2) ZnO:Er(2%) by CPP:

Powder XRD spectra of ZnO:Er(2%) synthesized by CPP is shown in Fig.4.2. The spectra showed crystalline phase of wurtzite ZnO according to JCPDS card no 36-1451, in addition a small peak at 21.82 degree (2 theta) due to unreacted Er_2O_3. (JCPDS card no. 43-1007).

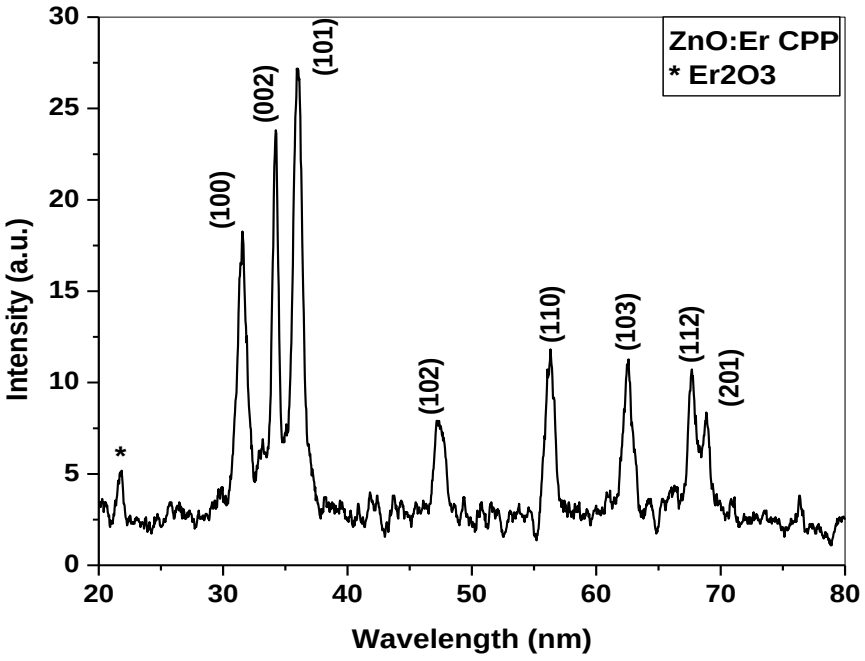

Fig. 4.2: XRD pattern of ZnO:Er(2%) by CPP method at pH=10

Table 4.2

Comparison between std. and observed values of phase for ZnO:Er(2%) by CPP

hkl	2θ(std.)	2θ(observed)	hkl	2θ(std.)	2θ(observed)
100	31.770	31.7681	**110**	56.603	56.3705
002	34.422	34.3536	**103**	62.864	62.6743
101	36.253	36.1261	**112**	67.939	67.8853
102	47.539	47.5211	**201**	69.100	68.9915

3) ZnO:Er(2%) annealed at 800°C by CPP:

ZnO:Er(2%) synthesized by CPP has poor Crystallinity and unreacted phase of the dopant precursor. To improve crystallinity, the sample was annealed at 800°C for 2 hours. The resulting XRD pattern as shown in Fig.4.3 that clearly exhibits much improved crystallinity and removal of dopant precursor phase suggesting better doping by the annealing process. All these phase are according to JCPDS card no. 36-1451.

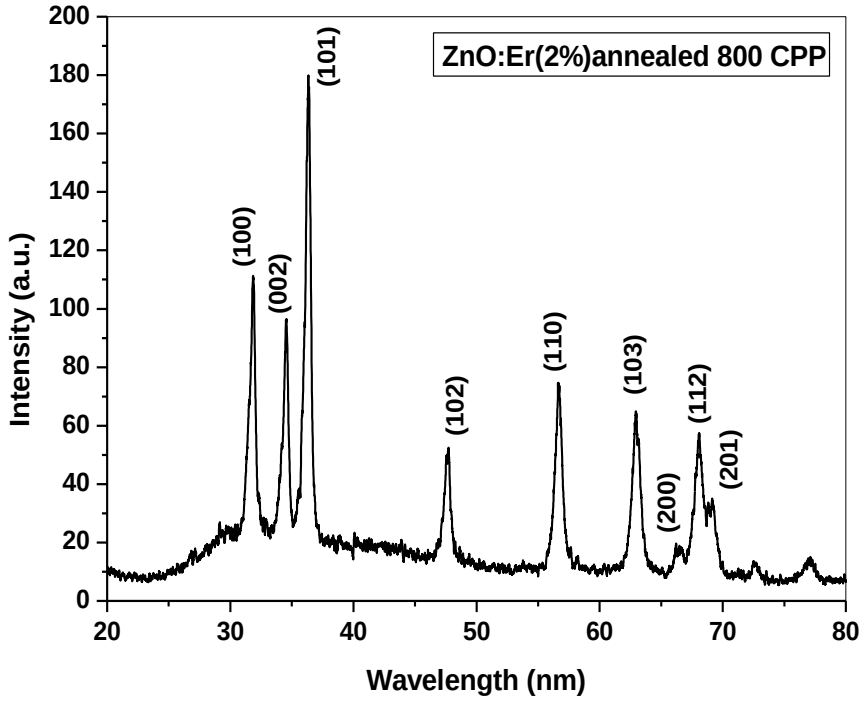

Fig. 4.3: XRD pattern of ZnO:Er(2%) annealed at 800°C by CPP method at pH=10

Table 4.3 gives a comparison between the standard and observed values of phase for undoped ZnO preparing by co-precipitation (CPP) method.

Table 4.3: Comparison of XRD peaks with standard values for ZnO:Er (2%) (CPP annealed at 800°C)

hkl	2θ(std.)	2θ(observed)	hkl	2θ(std.)	2θ(observed)
100	31.770	31.7843	**103**	62.864	62.7496
002	34.422	34.5173	**200**	66.380	66.3100
101	36.253	36.2473	**112**	67.939	67.9147
102	47.539	47.5804	**201**	69.100	68.9928
110	56.603	56.581			

4) ZnO:Ho(2%) by CPP:

XRD pattern of ZnO:Ho(2%) prepared by CPP method is shown in Fig.4.4. The phase conforms to JCPDS card no. 36-1451. Table 4.4 gives a comparison between the standard and observed values of phase for ZnO:Ho(2%) prepared by co-precipitation (CPP) method.

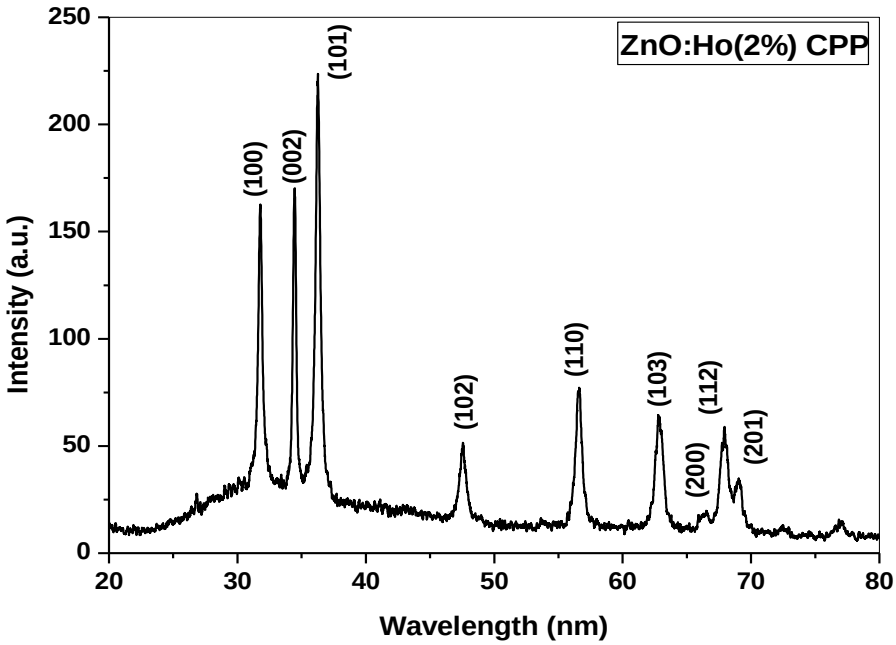

Fig. 4.4: XRD pattern of ZnO:Ho(2%) by CPP method at pH=10

Table 4.4: Comparison of XRD peaks with standard values for ZnO:Ho(2%) (CPP)

hkl	2θ(std.)	2θ(observed)	hkl	2θ(std.)	2θ(observed)
100	31.770	31.7843	**103**	62.864	62.7496
002	34.422	34.4170	**200**	66.380	66.5106
101	36.253	36.2473	**112**	67.939	67.8144
102	47.539	47.5801	**201**	69.100	68.9427
110	56.603	56.5816			

5) ZnO:Er(2%)Yb(10%) by CPP:

XRD pattern of ZnO:Er(2%)Yb(10%) prepared by CPP method is shown in Fig.4.5. The ZnO phase conforms to JCPDS card no 36-1451. In addition there are peaks corresponding to dopant precursors Er and Yb, indicating low solubility of rare earth dopants in ZnO when synthesized by room temperature CPP method (JCPDS card no. for Er_2O_3 card no. 43-1007 and for Yb_2O_3 card no. 65–3173.).

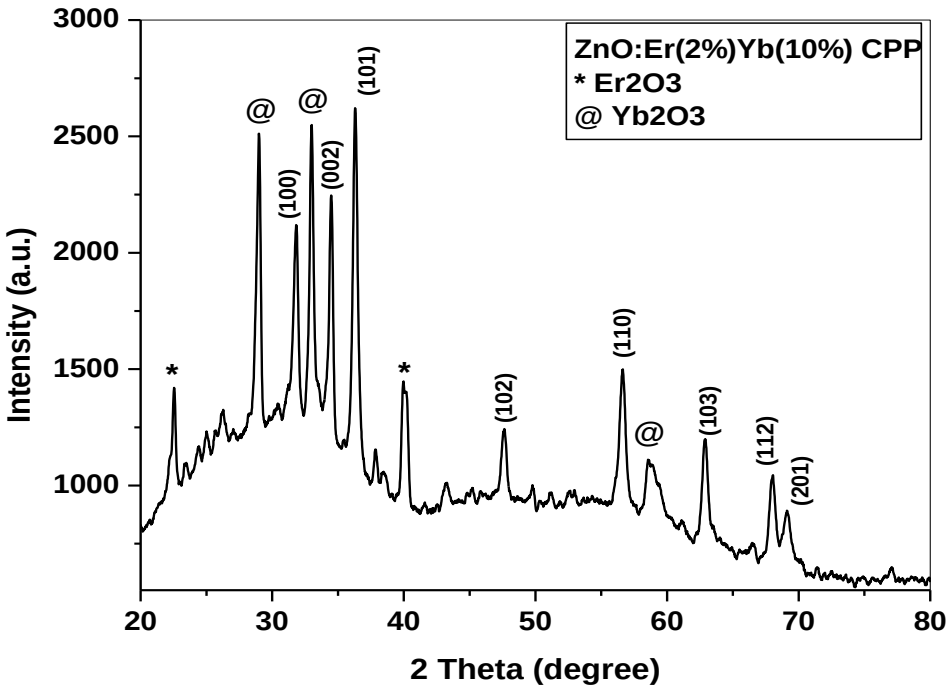

Fig. 4.5: XRD pattern of ZnO:Er(2%)Yb(10%) by CPP method at pH=10

6) ZnO:Er(2%)Yb(10%) annealed at 800°C by CPP:

To improve crystallinity the dopant incorporation, the ZnO:Er(2%)Yb(10%) powder sample prepared by CPP method was annealed at 800°C for 2 hrs. The XRD pattern of the annealed sample is shown in Fig. 4.6 which still shows peaks corresponding to dopant precursor phases. All these phase are according to JCPDS card No 36-1451 for ZnO and for Yb_2O_3 card No. 65–3173.

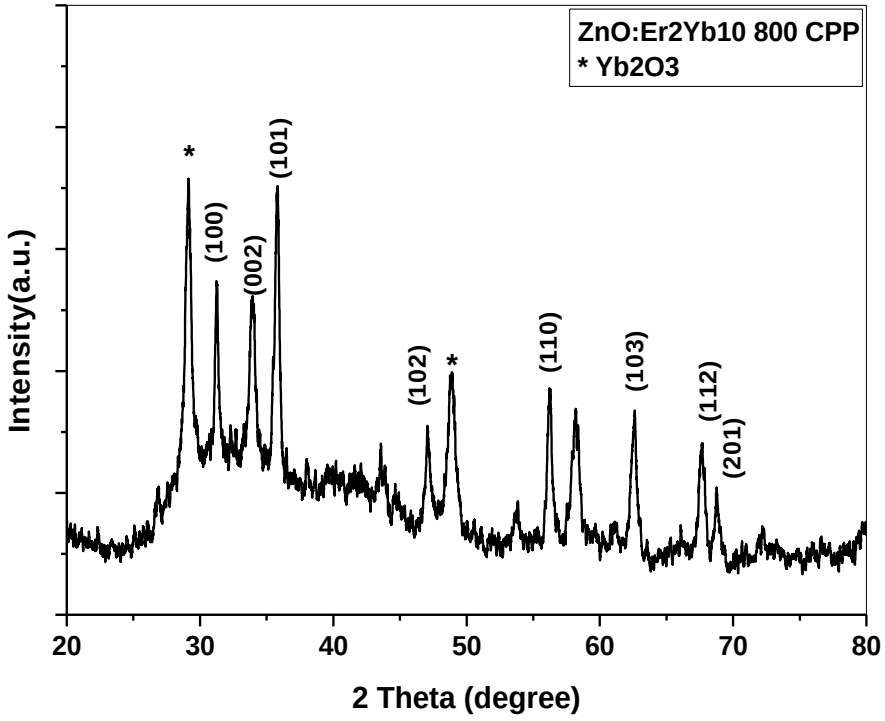

Fig. 4.6: XRD pattern of ZnO:Er(2%)Yb(10%)annealed at 800°C by CPP at pH=10

7) Undoped ZnO by SSR:

In order to ensure better doping of rare earth activator ions into ZnO lattice for achieving desired luminescence emission, solid state reaction route was employed. Undoped ZnO was synthesized by solid state reaction (as describe in 3.1.2) at 500°C. Powder XRD pattern is shown in Fig.4.7, which shows sharp peaks with high intensity indicating very well crystalline ZnO (JCPDS card No 36-1451).

Table 4.5 give a comparison between the standard and observed values of phase for Undoped ZnO preparing by solid state reaction (SRR) method.

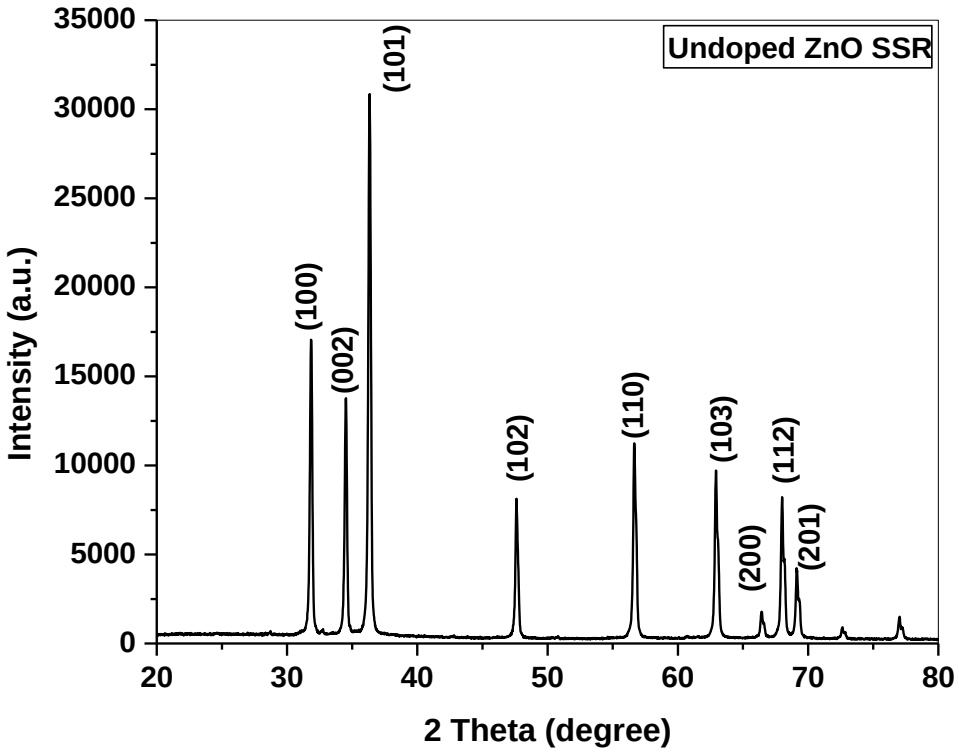

Fig. 4.7: XRD pattern of undoped ZnO by SSR.

Table 4.5: Comparison of XRD peaks with standard values for Undoped ZnO (SSR)

hkl	**2θ(std.)**	**2θ(observed)**	**hkl**	**2θ(std.)**	**2θ(observed)**
100	31.770	31.860	**103**	62.864	62.940
002	34.422	34.520	**200**	66.380	66.440
101	36.253	36.340	**112**	67.939	68.000
102	47.539	47.640	**201**	69.100	69.140
110	56.603	56.680			

8) ZnO:Er(2%) by SSR:

ZnO:Er(2%) was synthesized by solid state reaction at 500C. Powder XRD pattern is shown in Fig.4.8, which shows sharp peaks with high intensity indicating very well crystalline ZnO (JCPDS card No 36-1451). However, small peaks corresponding to dopant precursor phase is still observed (JCPDS card no. 43-1007). Table 4.6 gives a comparison between the standard and observed values of phase for ZnO:Er(2%) prepared by solid state reaction (SRR) method.

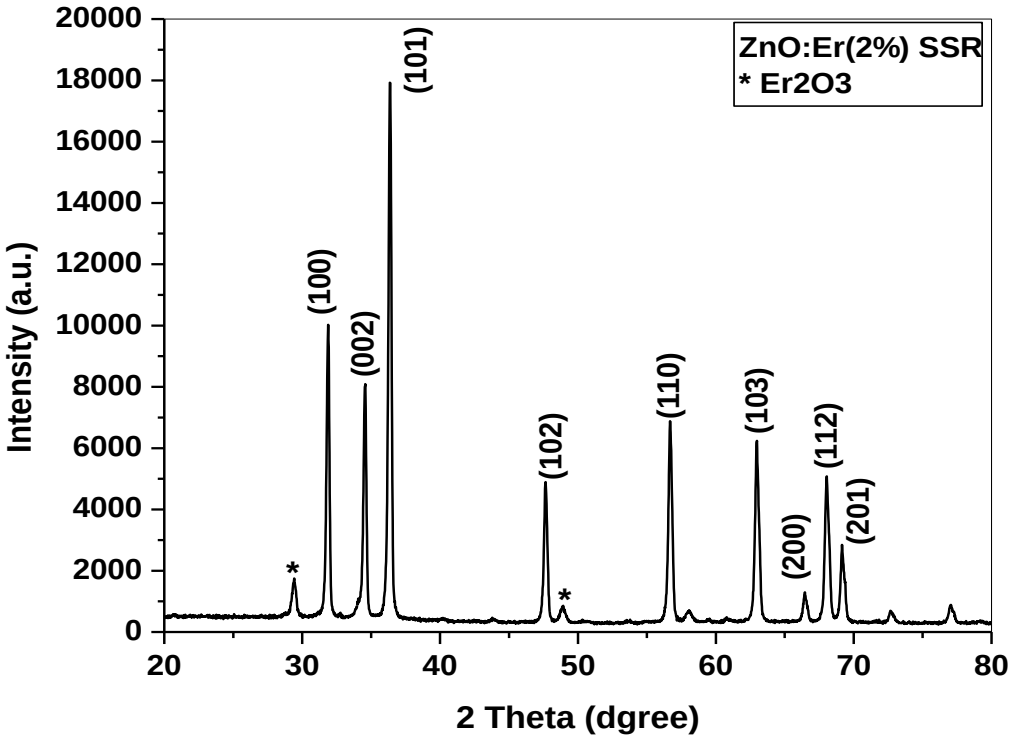

Fig. 4.8: XRD pattern of ZnO:Er(2%) by SSR.

Table 4.6: Comparison of XRD peaks with standard values for ZnO:Er(2%) (SSR)

hkl	2θ(std.)	2θ(observed)	hkl	2θ(std.)	2θ(observed)
100	31.770	31.880	**103**	62.864	62.980
002	34.422	34.560	**200**	66.380	66.460
101	36.253	36.380	**112**	67.939	68.040
102	47.539	47.660	**201**	69.100	69.160
110	56.603	56.700			

9) ZnO:Er(2%) Yb(10%) by SSR:

ZnO:Er(2%)Yb(10%) was synthesized by solid state reaction at 500°C. Powder XRD pattern is shown in Fig.4.9. The crystalline ZnO phase conforms to JCPDS card No 36-1451. However, small peaks at 29.680 degree and 49.380 degree (2 theta) corresponding to dopant precursor phase is observed (JCPDS card no. 43-1007 for Er_2O_3 and JCPDS card no. 65–3173 for Yb_2O_3). Table 4.7 gives a comparison between the standard and observed values of phase for ZnO:Er(2%)Yb(10%) prepared by solid state reaction (SRR) method.

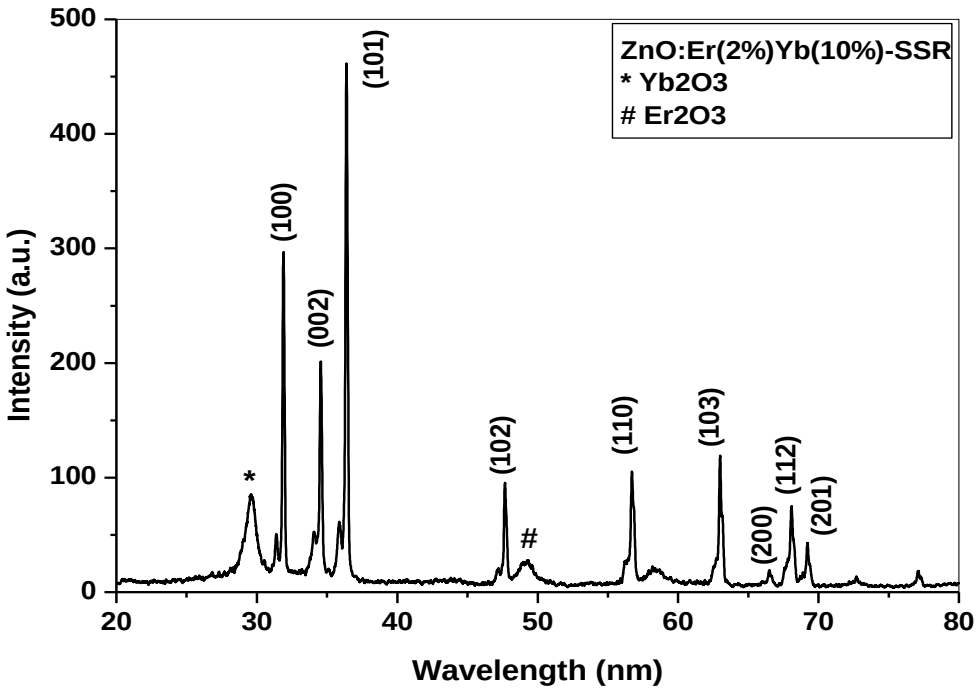

Fig. 4.9: XRD pattern of ZnO:Er(2%)Yb(10%) by SSR.

Table 4.7: Comparison of XRD peaks with std. values for ZnO:Er(2%)Yb(10%) (SSR)

hkl	2θ(std.)	2θ(observed)	hkl	2θ(std.)	2θ(observed)
100	31.770	31.7843	**103**	62.864	62.8499
002	34.422	34.5173	**200**	66.380	66.3602
101	36.253	36.2473	**112**	67.939	68.0150
102	47.539	47.5804	**201**	69.100	68.9928
110	56.603	56.5816			

10) ZnO:Er(2%) Yb(10%) annealed at 800°C by SSR:

ZnO:Er(2%)Yb(10%) sample was further annealed at 800°C for 4 hours**.** The crystallinity of ZnO phase improved considerably. However, peaks corresponding to dopant precursor phase also strengthened. Table 4.8 gives a comparison between the standard and observed values of phase for ZnO:Er(2%)Yb(10%) prepared by solid state reaction (SRR) method and further annealed. All these phase are according to JCPDS card No 36-1451 (ZnO), 43-1007 (Er_2O_3) and 65–3173 (Yb_2O_3).

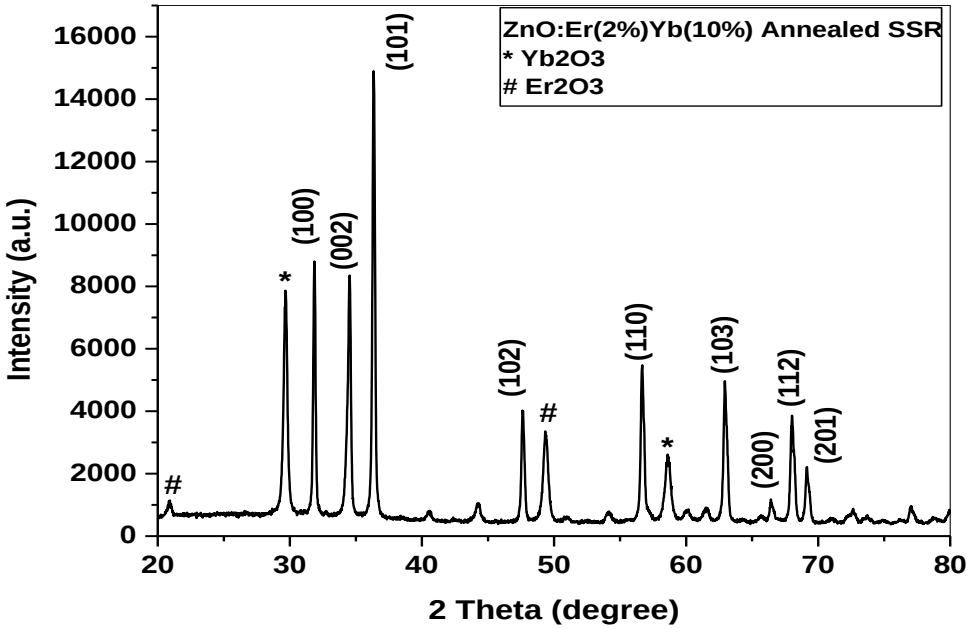

Fig. 4.10: XRD pattern of ZnO:Er(2%)Yb(10%) annealed at 800°C by SSR.

Table 4.8: Comparison of XRD peaks with standard values for ZnO:Er(2%)Yb(10%)

(Annealed at 800°C SSR)

hkl	2θ(std.)	2θ(observed)	hkl	2θ(std.)	2θ(observed)
100	31.770	31.860	**103**	62.864	62.960
002	34.422	34.520	**200**	66.380	66.440
101	36.253	36.360	**112**	67.939	68.020
102	47.539	47.640	**201**	69.100	69.160
110	56.603	56.680			

11) ZnO:Ho(2%) by SSR:

ZnO:Ho(2%) was synthesized by solid state reaction at 500C. Powder XRD pattern is shown in Fig.4.11. The crystalline ZnO phase conforms to JCPDS card No 36-1451. However, very small peaks corresponding to dopant precursor phase is observed. Table 4.9 gives a comparison between the standard and observed values of phase for ZnO:Ho(2%) prepared by solid state reaction (SRR) method.

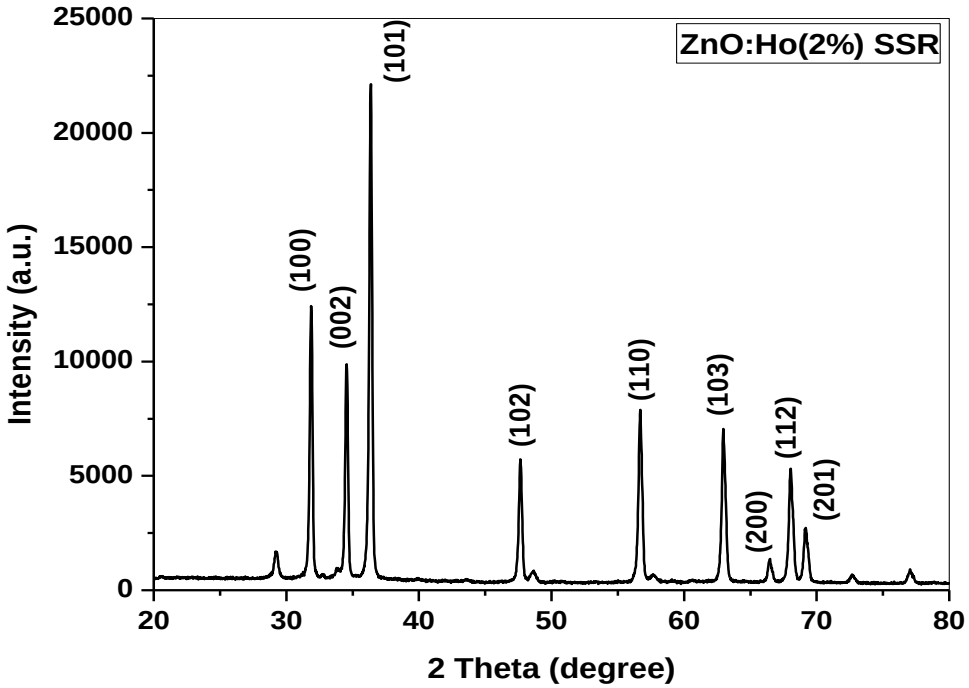

Fig. 4.11: XRD pattern of ZnO:Ho(2%) by SSR.

Table 4.9: Comparison of XRD peaks with standard values for ZnO:Ho(2%) (SSR)

hkl	2θ(std.)	2θ(observed)	hkl	2θ(std.)	2θ(observed)
100	31.770	31.880	**103**	62.864	62.980
002	34.422	34.560	**200**	66.380	66.460
101	36.253	36.360	**112**	67.939	68.040
102	47.539	47.660	**201**	69.100	69.180
110	56.603	56.700			

12) ZnO:Ho(2%)Yb(10%) by SSR:

ZnO:Ho(2%)Yb(10%) was synthesized by solid state reaction at 500°C. Powder XRD pattern is shown in Fig.4.12. The crystalline ZnO phase conforms to JCPDS card No 36-1451. However, in addition to small peaks corresponding to dopant (Ho) precursor phase, a strong peak corresponding to Yb phase is observed which shows low solubility of Yb in ZnO. (JCPDS card no. 47-1274 for Yb_2O_3 and 43-1018 for Ho_2O_3). Table 4.10 gives a comparison between the standard and observed values of phase for ZnO:Ho(2%)Yb(10%) prepared by solid state reaction (SRR) method.

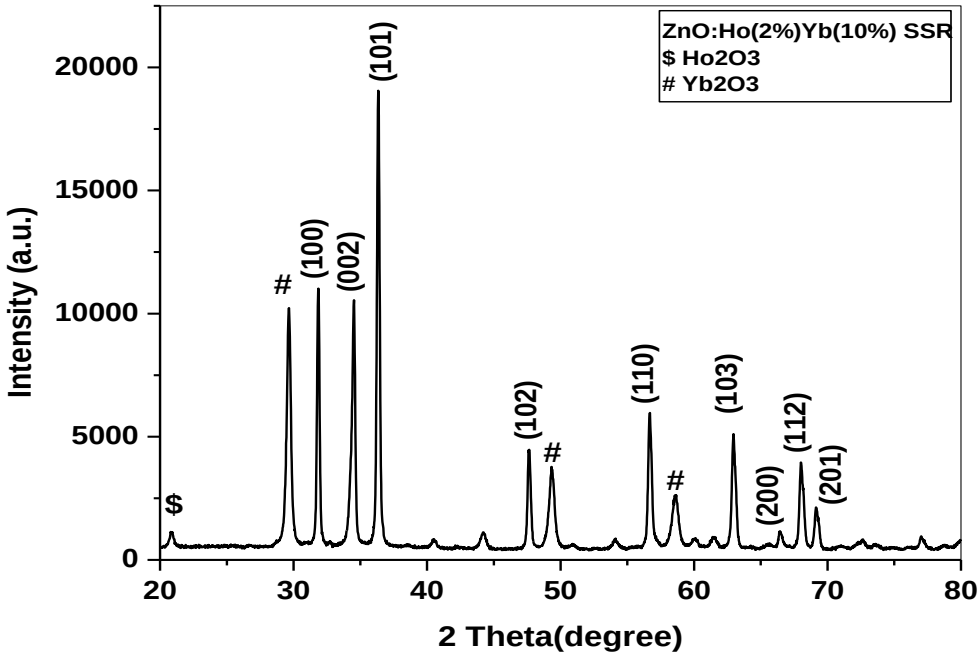

Fig. 4.12: XRD pattern of ZnO:Ho(2%)Yb(10%) by SSR.

Table 4.10

Comparison of XRD peaks with standard values for ZnO:Ho(2%)Yb(10%) (SSR)

hkl	2θ(std.)	2θ(observed)	hkl	2θ(std.)	2θ(observed)
100	31.860	31.880	**103**	62.864	62.960
002	34.422	34.520	**200**	66.380	66.460
101	36.253	36.340	**112**	67.939	68.020
102	47.539	47.640	**201**	69.100	69.160
110	56.603	56.680			

13) ZnO:Li(2%)Er(2%) by SSR:

ZnO:Li(2%)Er(2%) was synthesized by solid state reaction at 500°C. Monovalent Li was used for charge compensation since substitutional doping of trivalent rare earth ion in place of divalent Zinc may disturb overall charge neutrality in the lattice. Powder XRD pattern is shown in Fig.4.13. The crystalline ZnO phase conforms to JCPDS card No 36-1451. However, small peaks corresponding to dopant phase is observed. Table 4.11 gives a comparison between the standard and observed values of phase for ZnO:Li(2%)Er(2%) prepared by solid state reaction (SRR) method.

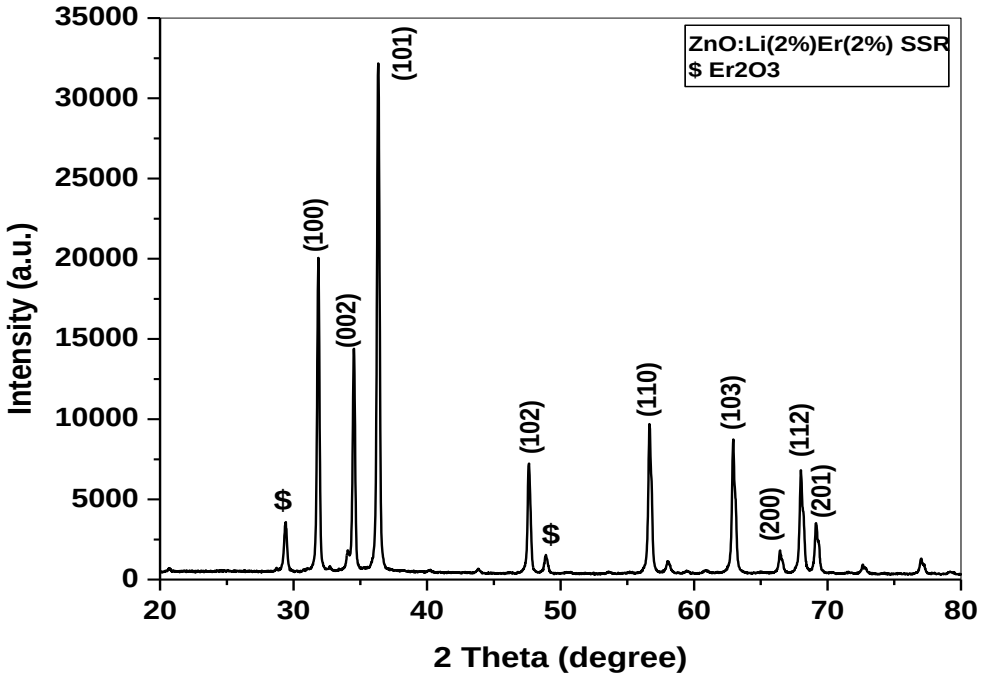

Fig. 4.13: XRD pattern of ZnO:Li(2%)Er(2%) by SSR.

Table 4.11

Comparison of XRD peaks with standard values for ZnO:Er(2%)Li(2%) (SSR)

hkl	2θ(std.)	2θ(observed)	hkl	2θ(std.)	2θ(observed)
100	31.860	31.860	**103**	62.864	62.940
002	34.422	34.520	**200**	66.380	66.460
101	36.253	36.340	**112**	67.939	68.020
102	47.539	47.640	**201**	69.100	69.160
110	56.603	56.680			

4.1.1 Interpretation of XRD :

The powder preparation procedure was very critical to obtain pure ZnO. All peaks in the XRD pattern of the resulting products ZnO; ZnO:Er; ZnO:ErYb; ZnO:Ho; ZnO:Ho,Yb; ZnO:Er,Li synthesized both by SSR and CPP method were indexed to "wurtzite hexagonal" phase of ZnO. The five peaks in the 30°-60° range of pattern indicate that the pure ZnO was obtained by slow precipitation at low temperature (90°C). *Hosnol et al* reported that washing with ethanol was very important. Our results suggest that washing by ethanol, alkaline pH(10) and slow drying at lower temperature (90°C) are critical for preparation of pure ZnO particles.

From the diffraction pattern, we found that the planes corresponding to [100], [002], [101] of the expected wurtzite hexagonal structure (JCPDS Card No. 36-1451). All diffraction peaks corresponding to wurtzite phases of ZnO, in addition trace of Erbium, Ytterbium and Holmium related phase were detected. The sharp peaks of ZnO indicate that the products were well crystallized.

The XRD patterns show that Er, Yb, Ho and Li doping of ZnO does not alter its wurtzite structure. The changes in peak intensities due to Er, Yb, Ho and Li doping is quite striking which clearly show that due to doping diffracted peak intensity decreases. A close comparison of the diffraction angle with different doping is shown in fig. 4.14. The peak shift in all XRD pattern indicted change in lattices parameters due to substitutional doping of Er^{3+}(effective ionic radii 0.175 nm), Yb^{3+}(effective ionic radii 0.176 nm), Ho^{3+}(effective ionic radii 0.176 nm), in place of Zn^{2+} (effective ionic radii 0.088 nm). The variation of lattice parameters 'a' and 'c' with doping of Er, Yb, Ho and Li in ZnO shown in table no. 4.12.

From the XRD patterns, lattice parameters were calculated using the equation:

$$\mathbf{1/d^2 = 4/3[(h^2+k^2+hk)/a^2] + (l^2/c^2)}$$

Where h,k,l are the Miller indices,

a & c are the lattice parameter, for hexagonal structure a=b.

The relevant data for ZnO wurtzite peak is given in table 4.12-4.13.

The crystallite sizes for different crystal planes have been calculated using Scherer's formula. The Scherer's formula for crystallite particle size determination is given by

$$D = K\lambda/(\beta \cos \theta)$$

Where

K is a proportionally constant and its value is (0.9), β the FWHM (full width half maximum) of the peak in radians (theoretically corrected from the instrumental broadening), D the size of the crystal in the direction perpendicular to the reflecting planes and λ the wavelength of the X-rays used (λ=1.54A°).

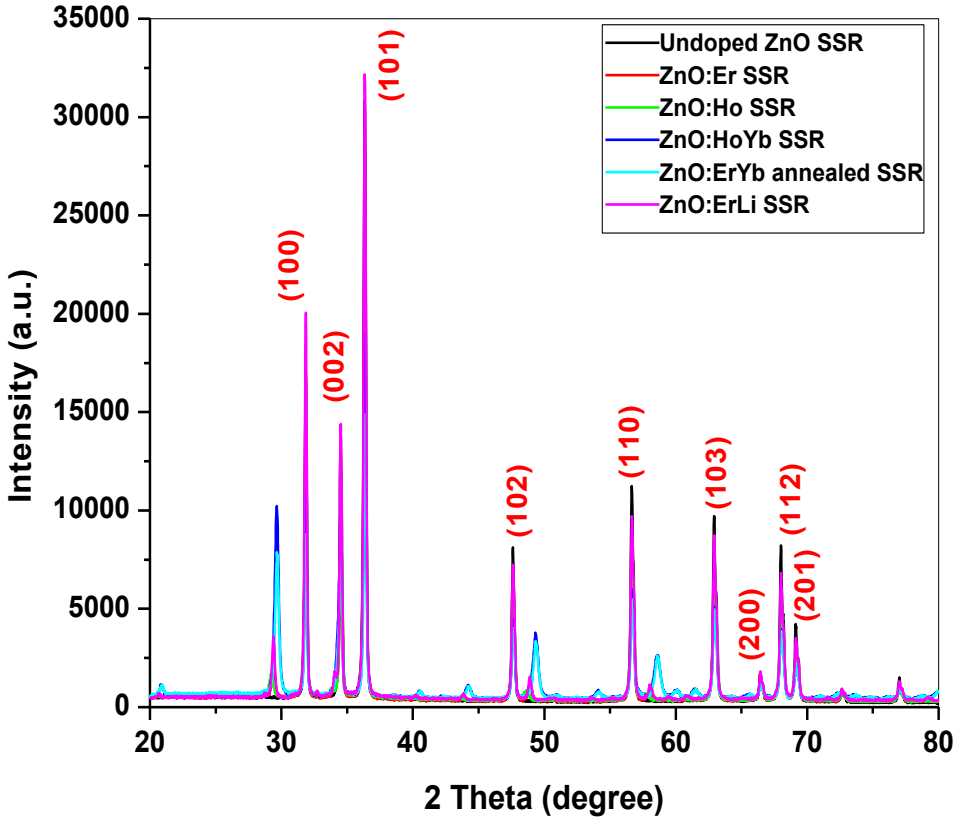

Fig. 4.14: Comparison between XRD patterns of ZnO with different doping by SSR.

In fig 4.14 ZnO:ErYb and ZnO:HoYb both give some extra peaks; these peaks are corresponding to ytterbium, erbium and holmium.. Fig 4.15 shows that there is negligible peak shift occur. Highest peaks are due to ZnO:Er(2%)Li(2%).

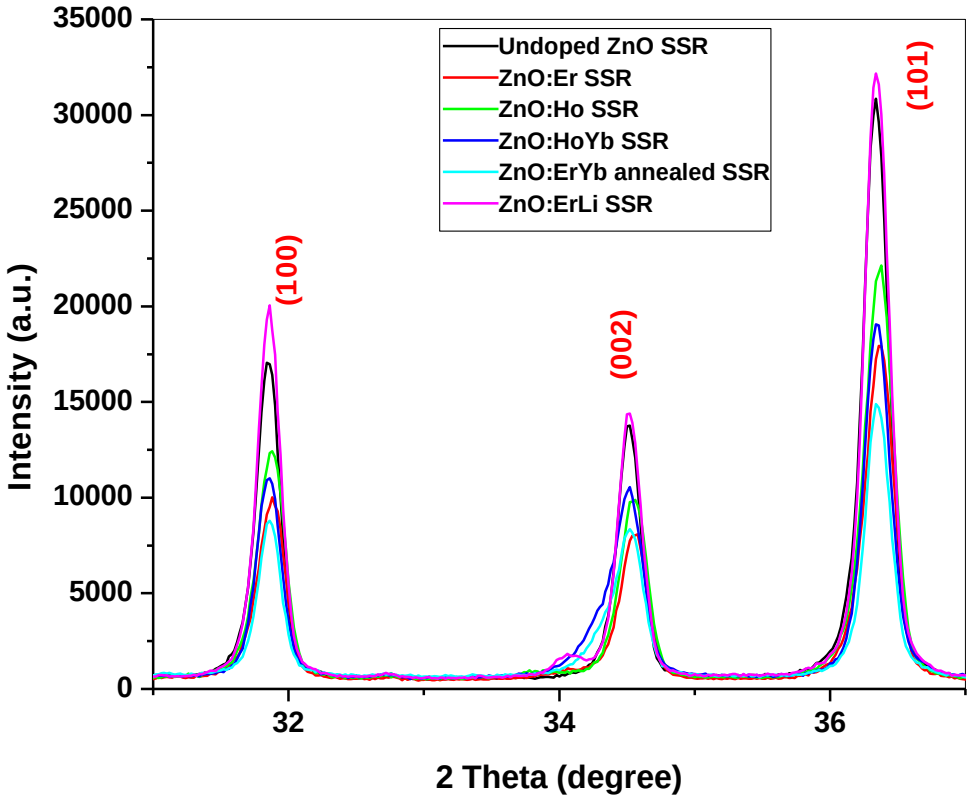

Fig. 4.15: Comparison between XRD patterns of ZnO with different doping by SSR in very small range.

TABLE 4.12

Crystalline parameters along different planes of sample prepared by Co- Precipitation method:

SAMPLE	d(A°)	2 Θ (degrees)	hkl	a=b≠c crystallite parameters (A°)
Undoped ZnO	**2.813**	**31.780**	**100**	**a=3.2486**
	2.602	**34.440**	**002**	**c=5.2039**
ZnO:Er(2%)	**2.597**	**31.494**	**100**	**a=2.9988**
	2.615	**34.247**	**002**	**c=5.2305**
ZnO:Er(2%) annealed	**2.812**	**31.784**	**100**	**a=3.2469**
	2.595	**34.517**	**002**	**c=5.1907**
ZnO:Ho	**2.812**	**31.784**	**100**	**a=3.2469**
	2.603	**34.417**	**002**	**c=5.2053**
ZnO:Er(2%)Yb(10%)	**2.808**	**31.840**	**100**	**a=3.2426**
	2.597	**34.500**	**002**	**c=5.1951**
ZnO:Er(2%)Yb(10%) annealed	**2.856**	**31.283**	**100**	**a=3.2977**
	2.639	**33.916**	**002**	**c=5.2799**

The average crystal size in ‘a’ and ‘c’ directions, for different doping of Er, Yb, Ho and Li in ZnO varied from 32nm to 51nm (table 4.12 and 4.13). The change in crystallite sizes is, however, small. Table 4.14 and 4.15 give the information about crystal size for ZnO with different doping of Er, Yb, Ho and Li and with SSR and CPP. For CPP materials a=32 nm (average) and c=52 nm (average). ZnO:Er by CPP have lowest size along a-axis among co-precipitated materials, whereas ZnO:ErYb annealed have largest size along a-axis among co-precipitated materials. (According to table no. 4.12)

TABLE 4.13

Crystalline parameters along different planes of sample prepared by solid state reaction method:

SAMPLE	d(A°)	2 Θ (degrees)	hkl	a=b≠c crystallite parameters (A°)
Undoped ZnO	2.806	31.860	100	a=3.2407
	2.596	34.520	002	c=5.1922
ZnO:Er(2%)	2.805	31.880	100	a=3.2387
	2.593	34.560	002	c=5.1864
ZnO:Er(2%)Yb(10%)	2.812	31.784	100	a=3.2469
	2.595	34.517	002	c=5.1907
ZnO:Er(2%)Yb(10%) annealed	2.806	31.860	100	a=3.2407
	2.596	34.520	002	c=5.1922
ZnO:Ho(2%)	2.805	31.880	100	a=3.2387
	2.593	34.560	002	c=5.1864
ZnO:Ho(2%)Yb(10%)	2.806	31.860	100	a=3.2407
	2.596	34.520	002	c=5.1922
ZnO:Er(2%)Li(2%)	2.806	31.860	100	a=3.2407
	2.596	34.520	002	c=5.1922

For ZnO synthesized by SSR, a=32 nm (average) and c=52 nm (average). ZnO:Er by SSR have lowest size along a-axis among solid state reaction method materials, whereas ZnO:Ho and ZnO:Er have lowest size along c-axis among solid state reaction method materials. (According to table no. 4.13)

.

TABLE 4.14

Crystalline size of sample prepared by Co-Precipitation method:

SAMPLE	β (Radians)	2 Θ (degrees)	hkl	Crystal size (nm)	Average crystal size D (nm)
Undoped ZnO	0.0104	31.780	100	13.911	15.08
	0.0089	34.440	002	16.254	
ZnO:Er(2%)	0.0179	31.493	100	8.0529	10.47
	0.0113	34.247	002	12.884	
ZnO:Er(2%) annealed	0.0122	31.784	100	11.766	11.71
	0.0125	34.517	002	11.642	
ZnO:Ho	0.0083	31.784	100	17.340	20.12
	2.6027	34.417	002	22.878	
ZnO:Er(2%)Yb(10%)	0.0083	31.840	100	17.425	19.94
	0.0065	34.500	002	22.459	
ZnO:Er(2%)Yb(10%) annealed	0.0063	31.283	100	22.694	18.11
	0.0107	33.916	002	13.521	

According to Table 4.14 and 4.15 we can see that size of crystal is much less in CPP syntheisized ZnO samples in comparison to SSR materials. The Crystallinity improves in solid state reaction method whereas in co-precipitated materials, one gets very small size particles. It can be noted that contrary to usual high temperature solid state reaction where particle size obtained is in micrometer range, the used low temperature solid state reaction procedure produced highly crystalline nanoparticles of undoped and doped ZnO in the 30 - 40 nm size range. Hence, in both the synthesis procedure used for

preparing undoped and rare earth doped ZnO, we could obtain nanoparticles in the range of 10-18 nm (CPP method) and 30 - 40 nm (SSR method).

TABLE 4.15

Crystal size of sample prepared by solid state reaction method:

SAMPLE	β(Radians)	2 Θ (degrees)	hkl	Crystal size (nm)	Average crystal size D (nm)
Undoped ZnO	0.0042	31.860	100	34.357	34.73
	0.0042	34.520	002	35.095	
ZnO:Er(2%)	0.0046	31.880	100	30.982	31.10
	0.0046	34.560	002	31.199	
ZnO:Er(2%)Yb(10%)	0.0035	31.784	100	41.184	39.45
	0.0038	34.517	002	37.707	
ZnO:Er(2%)Yb(10%) annealed	0.0037	31.860	100	38.726	33.40
	0.0052	34.520	002	28.076	
ZnO:Ho(2%)	0.0045	31.880	100	31.686	31.80
	0.0045	34.560	002	31.908	
ZnO:Ho(2%)Yb(10%)	0.0041	31.860	100	34.853	30.93
	0.0054	34.520	002	26.996	
ZnO:Er(2%)Li(2%)	0.0035	31.860	100	41.004	38.97
	0.0039	34.520	002	36.942	

4.2 Morphology by Scanning Electron Microscope:

The morphology of the synthesized ZnO powder samples were inspected using a LEO 440 PC based digital scanning electron microscope. The micrographs for ZnO with different rare earth doping by SSR and CPP method are shown below:

1. Undoped ZnO by CPP:

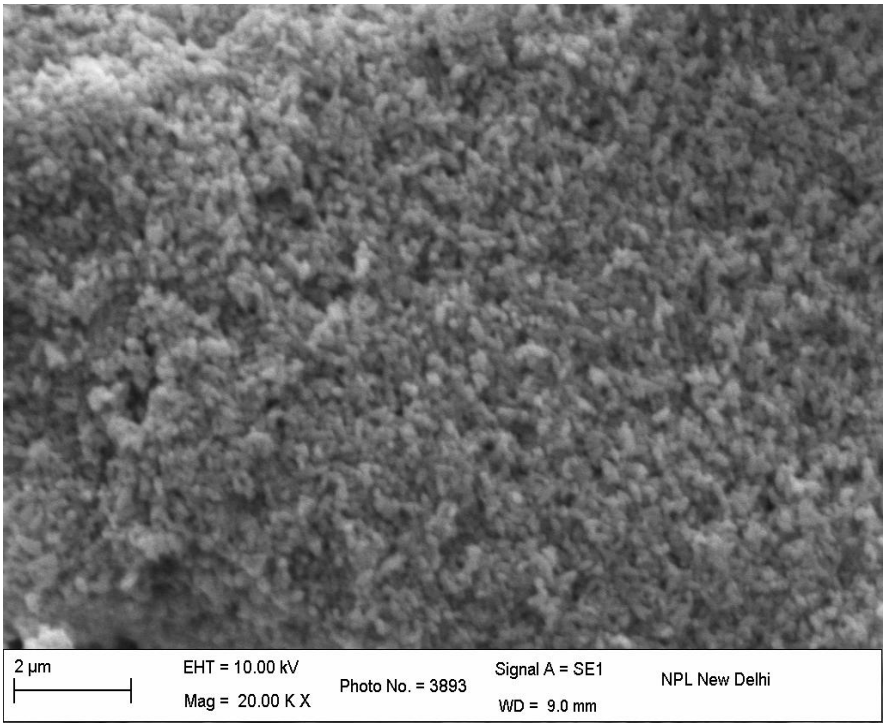

Fig. 4.16: SEM image of undoped ZnO particles by CPP at 20.00 KX.

Fig 4.16 shows the scanning electron micrographs of undoped ZnO synthesized by the co-precipitation method. The particles tend to agglomerate.

2. ZnO:Er(2%) by CPP:

Fig 4.17, 4.18 & 4.19 show the scanning electron micrographs of ZnO:Er(2%) synthesized by the co-precipitation method.. Particles found in flower shape.

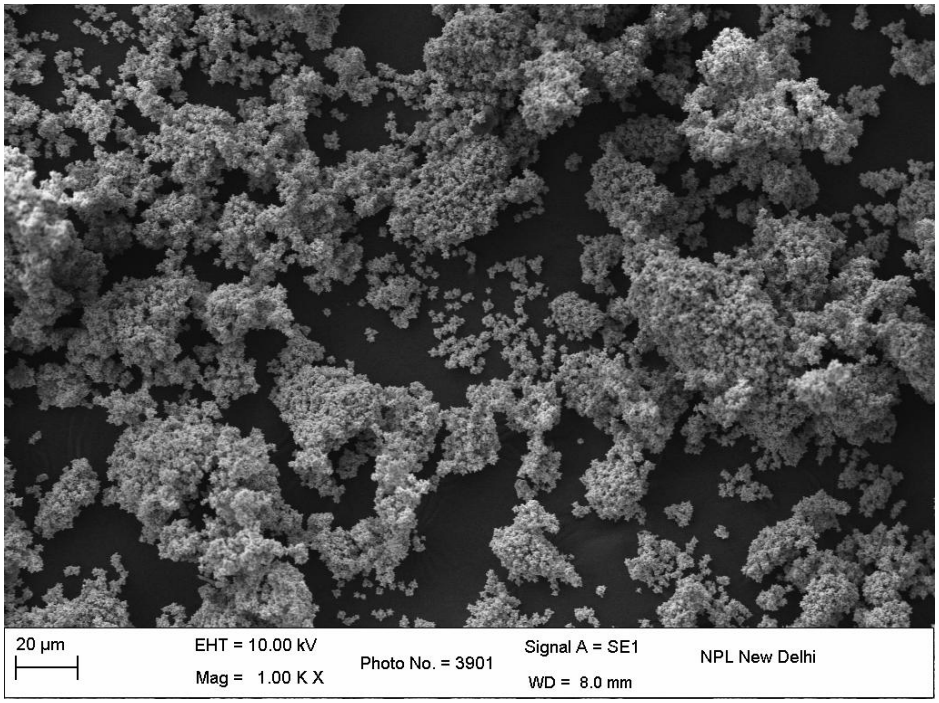

Fig. 4.17: SEM image of ZnO:Er particles by CPP at 1.00 KX.

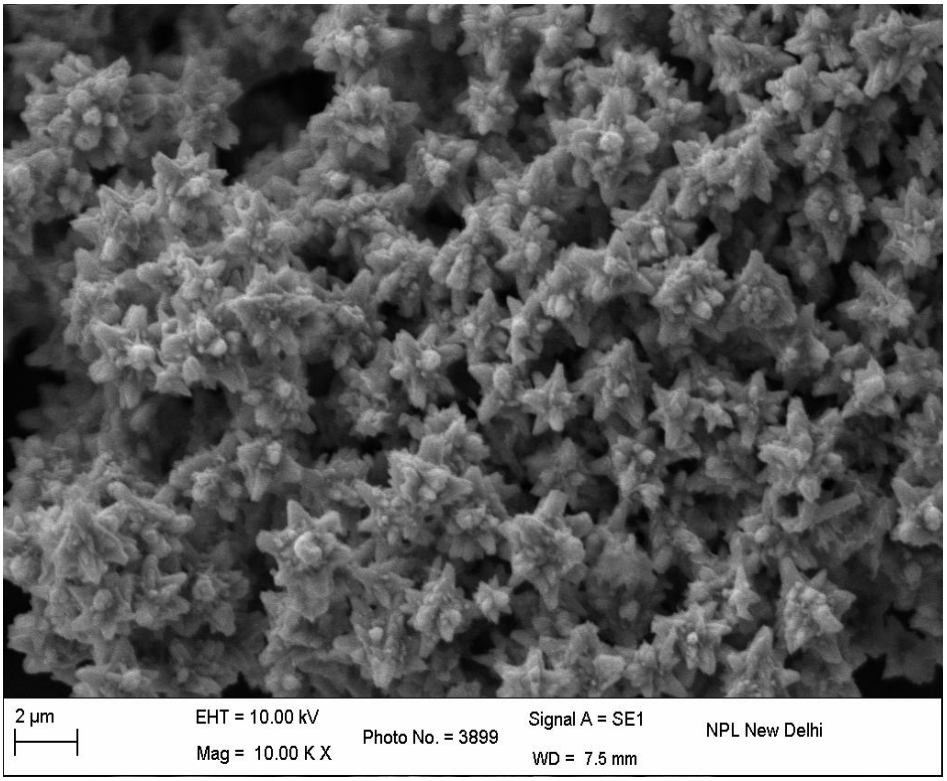

Fig. 4.18: SEM image of ZnO:Er particles by CPP at 10.00 KX.

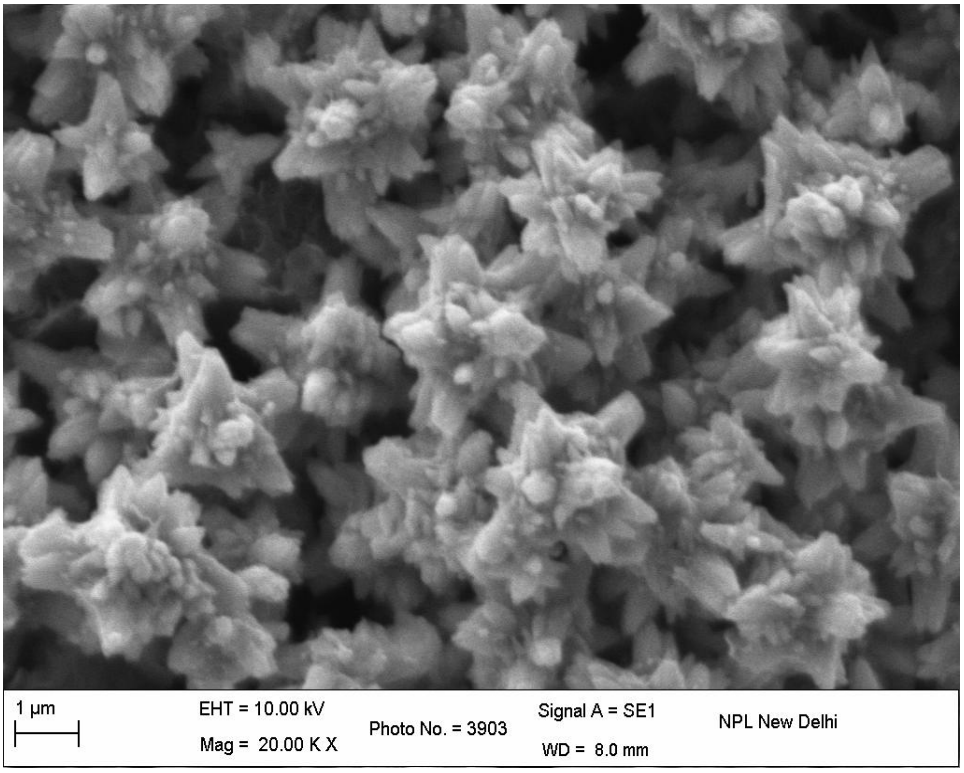

Fig. 4.19: SEM image of ZnO:Er particles by CPP at 20.00 KX.

3. ZnO:Er(2%) annealed at 800°C by CPP:

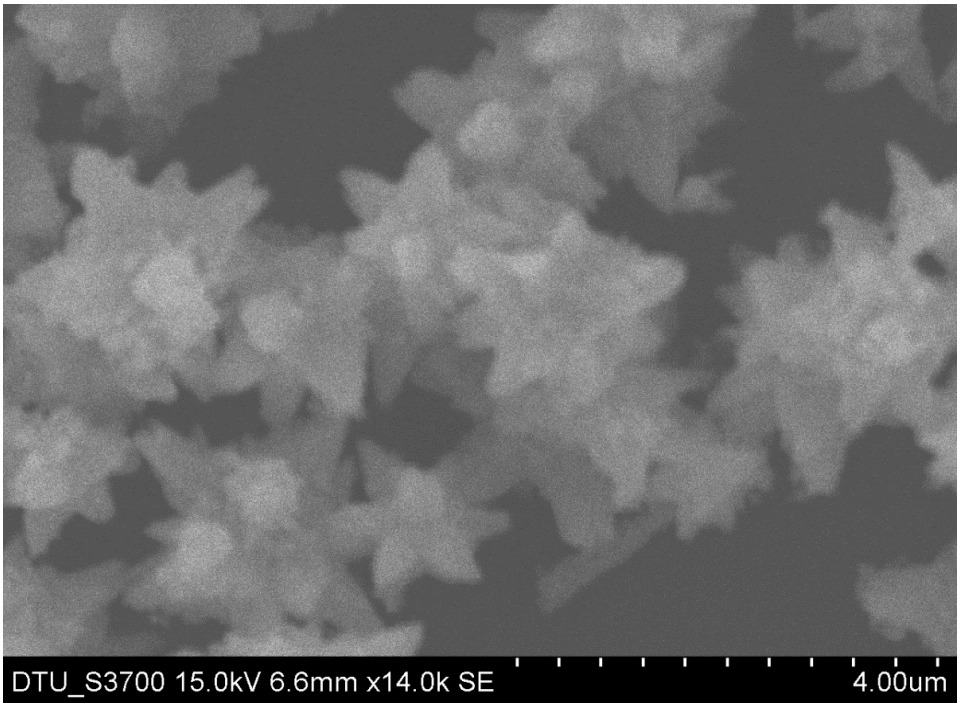

Fig. 4.20: SEM image of ZnO:Er annealed at 800°C particles by CPP at 14.00 KX.

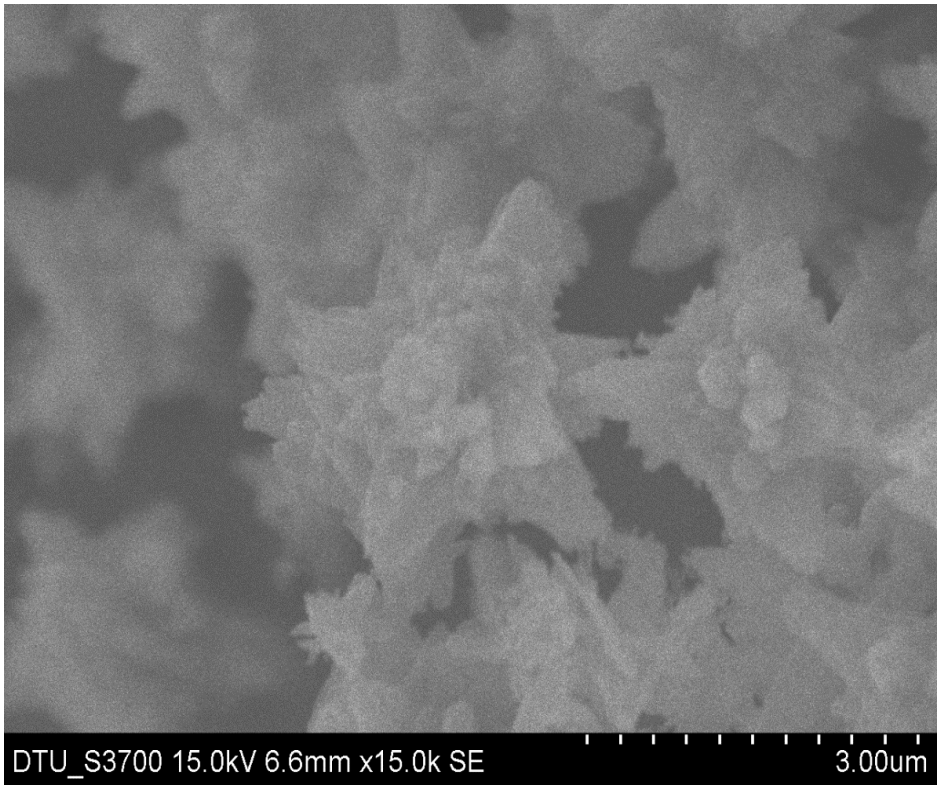

Fig. 4.21: SEM image of ZnO:Er annealed at 800°C particles by CPP at 15.00 KX.

4. ZnO:Er(2%)Yb(10%) by CPP:

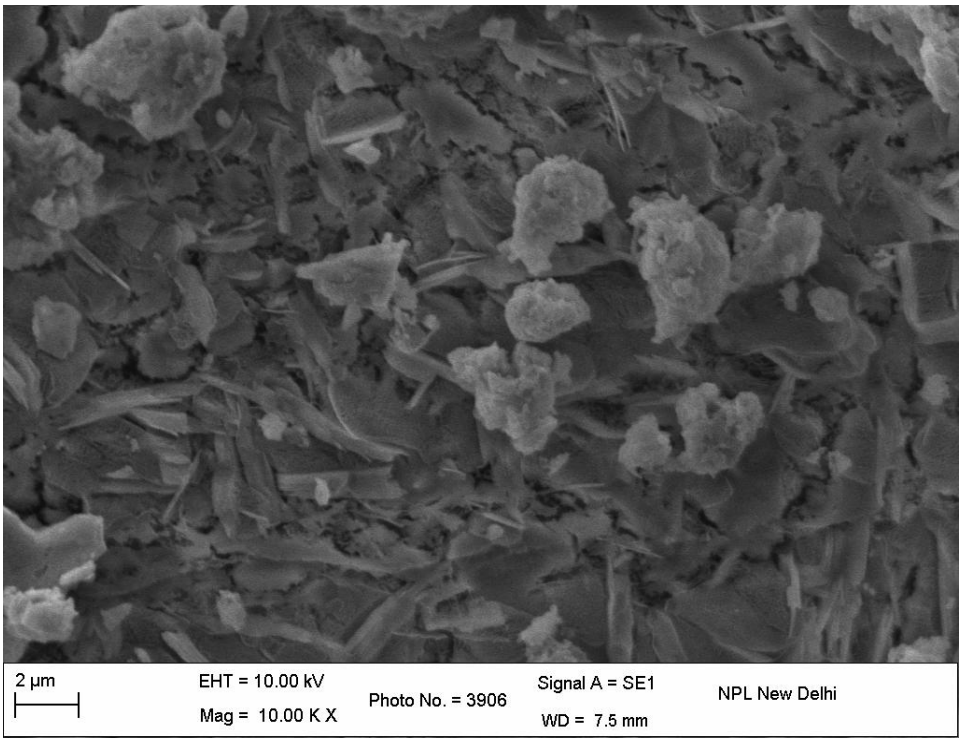

Fig. 4.22: SEM image of ZnO:Er(2%)Yb(10%) particles by CPP at 10.00 KX.

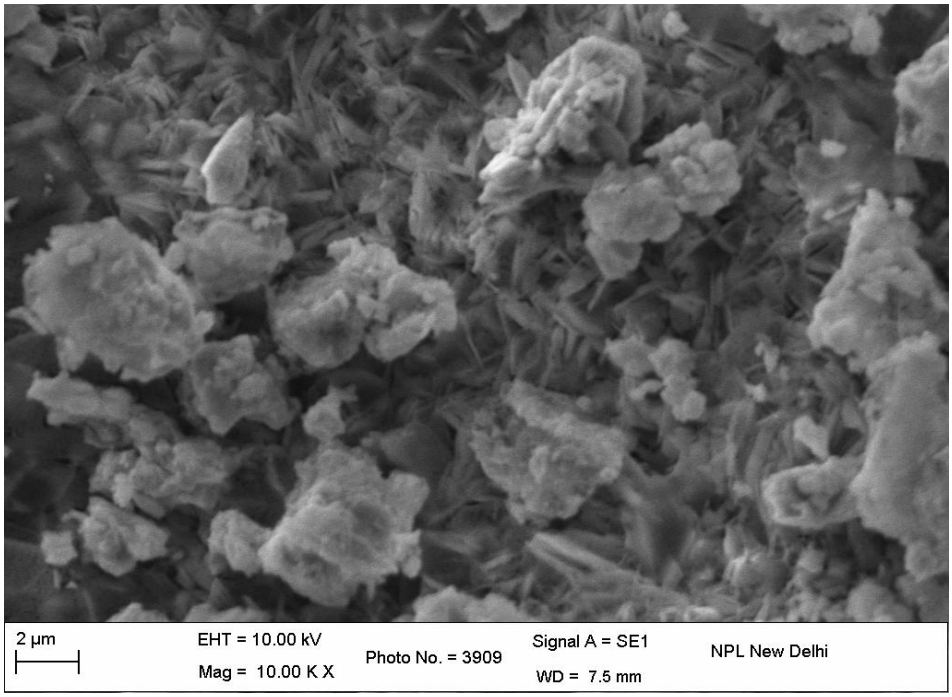

Fig. 4.23: SEM image of ZnO:Er(2%)Yb(10%) particles by CPP at 10.00 KX.

In addition to flower like particles, some rod and flake like formations are also observed in SEM micrographs of ZnO:Er(2%)Yb(10%) samples prepared by CPP method.

5. ZnO:Er(2%)Yb(10%) annealed at 800°C by CPP:

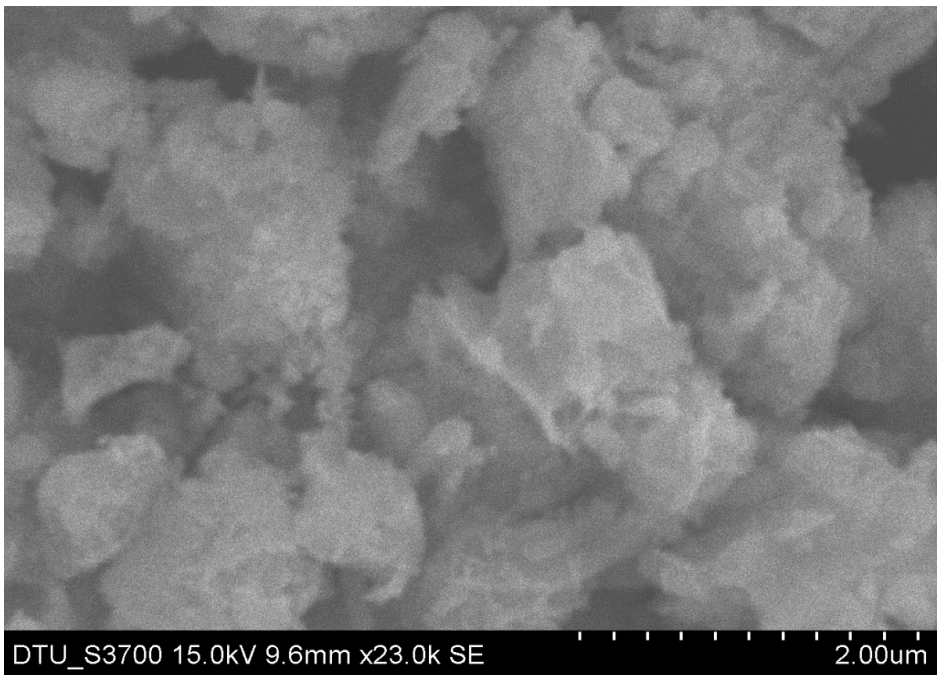

Fig. 4.24: SEM image of ZnO:Er(2%)Yb(10%) annealed particles by CPP at 23.00 KX.

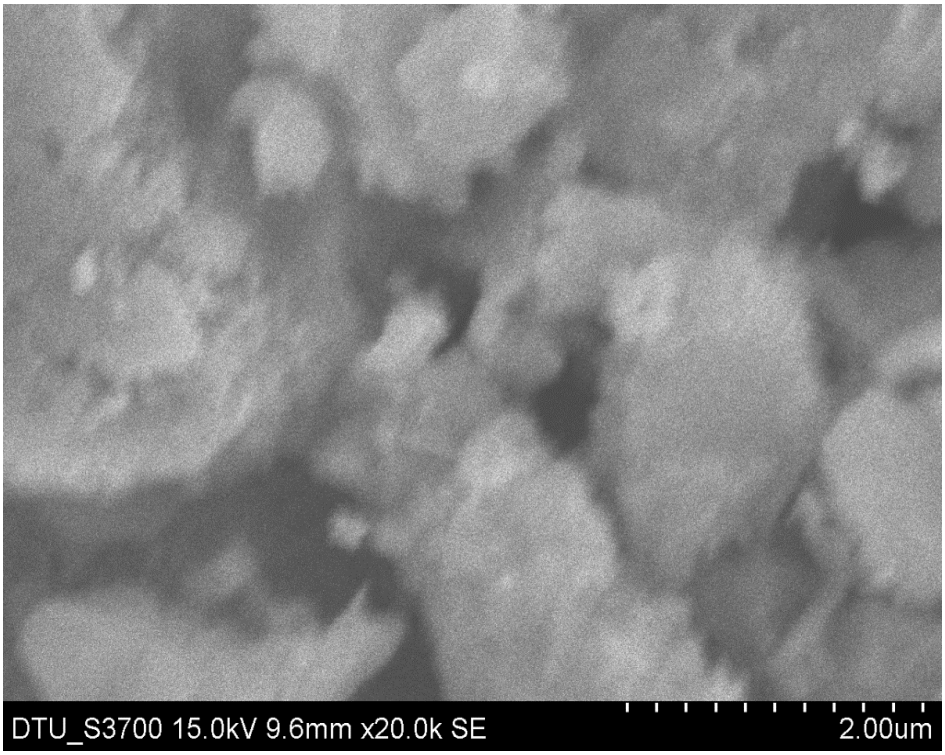

Fig. 4.25: SEM image of ZnO:Er(2%)Yb(10%) annealed particles by CPP at 20.00KX.

Fig 4.24 & 4.25 show the scanning electron micrographs of ZnO:Er(2%)Yb(10%) annealed at 800°C synthesized by the co-precipitation method. The particle tended to agglomerate. Here due to annealing size is disturbed and the reason of this change is agglomeration of crystals.

6. ZnO:Ho(2%) by CPP:

Fig 4.26, 4.27, 4.28 & 4.29 show the scanning electron micrographs of ZnO:Ho(2%) synthesized by the co-precipitation method. The particle tended to agglomerate. Particles found in flower shape.

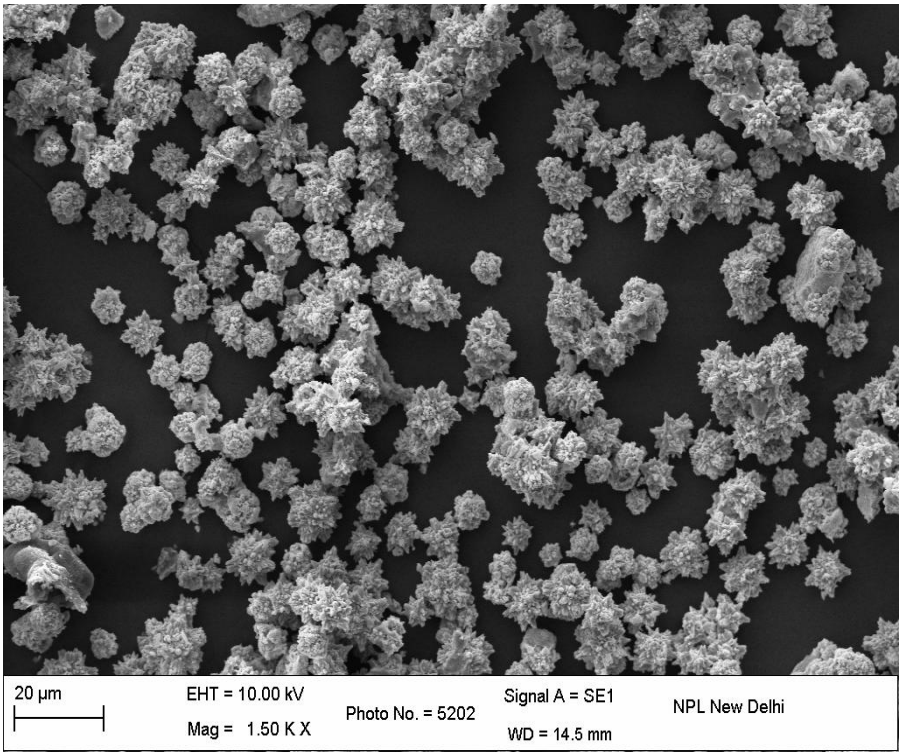

Fig. 4.26: SEM image of ZnO:Ho(2%) particles by CPP at 1.50 KX.

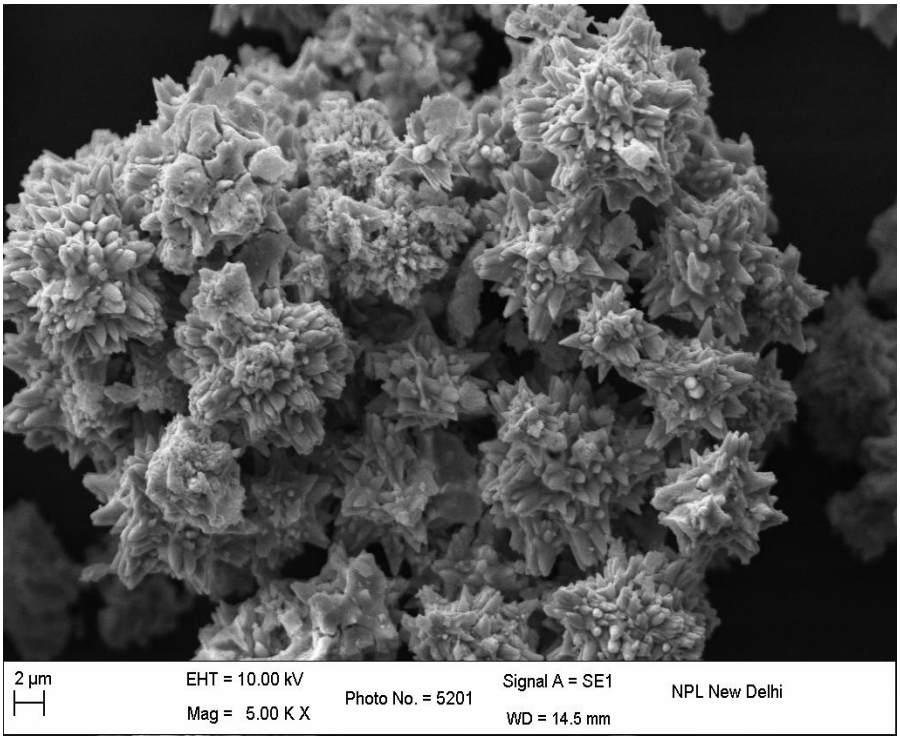

Fig. 4.27: SEM image of ZnO:Ho(2%) particles by CPP at 5.00 KX.

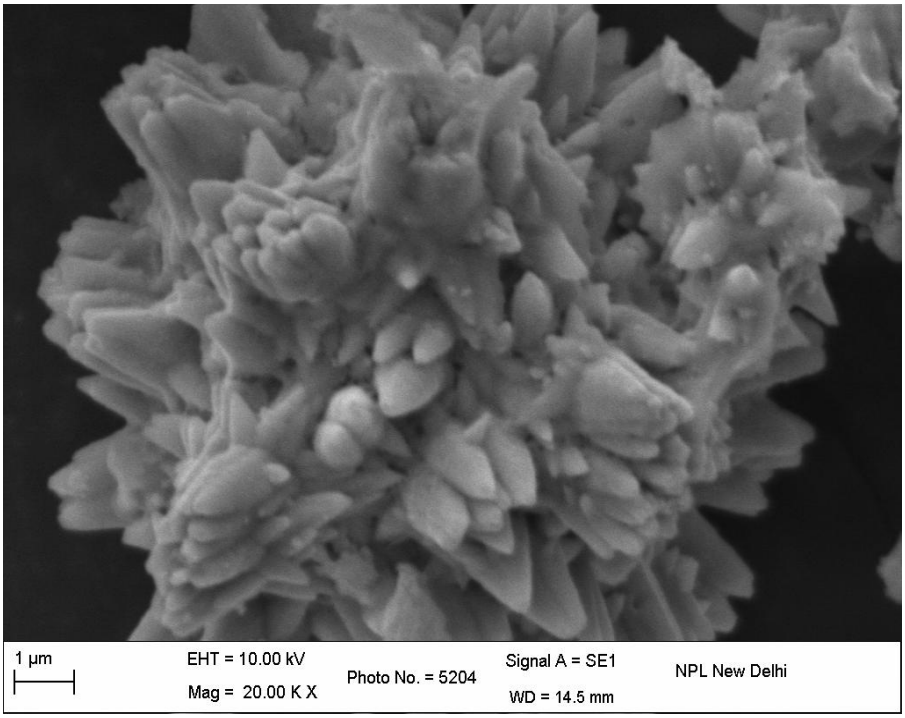

Fig. 4.28: SEM image of ZnO:Ho(2%) particles by CPP at 20.00 KX.

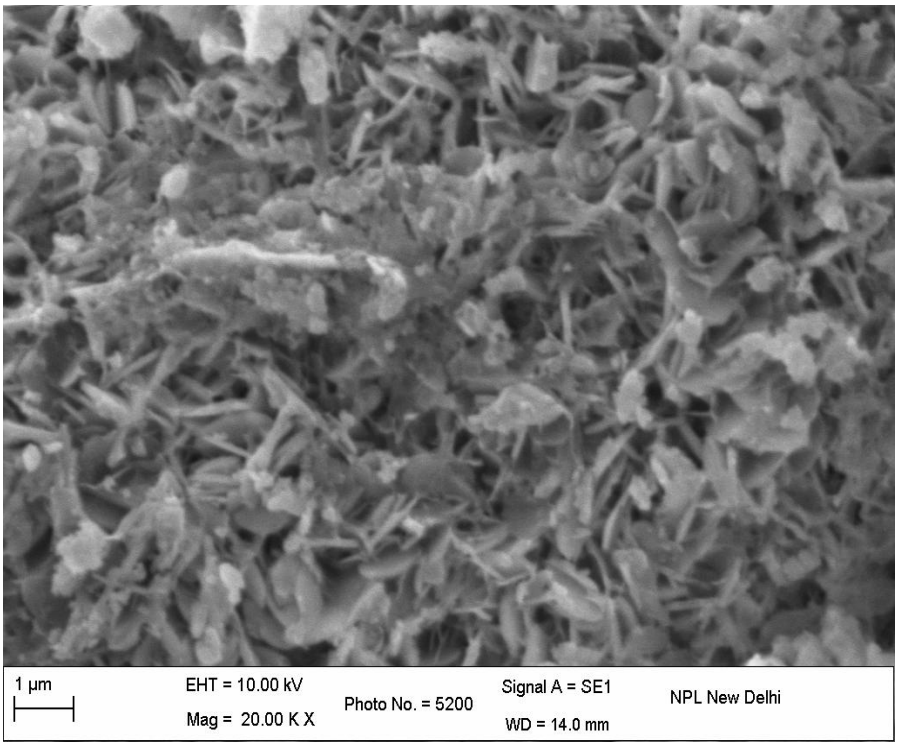

Fig. 4.29: SEM image of ZnO:Ho(2%) particles by CPP at 20.00 KX.

Fig 4.26 to 4.29 show the scanning electron micrographs of ZnO:Ho(2%) synthesized by the co-precipitation method. Longitudinal flakes of triangular morphology and hierarchical flower type structure made of such ZnO flakes as petals are seen in the micrographs.

7. Undoped ZnO by SSR:

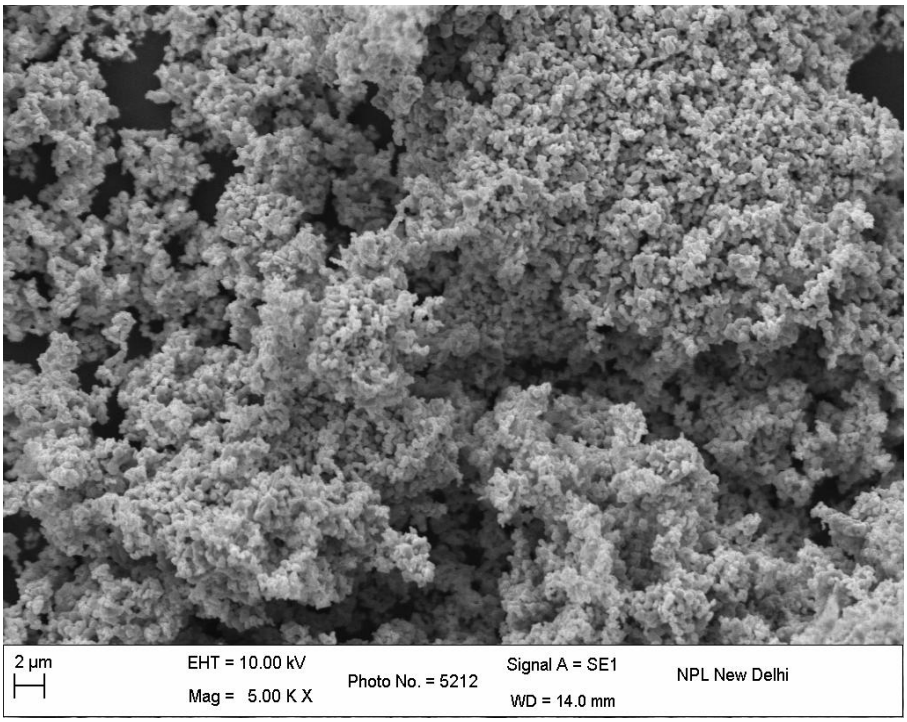

Fig. 4.30: SEM image of Undoped ZnO particles by SSR at 5.00 KX.

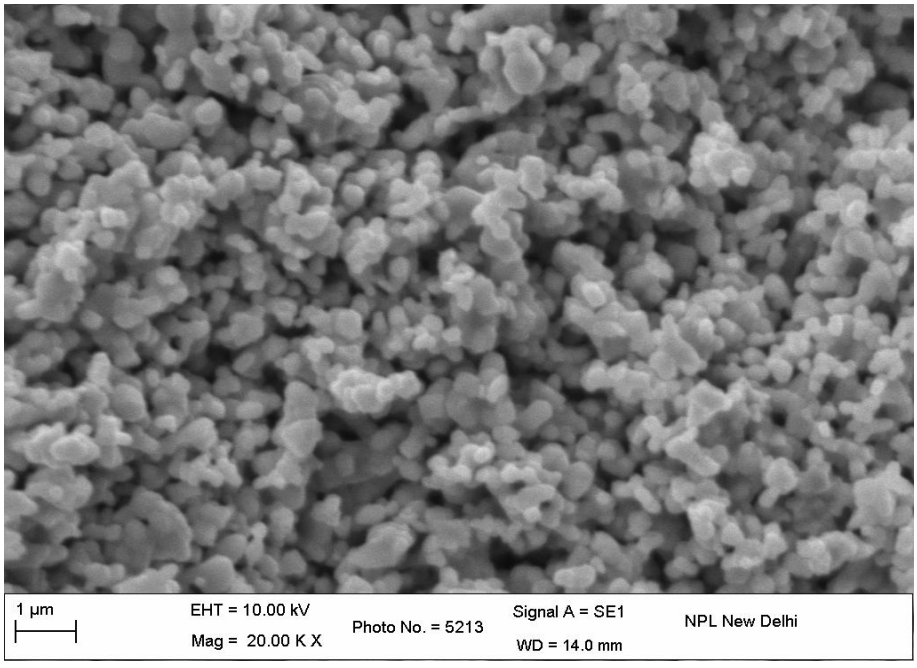

Fig. 4.31: SEM image of Undoped ZnO particles by SSR at 20.00 KX.

Rounded morphology and agglomerated particles are observed in the SEM micrographs.

8. ZnO:Er(2%) by SSR:

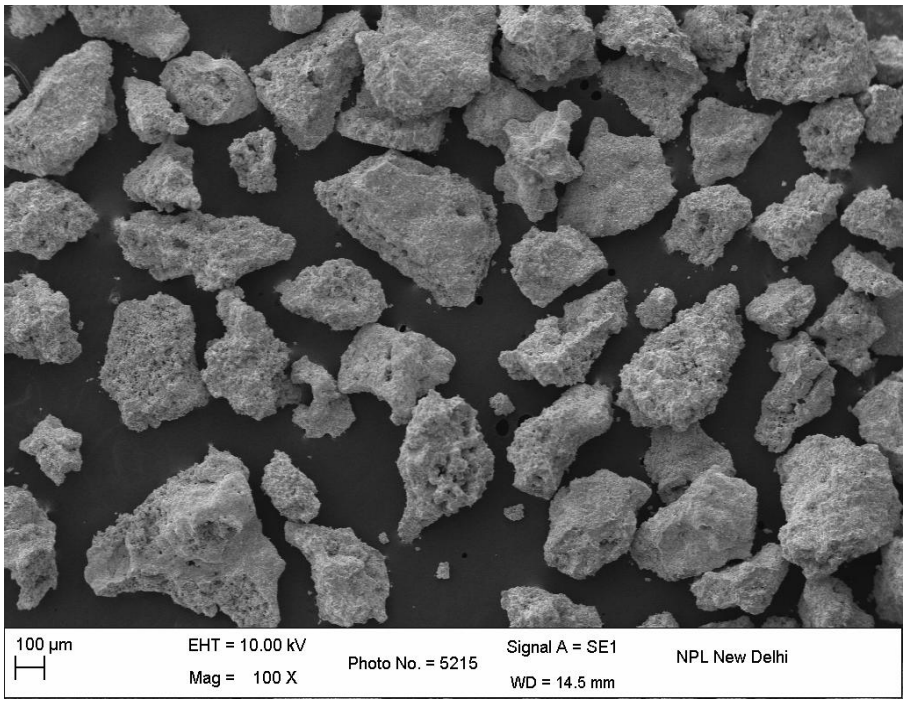

Fig. 4.32: SEM image of ZnO:Er particles by SSR at 100 X.

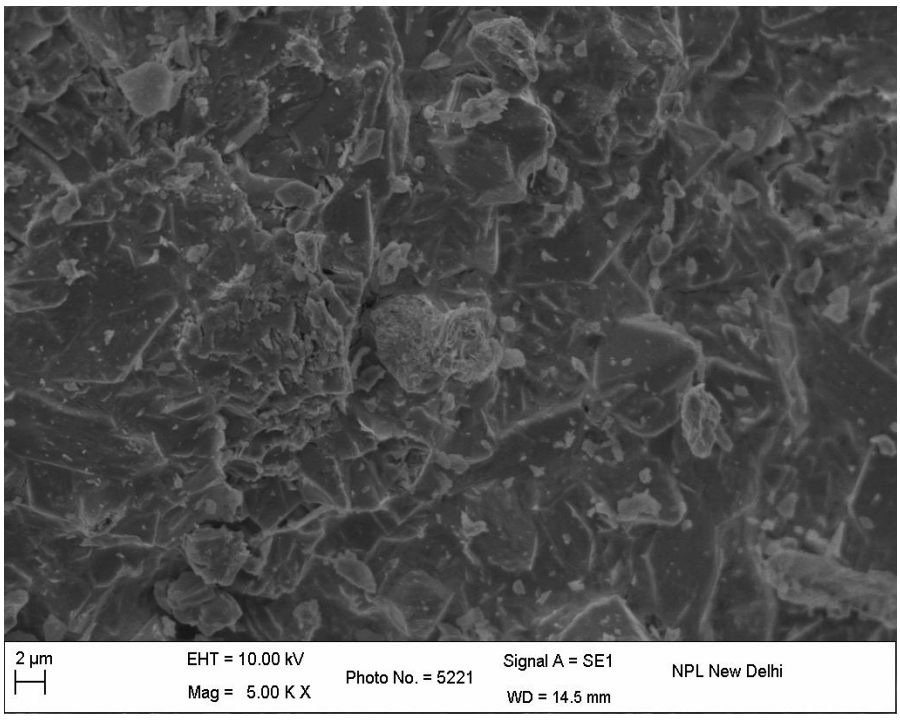

Fig. 4.33: SEM image of ZnO:Er particles by SSR at 5.00 KX.

9. ZnO:Er(2%)Li(2%) by SSR:

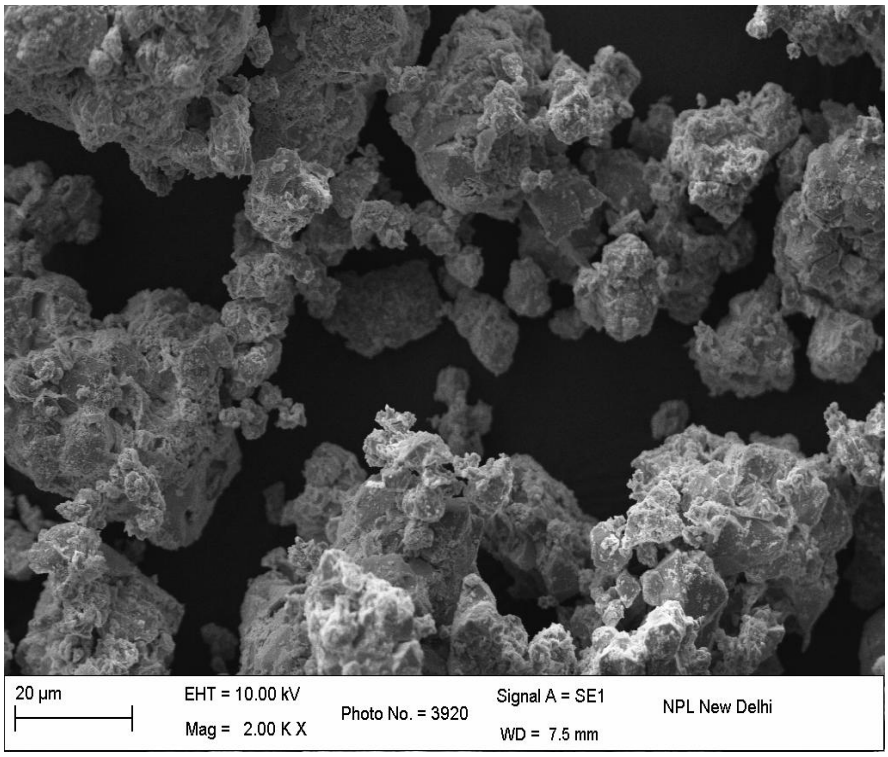

Fig. 4.34: SEM image of ZnO:ErLi particles by SSR at 2.00 KX.

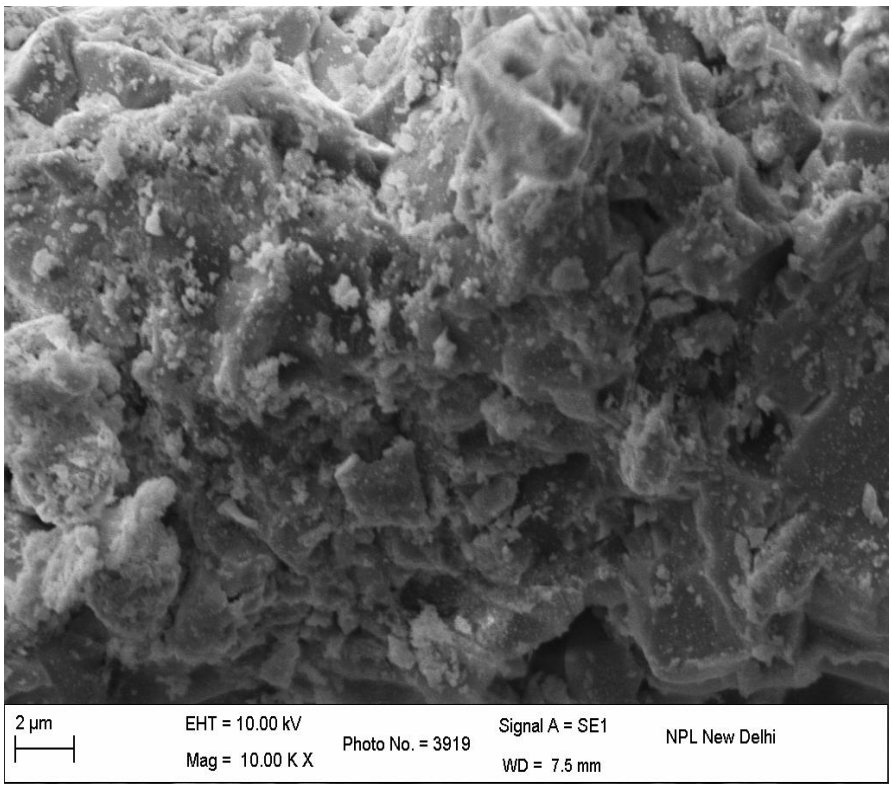

Fig. 4.35: SEM image of ZnO:ErLi particles by SSR at 10.00 KX

10.ZnO:Er(2%)Yb(10%) by SSR:

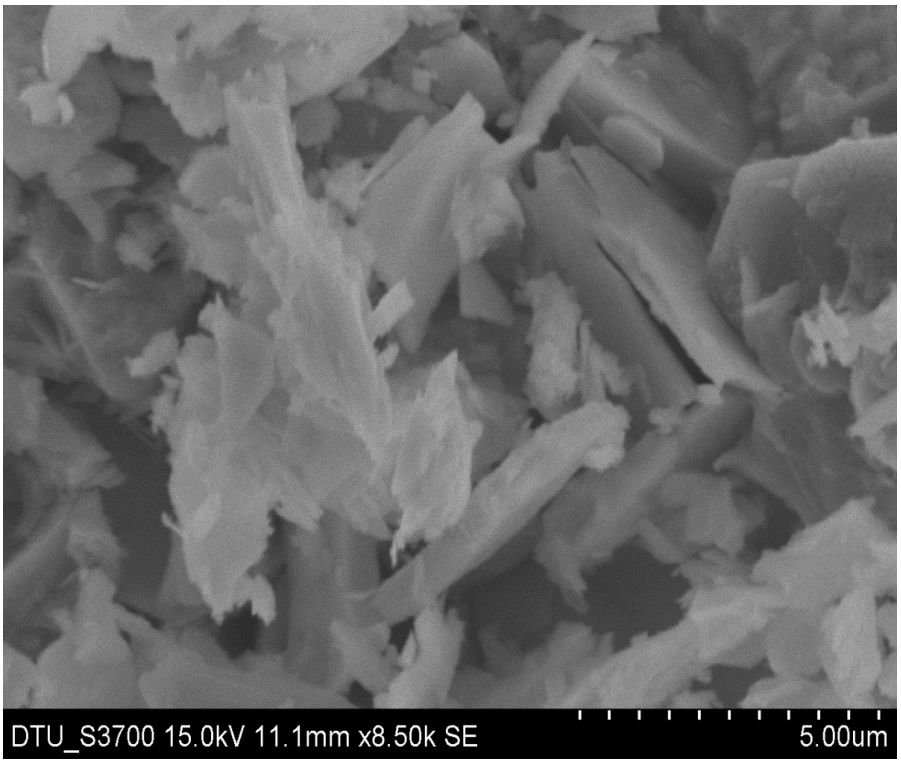

Fig. 4.36: SEM image of ZnO:ErYb particles by SSR at 8.50 KX.

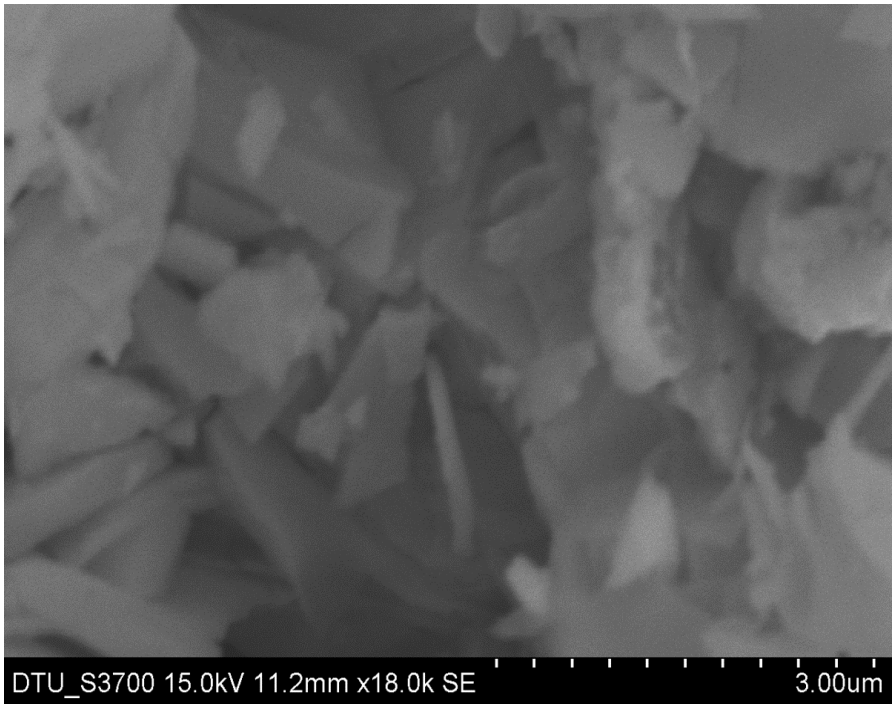

Fig. 4.37: SEM image of ZnO:ErYb particles by SSR at 18.0 KX.

11.ZnO:Er(2%)Yb(10%) annealed at 800°C by SSR:

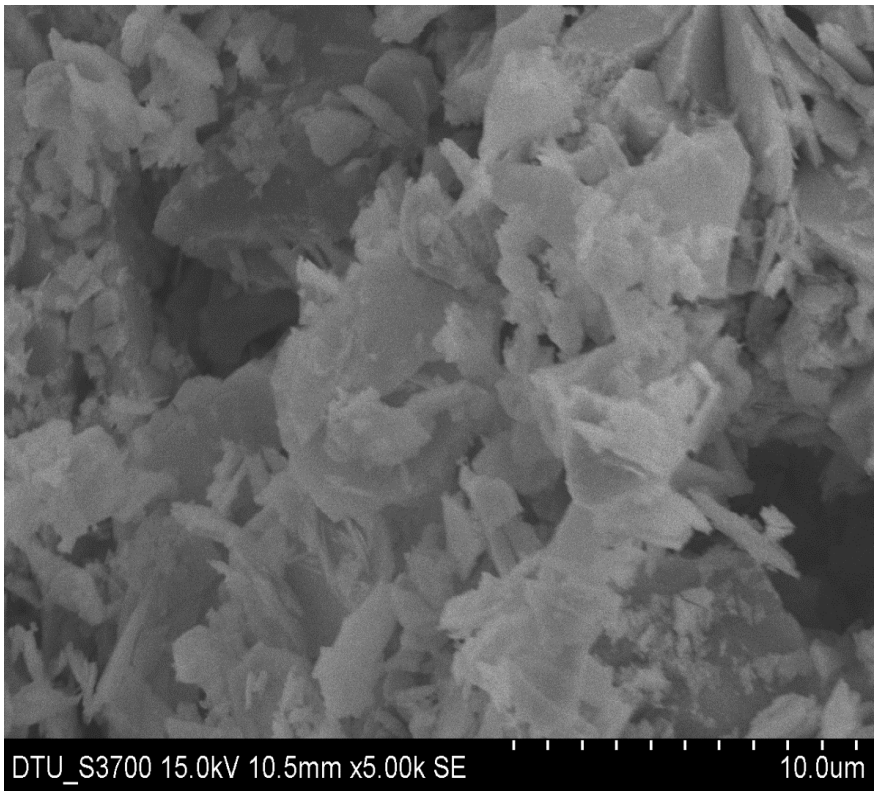

Fig. 4.38: SEM image of ZnO:ErYb annealed at 800°C particles by SSR at 5.0 KX.

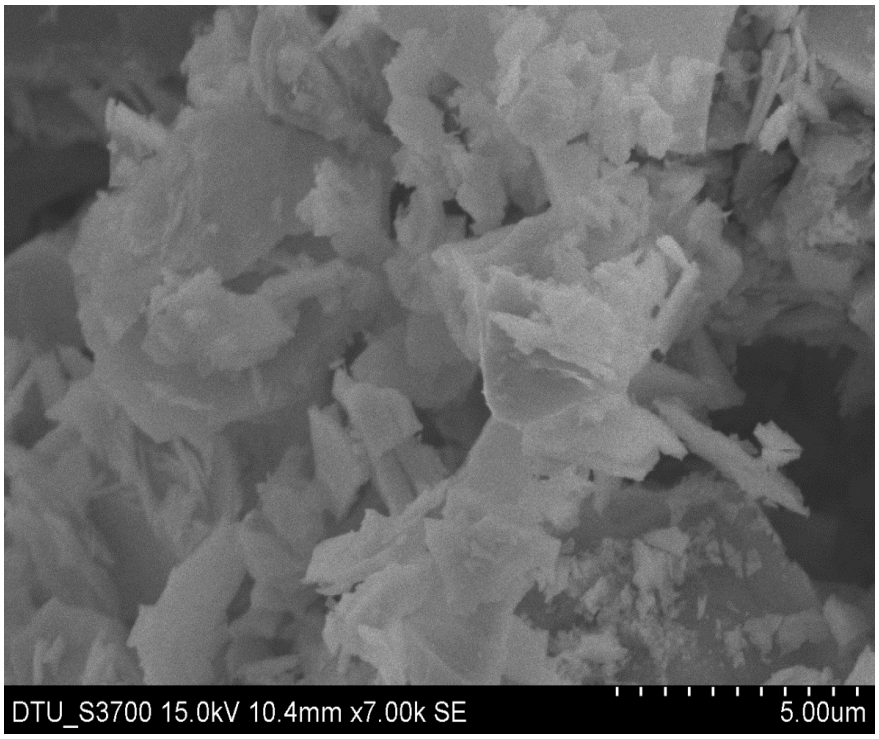

Fig. 4.39: SEM image of ZnO:ErYb annealed at 800°C particles by SSR at 7.0 KX.

Fig 4.38 to 4.39 show the scanning electron micrographs of ZnO:Er(2%)Yb(10%) annealed at 800°C synthesized by the Solid State Reaction method. Flake like morphology has been observed.

12.ZnO:Ho(2%) by SSR:

Fig 4.40 to 4.41 show the scanning electron micrographs of ZnO:Ho(2%) synthesized by the Solid State Reaction method.

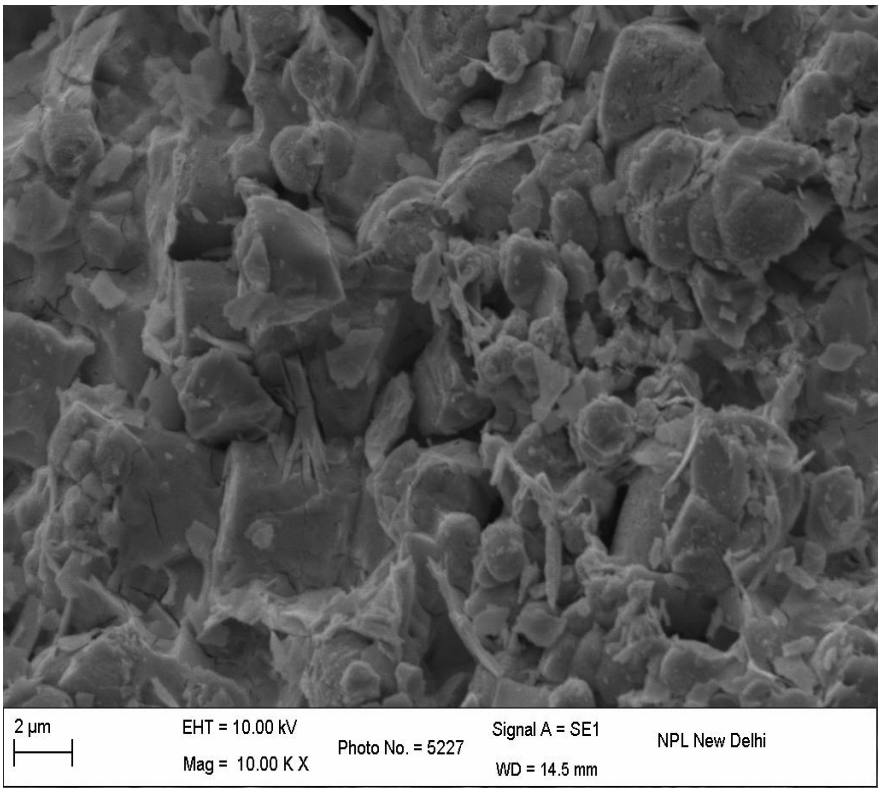

Fig. 4.40: SEM image of ZnO:Ho particles by SSR at 10.00 KX.

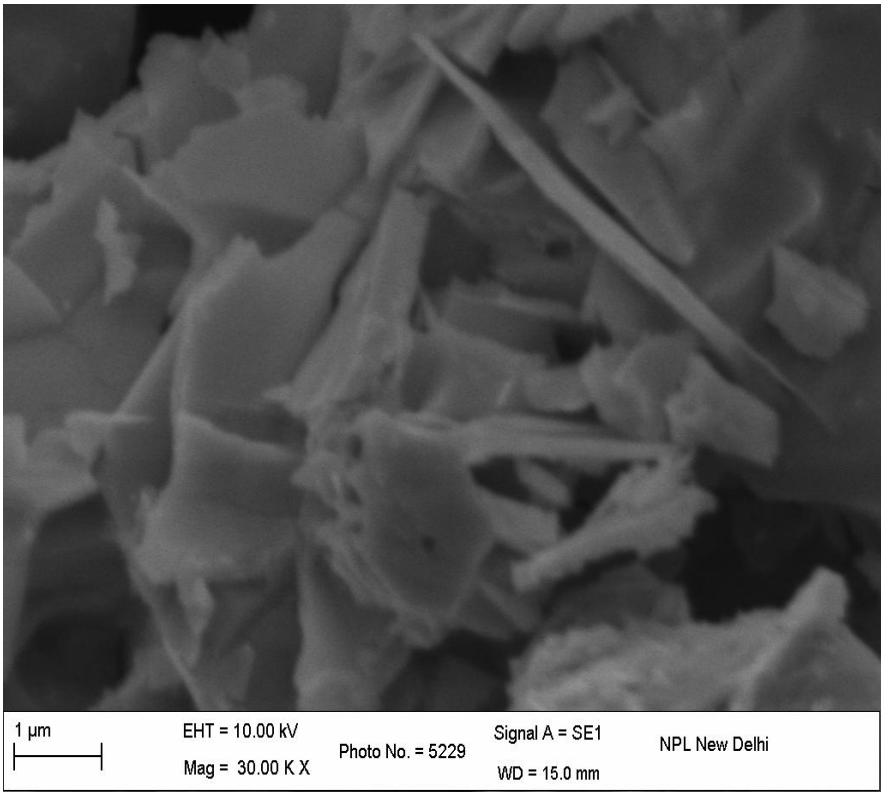

Fig. 4.41: SEM image of ZnO:Ho particles by SSR at 30.00 KX.

13.ZnO:Ho(2%)Yb(10%) by SSR:

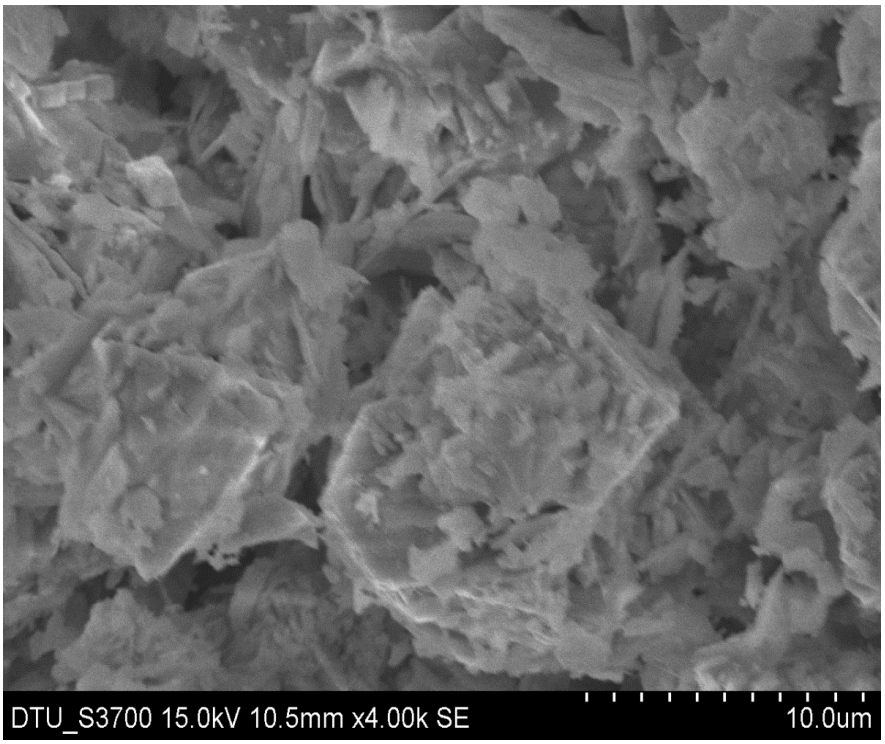

Fig. 4.42: SEM image of ZnO:HoYb particles by SSR at 4.00 KX.

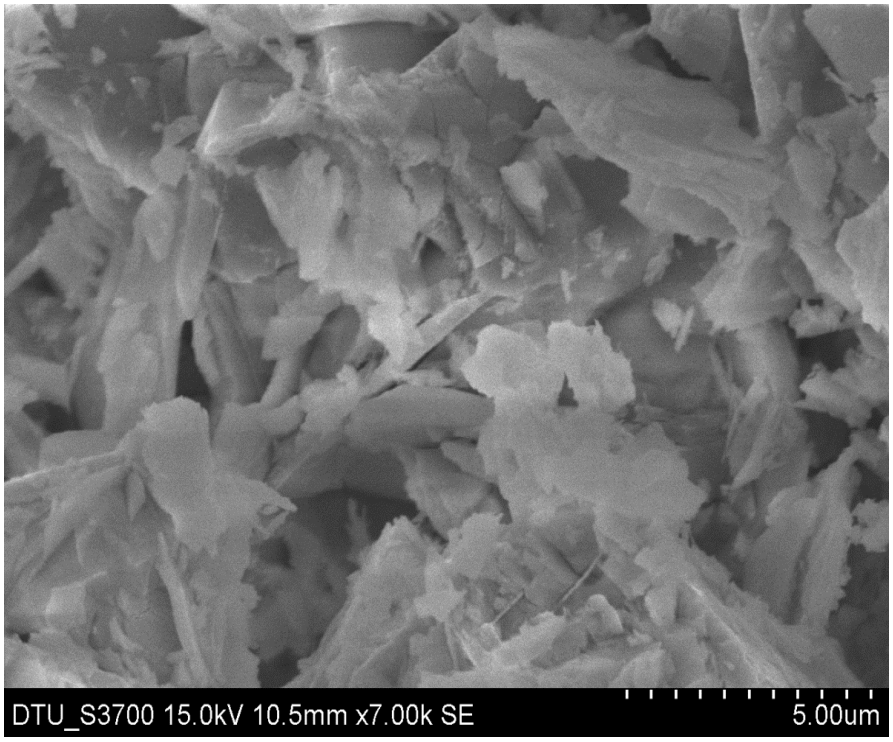

Fig. 4.43: SEM image of ZnO:HoYb particles by SSR at 7.00 KX.

Fig 4.41 to 4.42 show the scanning electron micrographs of ZnO:Ho(2%)Yb(10%) synthesized by the Solid State Reaction method. The particle exbibit flake like morphology.

4.2.1 Observation from SEM images:

ZnO samples doped with different rare earth ions, synthesized by CPP method indicate very small particles as shown in fig. 4.15 to 4.29. The particle size is in few nanometres and they form flower like structure. To further investigate the morphology of the nanoparticles synthesized by Co-Precipitation methods, Transmission electron Microscopy (TEM) has been used.

On the other hand, fig 4.30 to 4.43 show the SEM images of ZnO doped with different rare earth elements synthesized by solid state reaction methods. In the case where the SSR method was used, the particles are well formed with flake like morphology.

4.3 Morphology by Transmission Electron Microscope [TEM]:

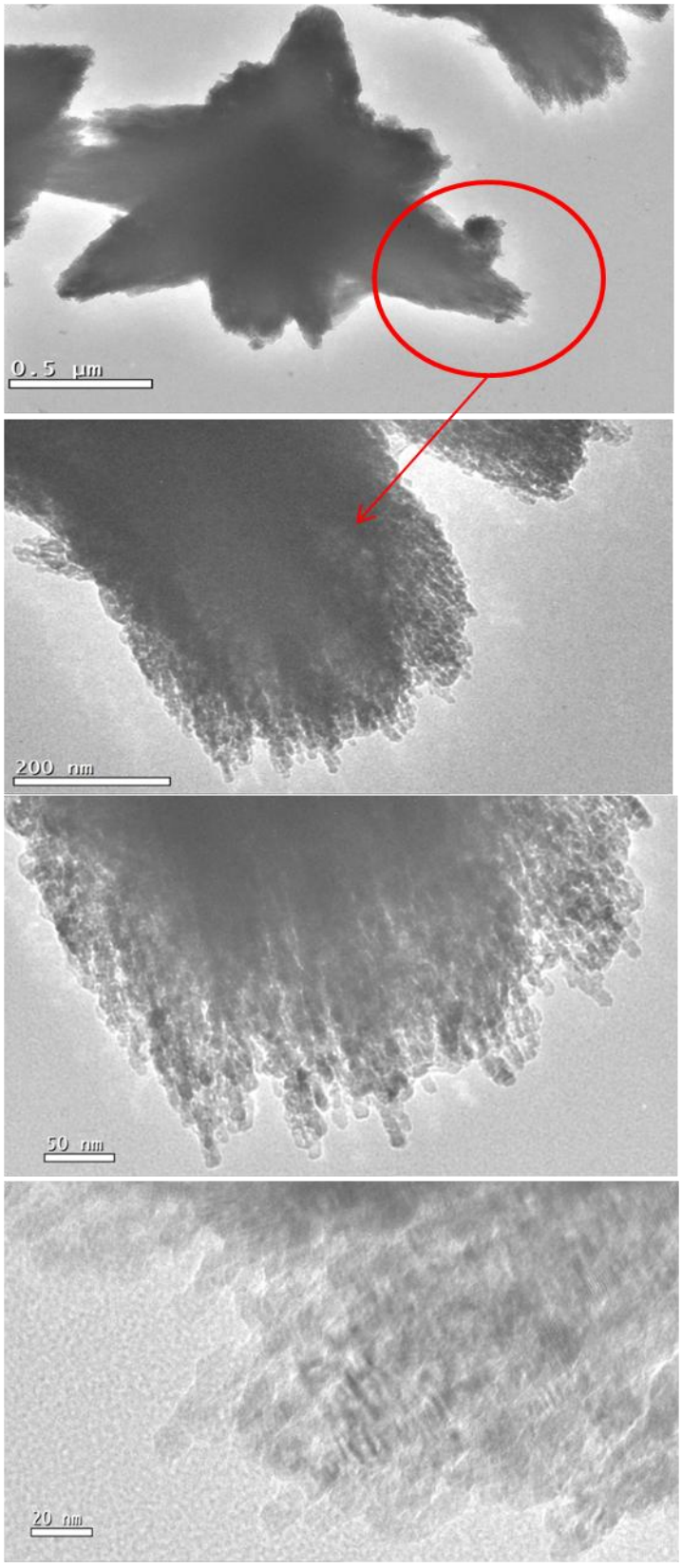

Fig 4.44: TEM images of ZnO:Er(2%) by CPP.

4.3.1 Observation from TEM images:

The size and morphology of ZnO:Er nanoparticles synthesized by CPP method were studied by TEM. From the TEM micrographs of ZnO:Er sample, it is clearly seen that flower type structure is formed by large number of small particles and size of individual nanoparticles range from 5nm to 10nm.

4.4 Photoluminescence (PL):

The luminescence characteristic of ZnO doped with different rare earth dopants with different morphology and sizes were investigated using combined steady state fluorescence and phosphorescence life time spectrometer (Edinburgh Instruments FLSP920 system).

4.4.1 Down Conversion (Excitation by UV):

1. Undoped ZnO by CPP:

The photoluminescence emission and excitation spectra of undoped ZnO powder sample are shown in the following figures.

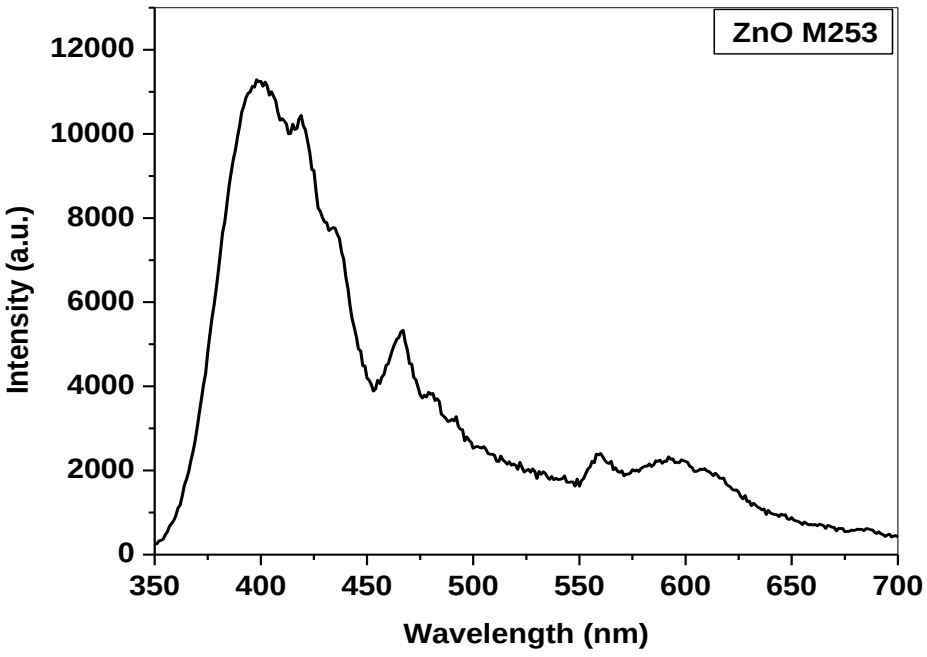

Fig 4.45: Emission spectra of undoped ZnO by CPP at 253 nm.

The emission and excitation spectra of Undoped ZnO by CPP are shown in fig 4.49. For this sample a violet light was observed, which consists of the typical emission at 406 nm. The excitation spectra (λ_{em}=406 nm) have a narrow excitation band around 394 nm.

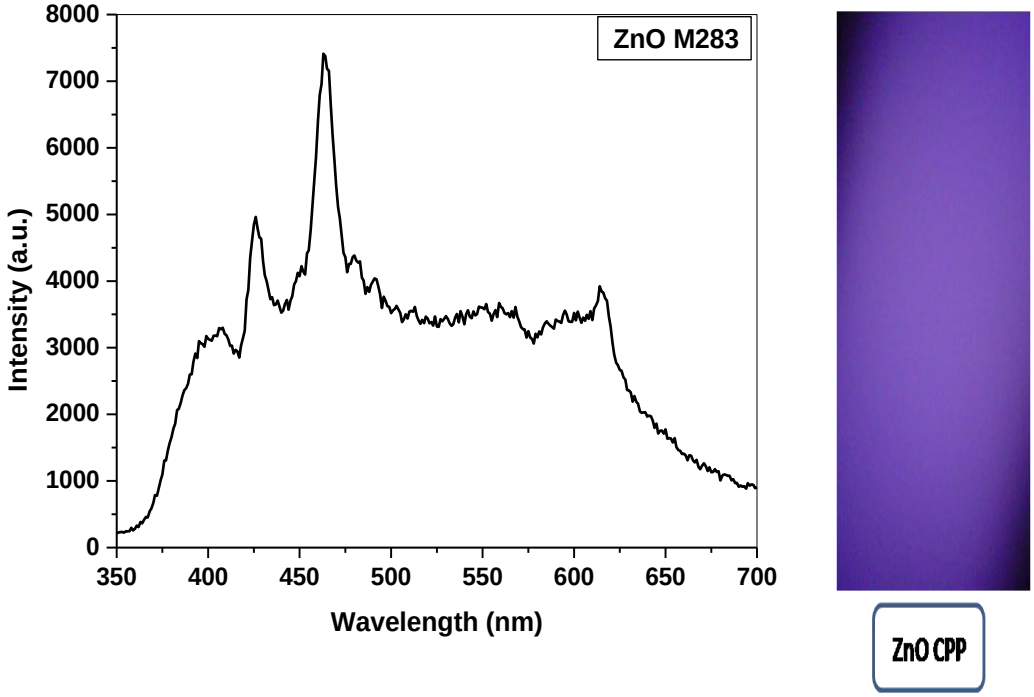

Fig 4.46: Emission spectra of undoped ZnO by CPP at 283 nm.

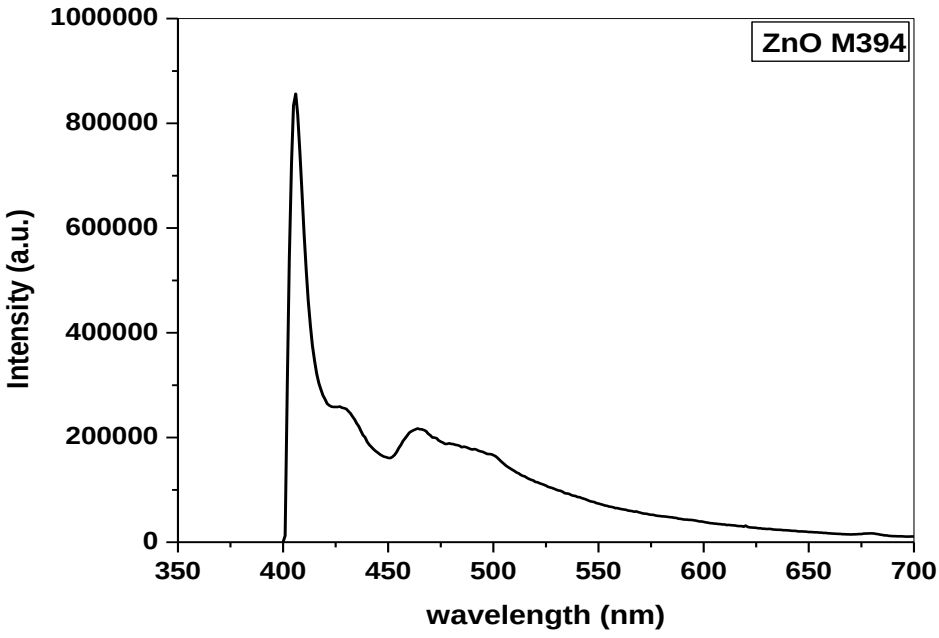

Fig 4.47: Emission spectra of undoped ZnO by CPP at 394 nm.

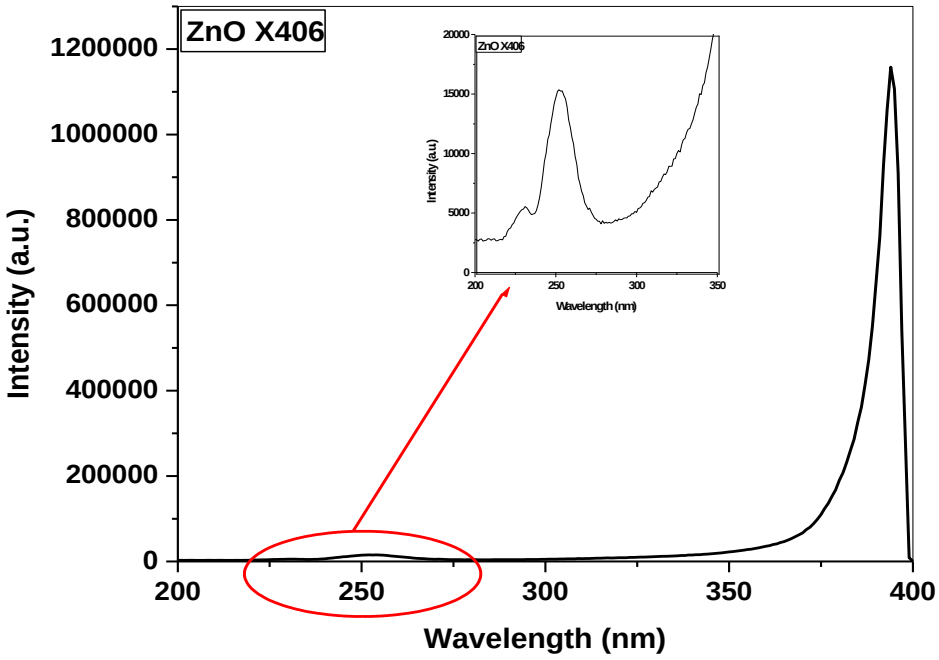

Fig 4.48: Excitation spectra of undoped ZnO by CPP at 406 nm.

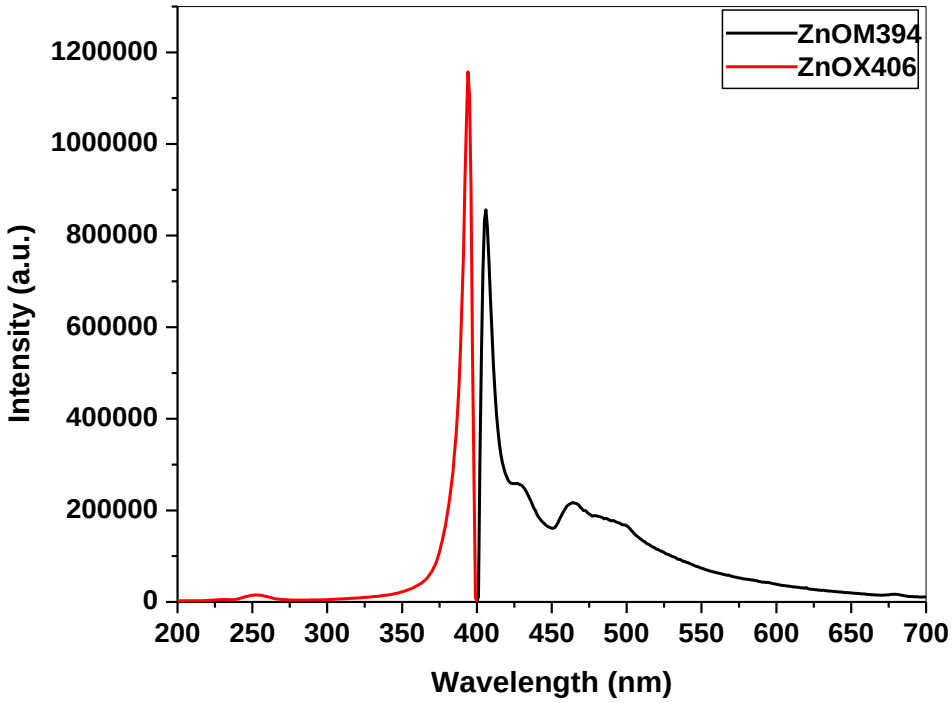

Fig 4.49: Photoluminescence Excitation and Emission spectra of undoped ZnO

Emission line at 406 nm is due to interstitial defects. Fig 4.50 shows broad band emission spectra at the excitation wavelength of 283 nm. At this wavelength sample gives white light but dominated by violet region. Emission spectrum at the excitation wavelength of 394 nm gives a sharp peak at 406 nm and gives violet light. Fig 4.49 shows excitation and emission spectra of undoped ZnO at the wavelength of 406 and 394 nm respectively.

2. ZnO:Er(2%) by CPP:

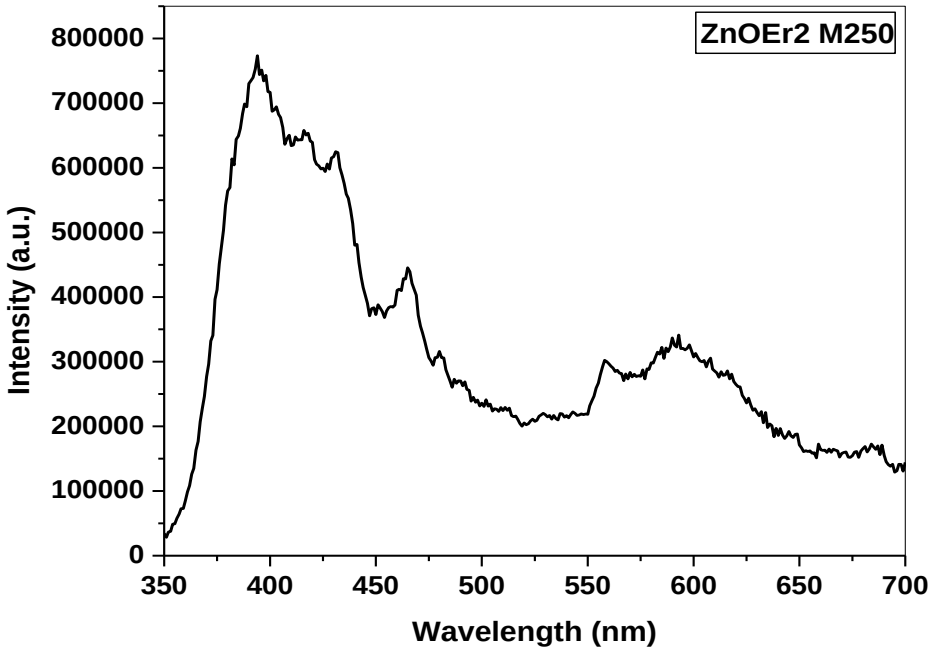

Fig 4.50: Emission spectra of ZnO:Er by CPP at 250 nm.

The emission and excitation spectra of ZnO:Er(2%) by CPP is shown in fig 4.50, 4.51, 4.52 and 4.53. For this sample a blue light was observed, which consists of the typical emission at 394 nm. The excitation spectra (λ_{em}=430 nm) have a narrow excitation band around 340 nm. Fig 4.50 shows emission spectra at excitation wavelength of 253 nm which gives broad spectrum with highest peak at 394 and dominated by blue region. Thus colour of this sample is light blue. Emission spectra at wavelength 283 nm also give broad band spectrum; peaks at 394, 428 and 465 nm.

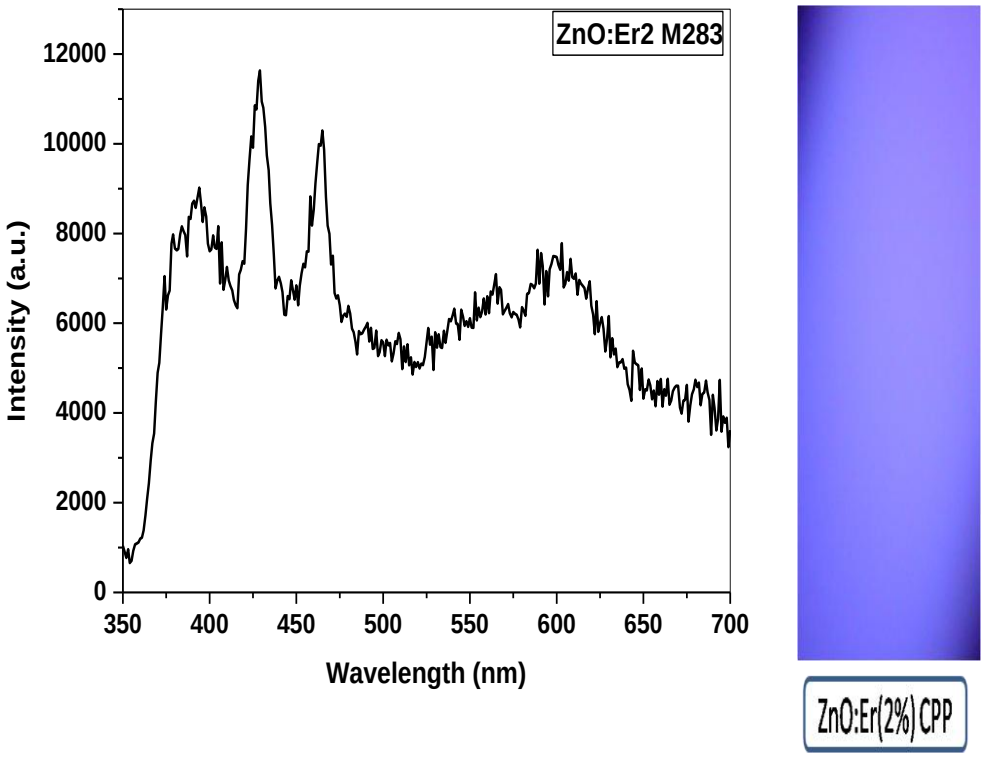

Fig 4.51: Emission spectra of ZnO:Er by CPP at 283 nm.

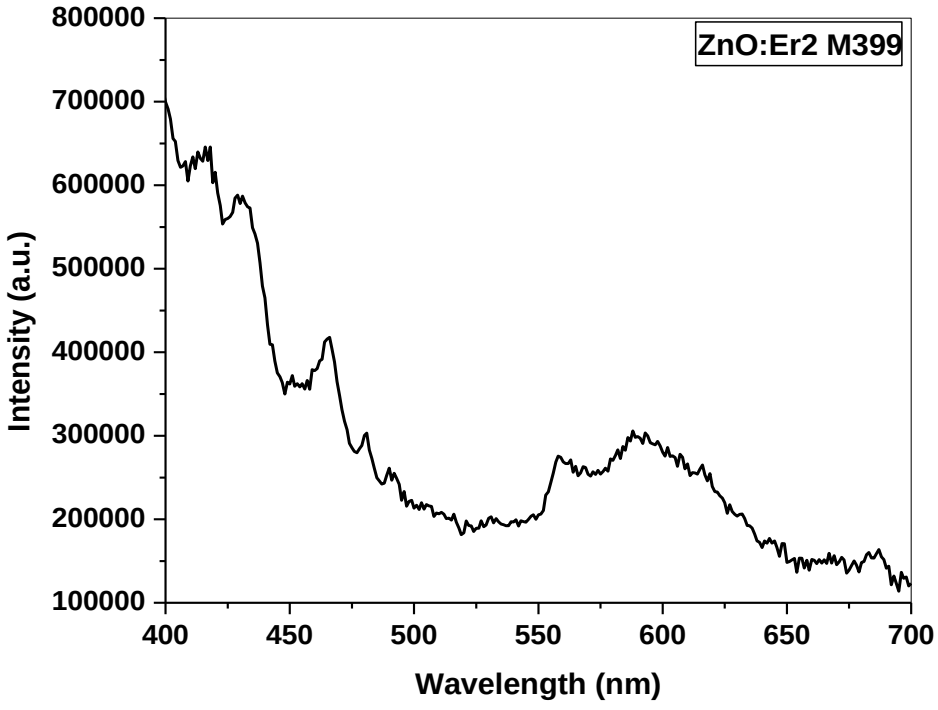

Fig 4.52: Emission spectra of ZnO:Er by CPP at 399 nm.

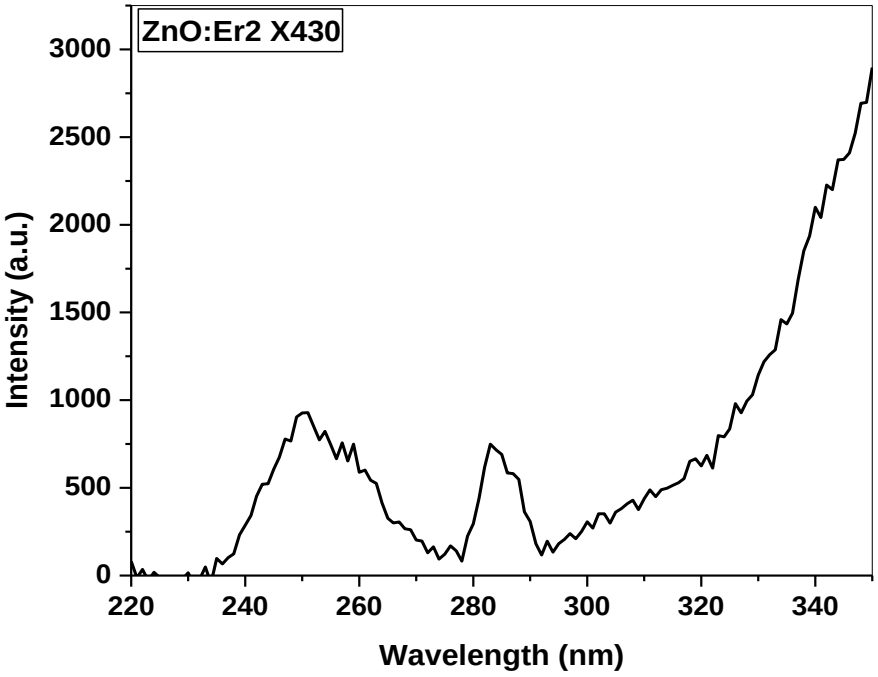

Fig 4.53: Excitation spectra of ZnO:Er by CPP at 430 nm.

3. ZnO:Er(2%)Yb(10%) by CPP:

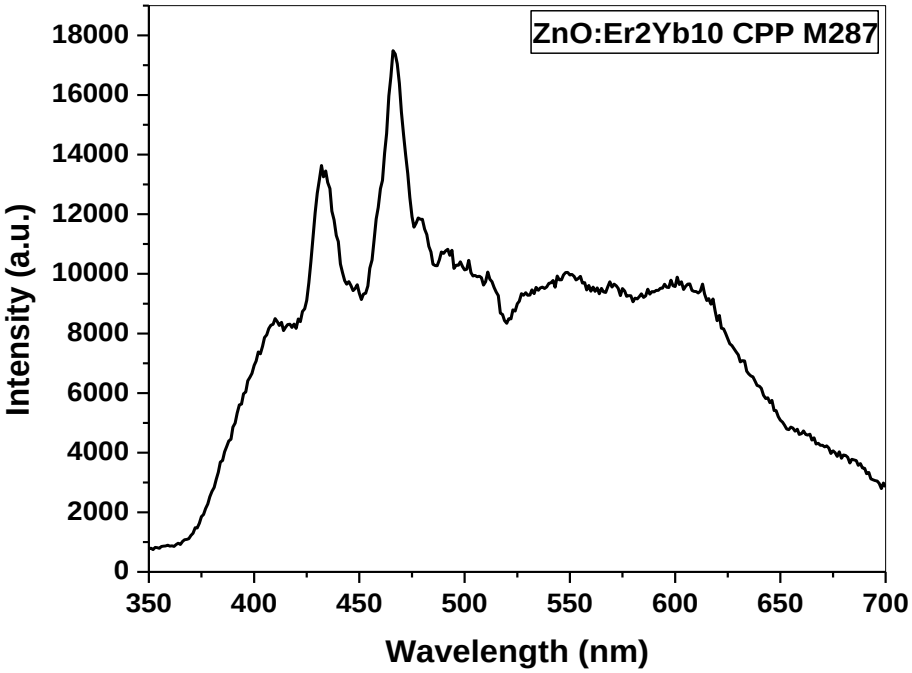

Fig 4.54: Emission spectra of ZnO:ErYb by CPP at 287 nm.

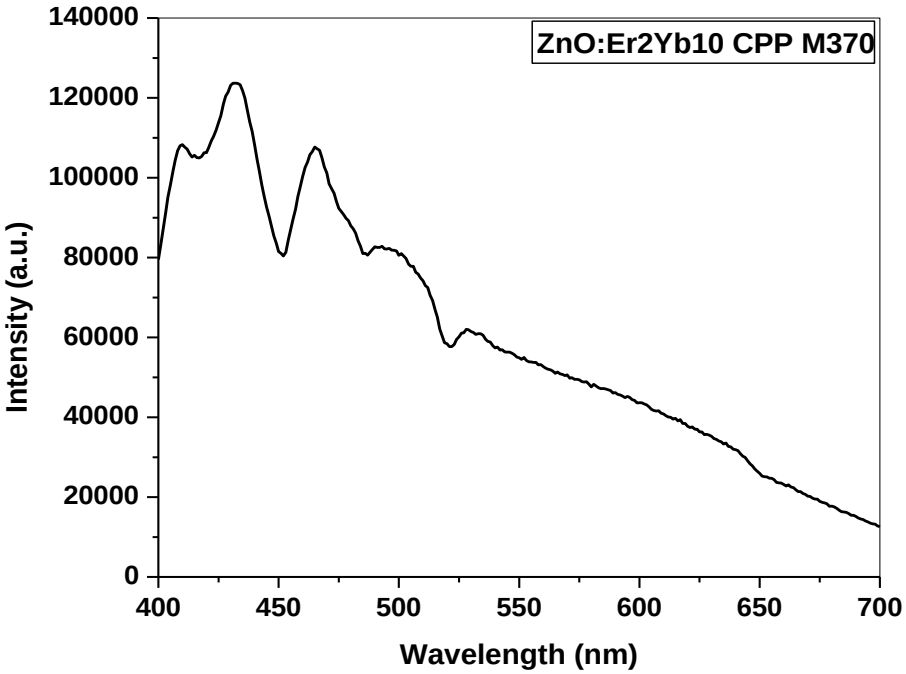

Fig 4.55: Emission spectra of ZnO:ErYb by CPP at 370 nm.

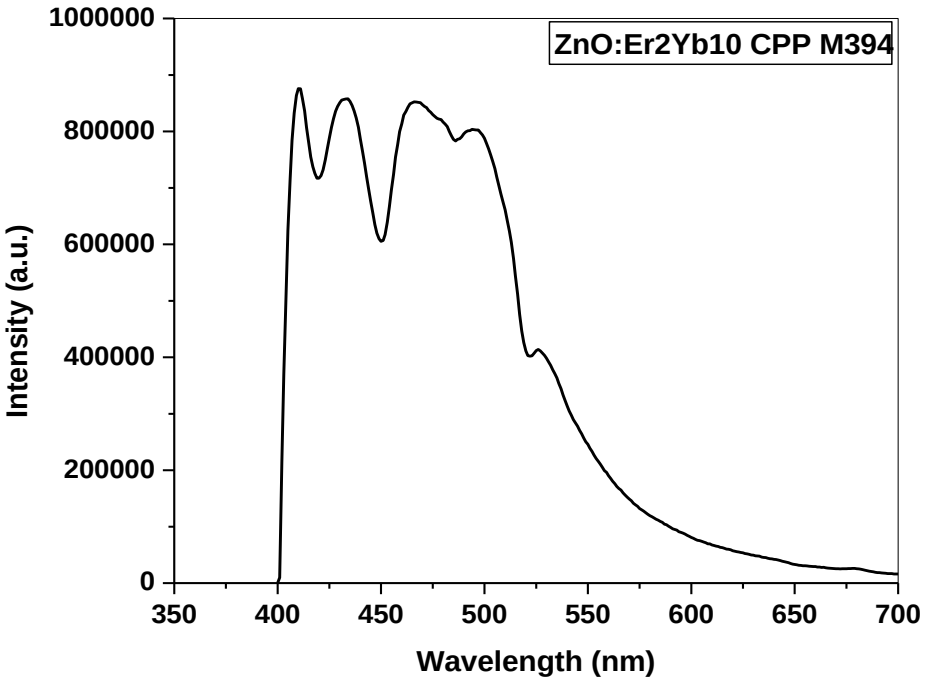

Fig 4.56: Emission spectra of ZnO:ErYb by CPP at 394 nm.

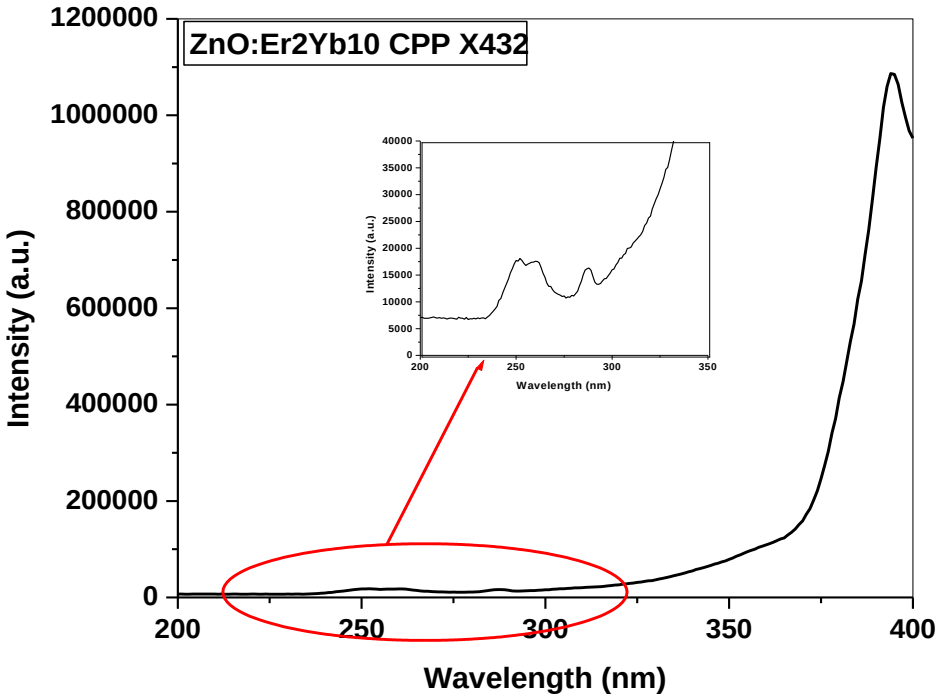

Fig 4.57: Excitation spectra of ZnO:ErYb by CPP at 432 nm.

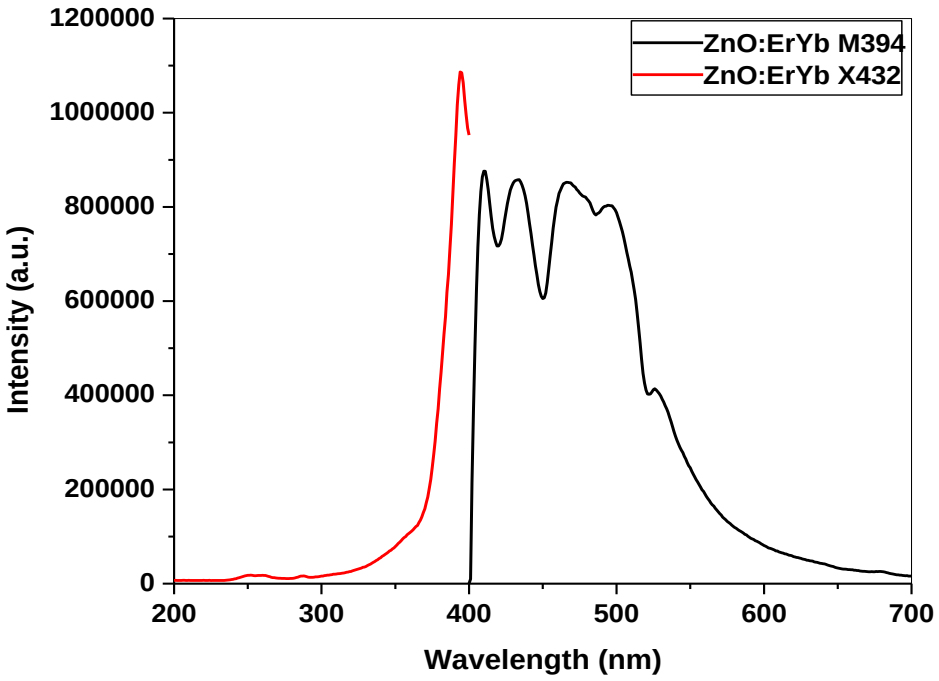

Fig 4.58: Excitation and Emission spectra of ZnO:ErYb by CPP.

The emission and excitation spectra of ZnO:Er(2%)Yb(10%) by CPP are shown in fig 4.54, 4.55, 4.56, 4.57 and 4.58. For this sample a blue light (brighter than ZnO:Er by CPP) was observed, which consists of the typical emission at 409 nm. The excitation spectra (λ_{em}=432 nm) have a narrow excitation band around 394 nm. Fig 4.56 shows emission spectra at excitation wavelength of 394 nm which gives broad spectrum with peak at 410, 432, 467 and 497 and dominated by blue region. Thus colour of this sample is brighter than ZnO:Er. Here also blue colour is due to more doping this sample has more defects thus blue light is more intense.

4. ZnO:Ho(2%) by CPP:

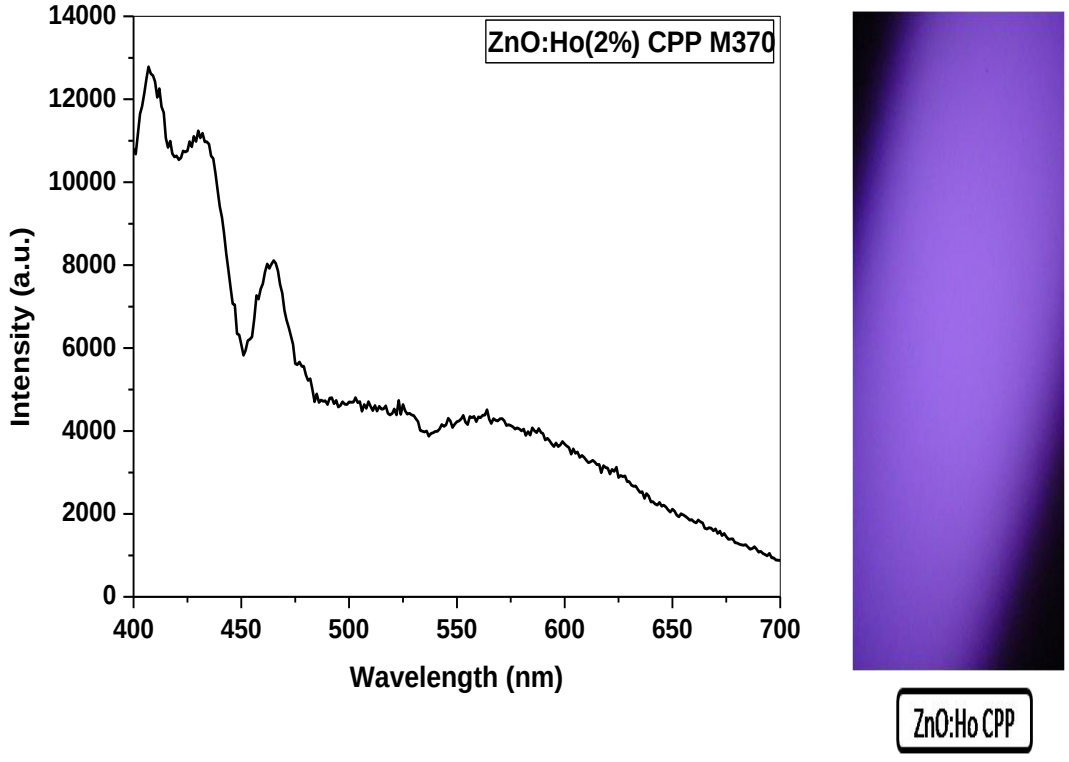

Fig 4.59: Emission spectra of ZnO:Ho by CPP at 370 nm.

The emission and excitation spectra of ZnO:Ho(2%) by CPP are shown in fig 4.59, 4.60, and 4.61. For this sample violet light was observed, which consists of the typical emission at 407 nm. The excitation spectra (λ_{em}=563 nm) have a narrow excitation band around 394 nm. Fig 4.59 shows emission spectra at excitation wavelength of 370 nm which gives broad spectrum with peak at 407, 430 and 465; dominated by violet region. Thus colour of this sample is violet (brighter than undoped

ZnO). Here also colour is due to interstitial defects and due to doping this sample have more defects thus violet light is more intense compare to undoped ZnO.

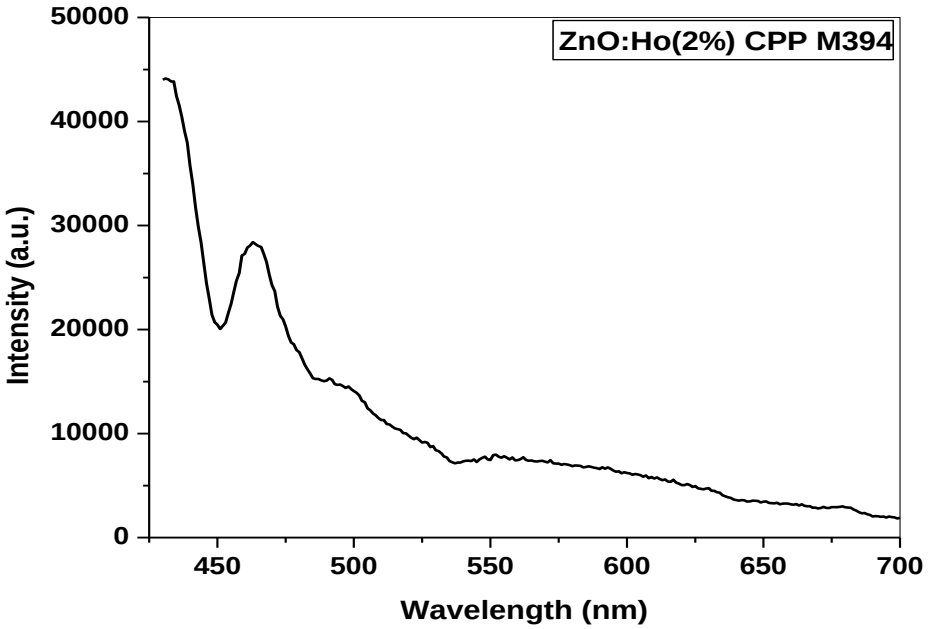

Fig 4.60: Emission spectra of ZnO:Ho by CPP at 394 nm.

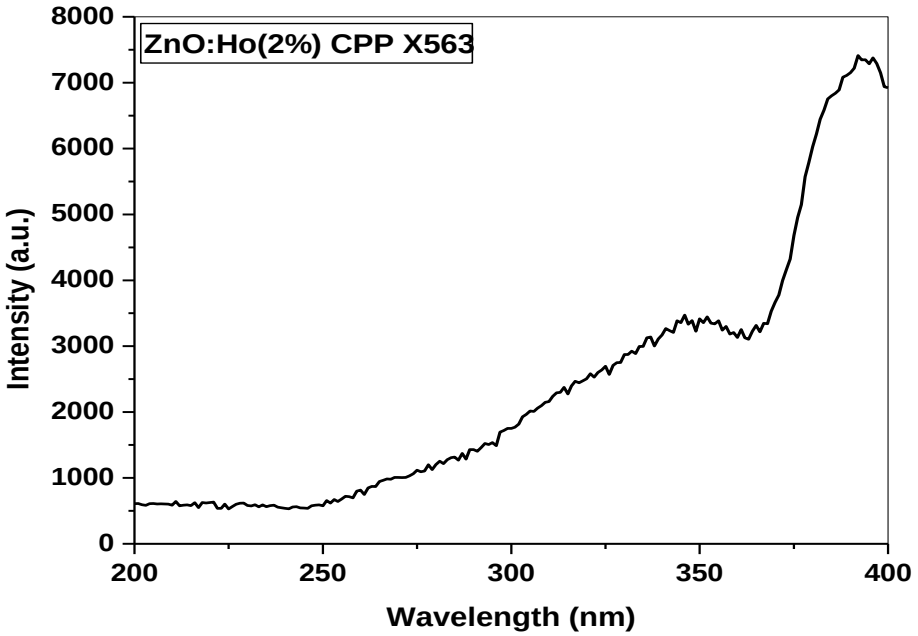

Fig 4.61: Excitation spectra of ZnO:Ho by CPP at 563 nm.

5. Comparison of down conversion emission spectra of undoped and doped ZnO prepared by room temperature CPP method:

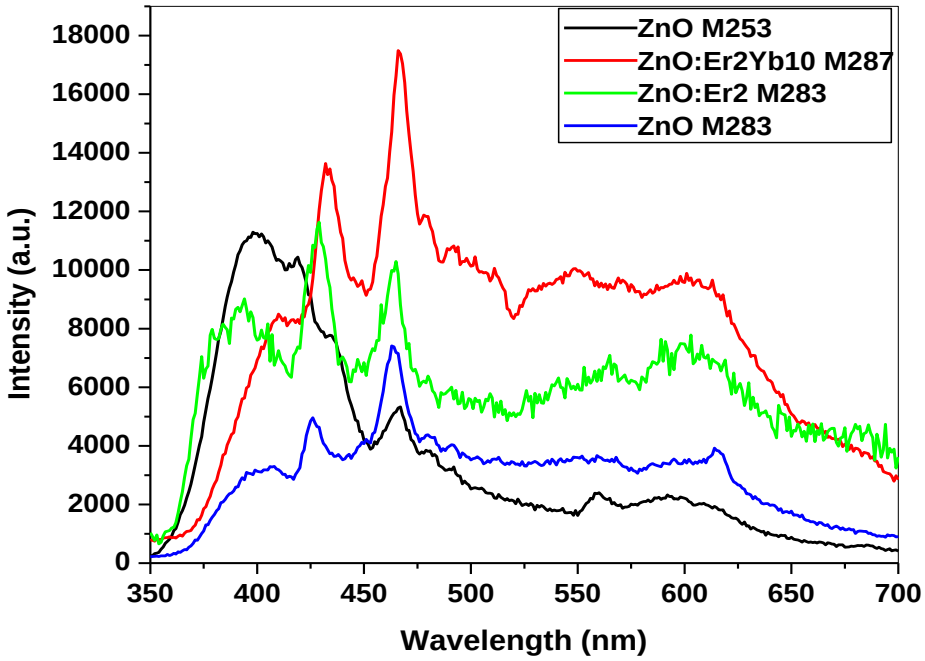

Fig 4.62: Comparison between emission spectra of doped ZnO by CPP at 287 nm

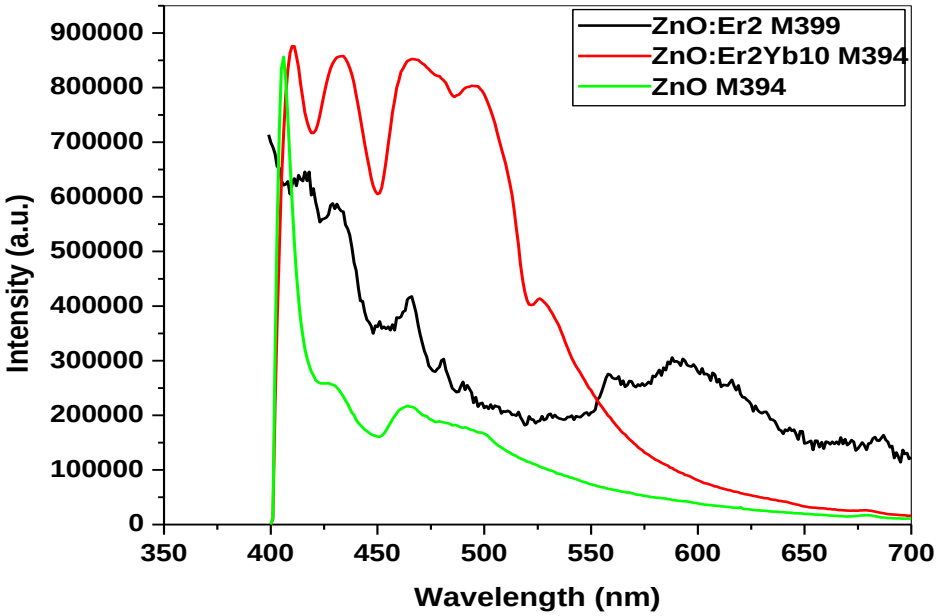

Fig 4.63: Comparison between emission spectra of doped ZnO by CPP at 394 nm

Comparison of emission spectra of undoped and rare earth doped ZnO at two different excitation wavelength indicate that photoluminescence intensity increases with rare earth doping, though peak positions in undoped and doped ZnO samples remain same. Maximum intensity has been observed for ZnO:Er,Yb sample. The PL emission spectra is quite broad and the samples show bright white to reddish under UV light. The observation indicate that the fluorescence emission from undoped as well as rare earth doped ZnO samples under UV excitation (band to band) arises due to intrinsic defects of ZnO e.g., zinc vacancy, oxygen vacancy, zinc interstitial etc. Due to doping of trivalent rare earth ion in place of divalent zinc, charge compensation would require creation of more vacancy/interstitial defects leading to increased emission. Such defects may form either donor (e.g., zinc interstitial) or acceptor (e.g., zinc vacancy) type defects and PL arises due to recombination of charges trapped in such defects upon UV excitation.

6. Undoped ZnO by SSR:

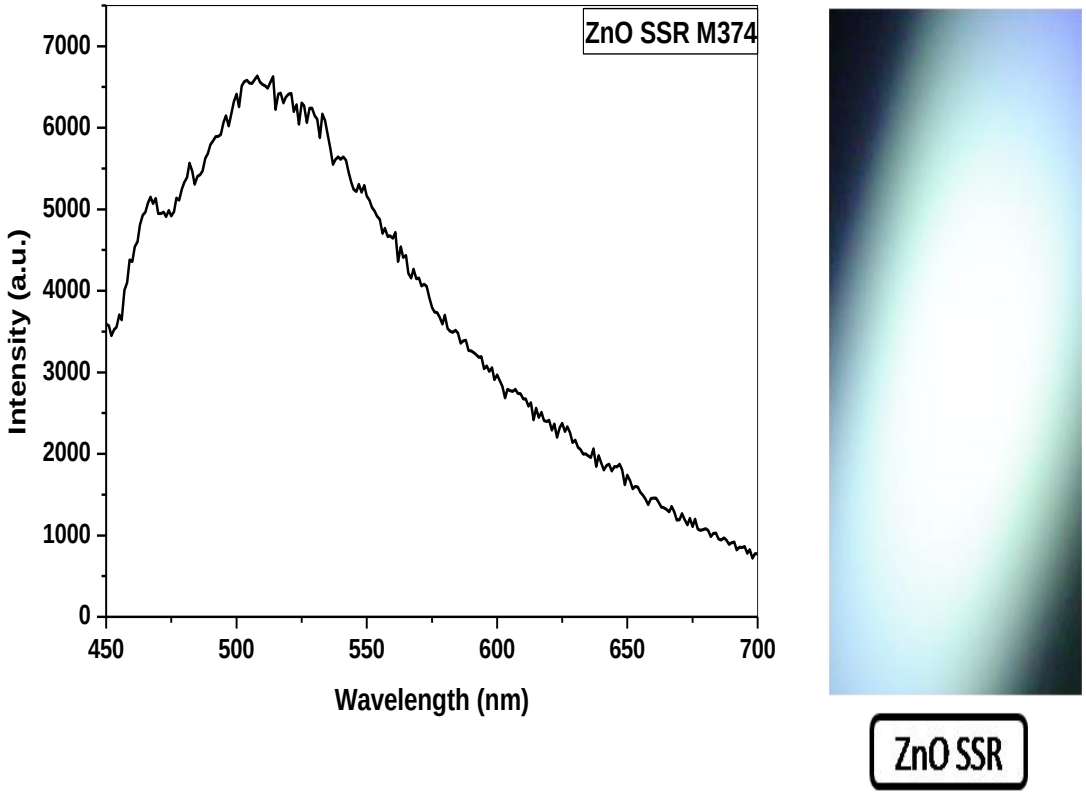

Fig 4.64: Emission spectra of Undoped ZnO by SSR at 374 nm.

The emission and excitation spectra of undoped ZnO prepared by SSR are shown in fig 4.64, 4.65, and 4.66. For this sample greenish white light was observed, which consists of the typical emission at 511 nm. The excitation spectra (λ_{em}=511 nm) have a broad excitation band around 372 nm. Fig 4.64 shows emission spectra at excitation wavelength of 374 nm which gives broad spectrum around 511nm. In this spectrum only broad band occurs and not any particular peak exists thus colour of this sample is greenish white. Here also colour is due to intrinsic point defects such as oxygen vacancy.

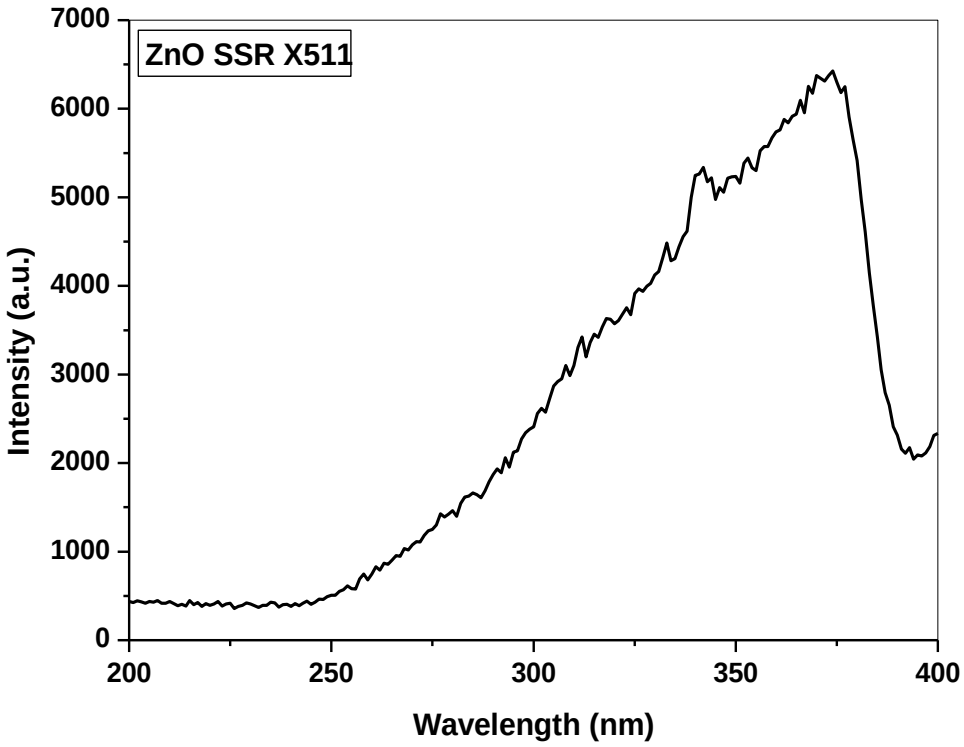

Fig 4.65: Excitation spectra of Undoped ZnO by SSR at 511 nm.

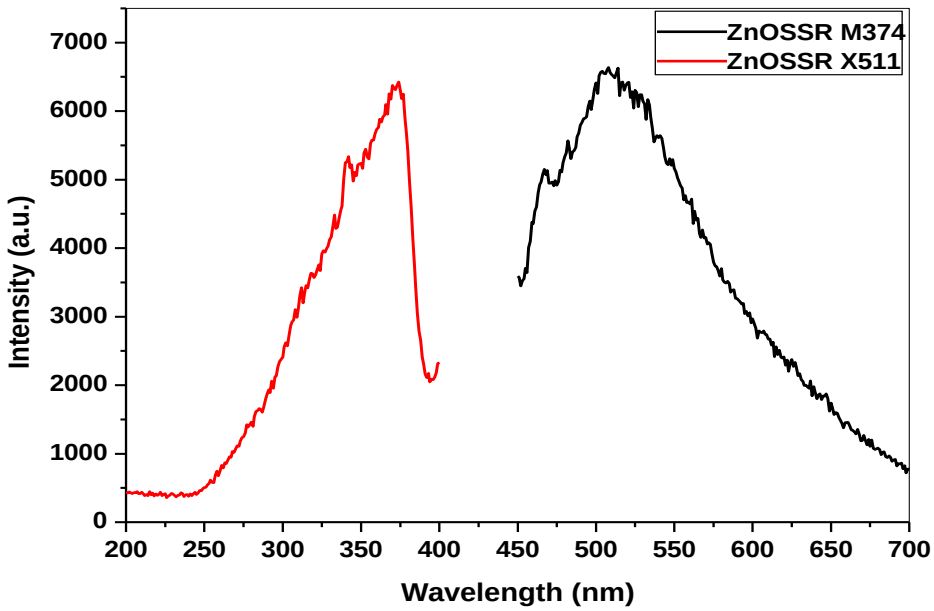

Fig 4.66: Emission & Excitation spectra of Undoped ZnO by SSR.

The PL excitation spectra (red) shows typical sharp band edge excitation peak at 374nm. The emission spectra (black) show broad visible emission with peak in the green region (511nm).

7. ZnO:Er(2%) by SSR:

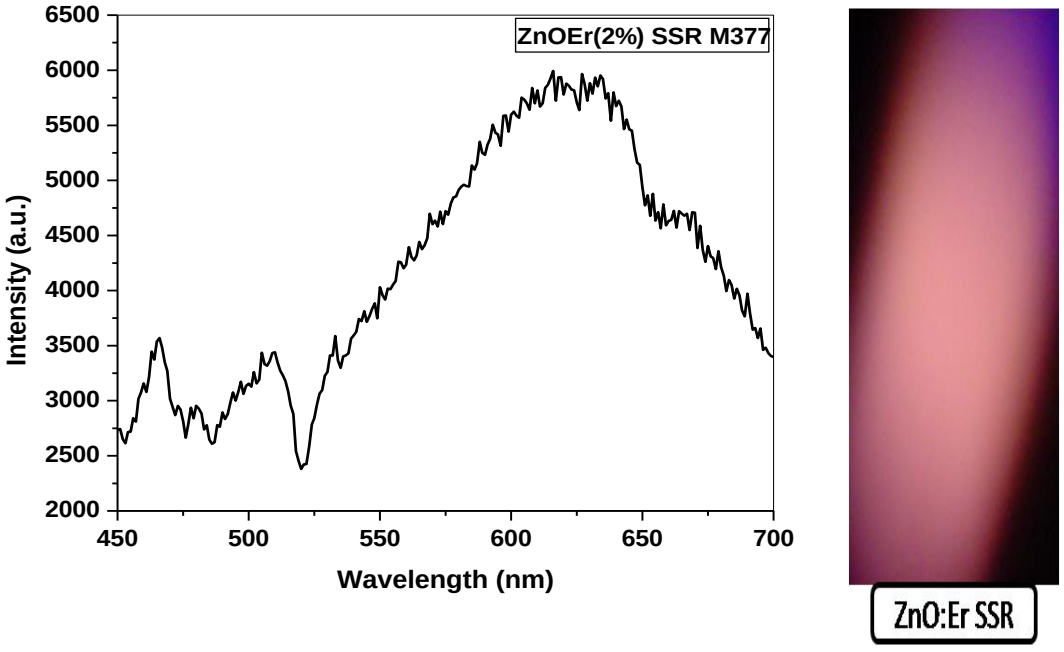

Fig 4.67: Emission spectra of ZnO:Er by SSR at 377 nm.

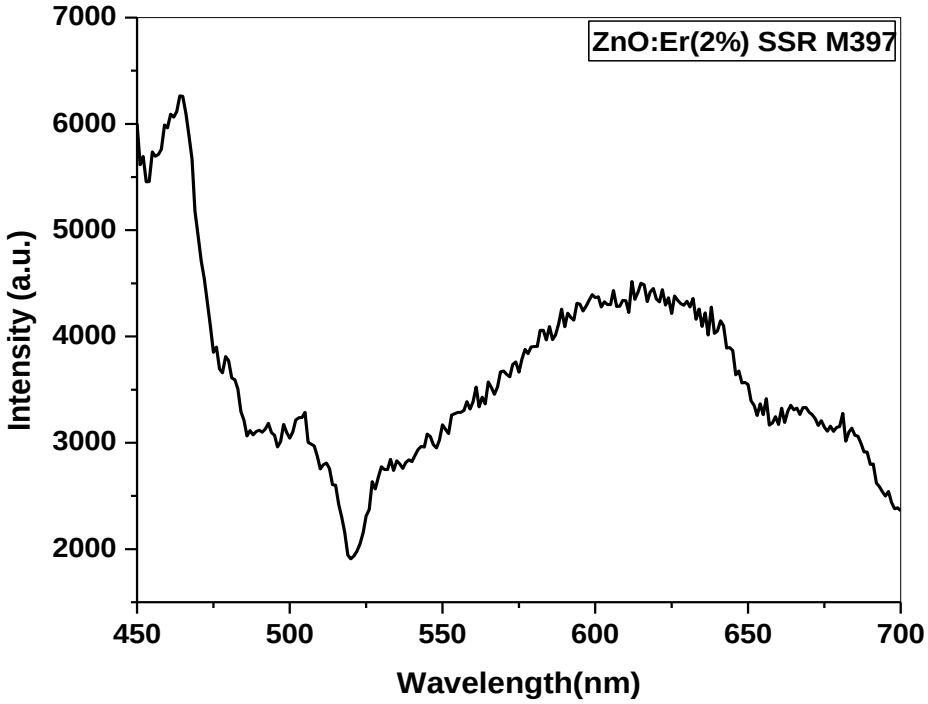

Fig 4.68: Emission spectra of ZnO:Er by SSR at 397 nm.

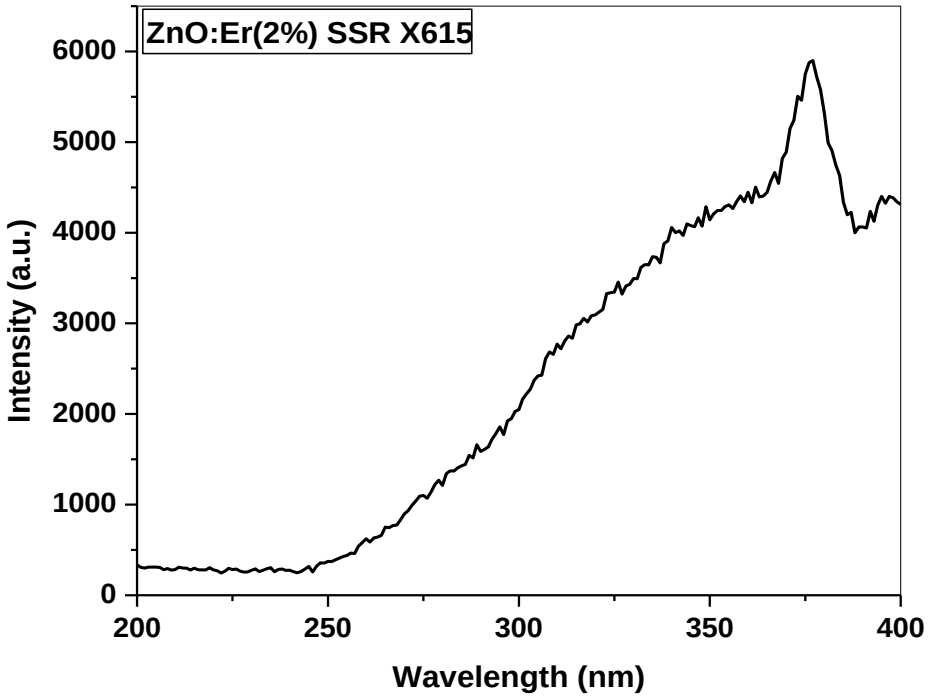

Fig 4.69: Excitation spectra of ZnO:Er by SSR at 615 nm.

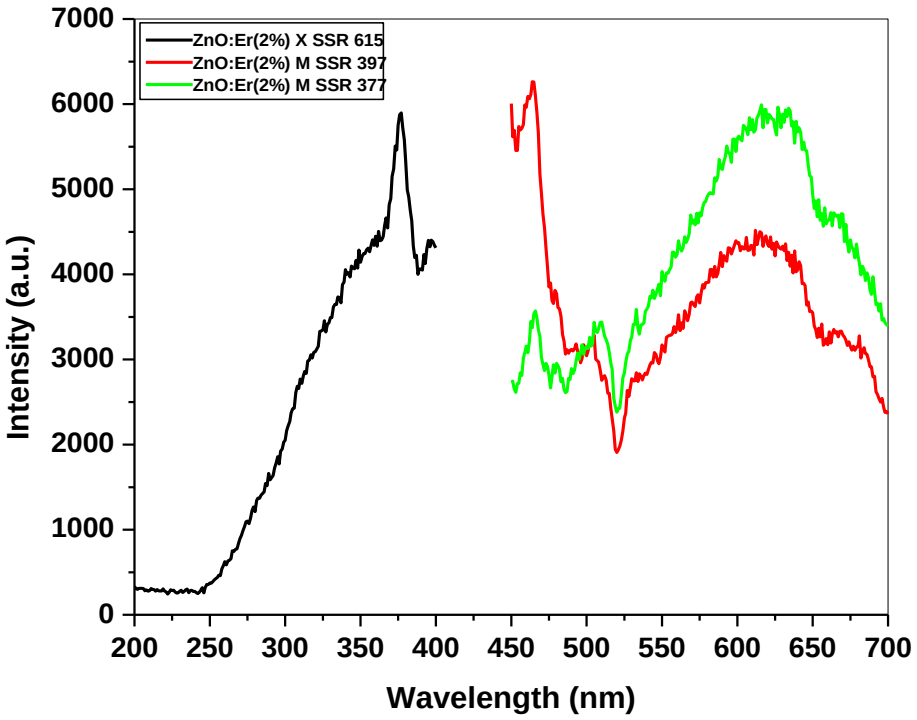

Fig 4.70: Comparison between Emission & Excitation spectra of ZnO:Er by SSR.

The emission and excitation spectra of ZnO:Er(2%) prepared by SSR are shown in fig 4.67, 4.68, 4.69 and 4.70. For this sample orange red light was observed, which consists of the broad emission with peak at 615 nm. The excitation spectra (λ_{em}=615 nm) have a sharp peak at 377 nm. Fig 4.67 shows emission spectra at excitation wavelength of 377 nm which gives broad spectrum around 615 nm. In this spectrum broad band emission occurs which peaks in the orange red region and thus colour of this sample is orange red. The excitation spectra (in Fig 4.70) show sharp band edge absorption peak and emission spectra is broad covering orange red region, in addition to a sharp peak in the blue part of the spectral region for both excitation wavelengths i.e., 377nm, 394nm. The orange red emission probably arises from dopant Er related defect centers.

8. ZnO:Er(2%)Li(2%) by SSR:

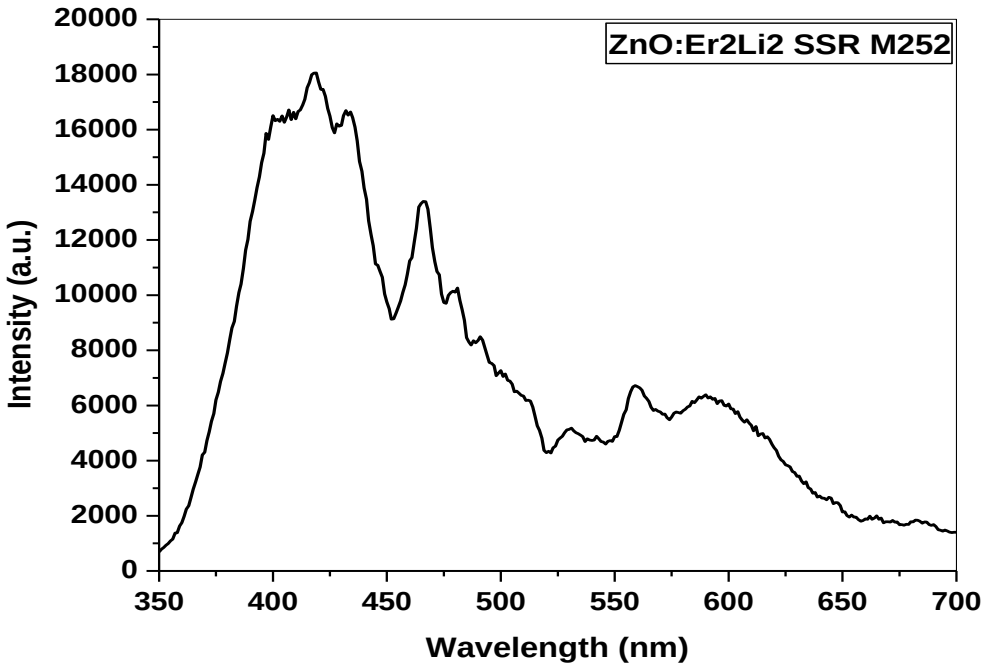

Fig 4.71: Emission spectra of ZnO:ErLi by SSR at 252 nm.

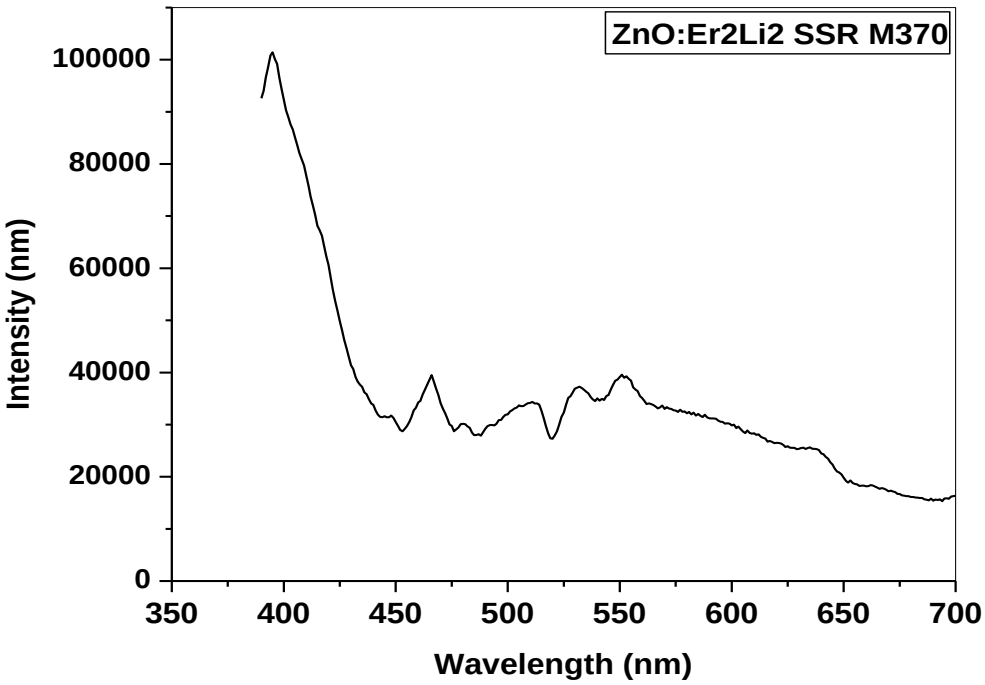

Fig 4.72: Emission spectra of ZnO:ErLi by SSR at 370 nm.

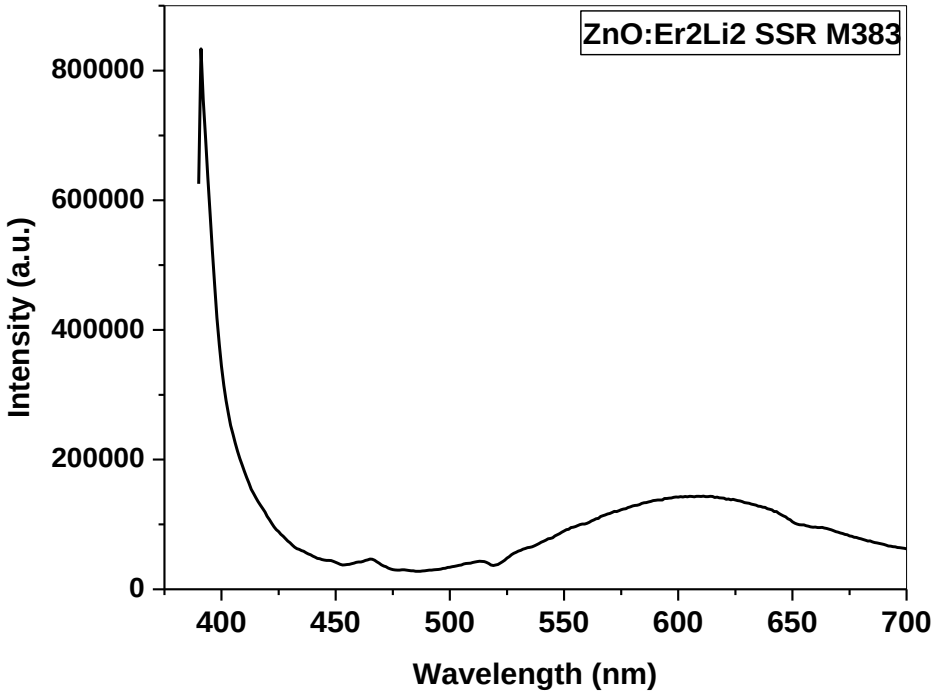

Fig 4.73: Emission spectra of ZnO:ErLi by SSR at 383 nm.

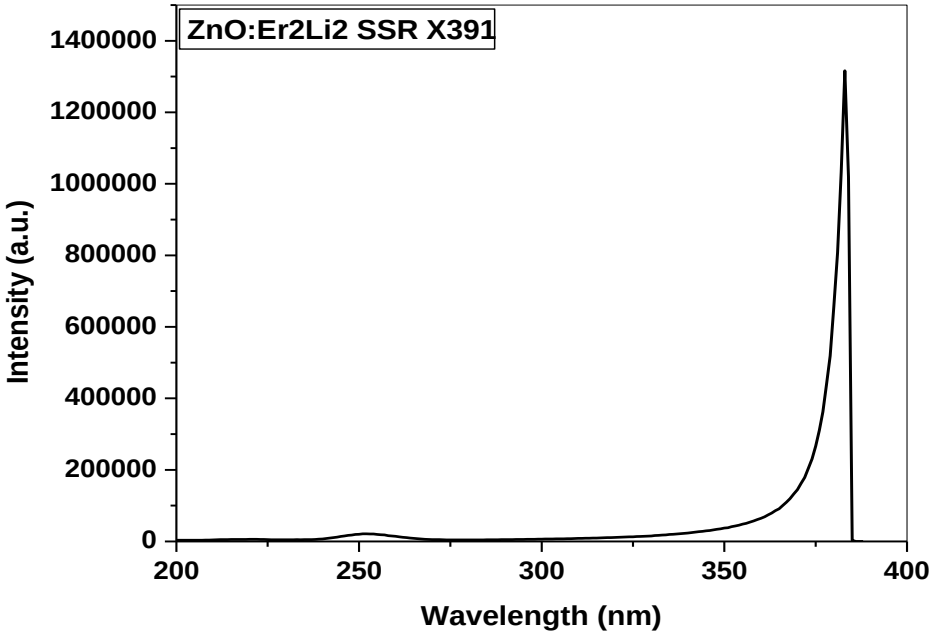

Fig 4.74: Excitation spectra of ZnO:ErLi by SSR at 391 nm.

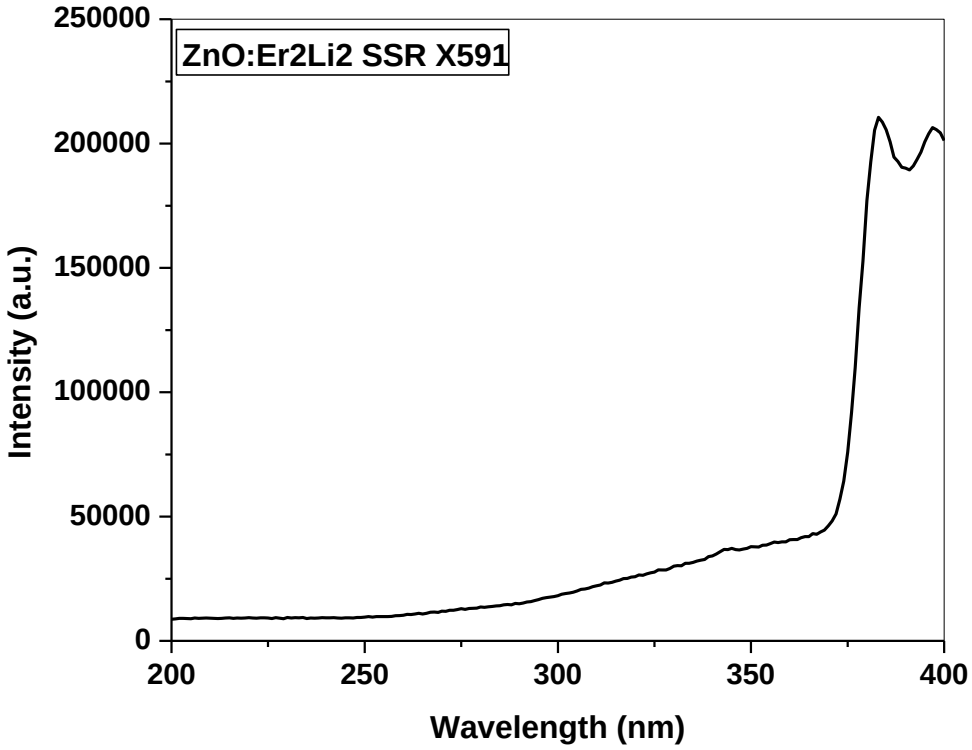

Fig 4.75: Excitation spectra of ZnO:ErLi by SSR at 591 nm.

The emission and excitation spectra of ZnO:Er(2%)Li(2%) prepared by SSR are shown in fig 4.71, 4.72, 4.73, 4.74 and 4.75. For this sample violet light was observed, which consists of the typical emission at 391 nm. The excitation spectra (λ_{em}=591 nm) have a narrow excitation band around 382 nm. Fig 4.72 shows emission spectra at excitation wavelength of 370 nm which gives narrow band spectrum around 391 nm.

9. ZnO:Ho(2%) by SSR:

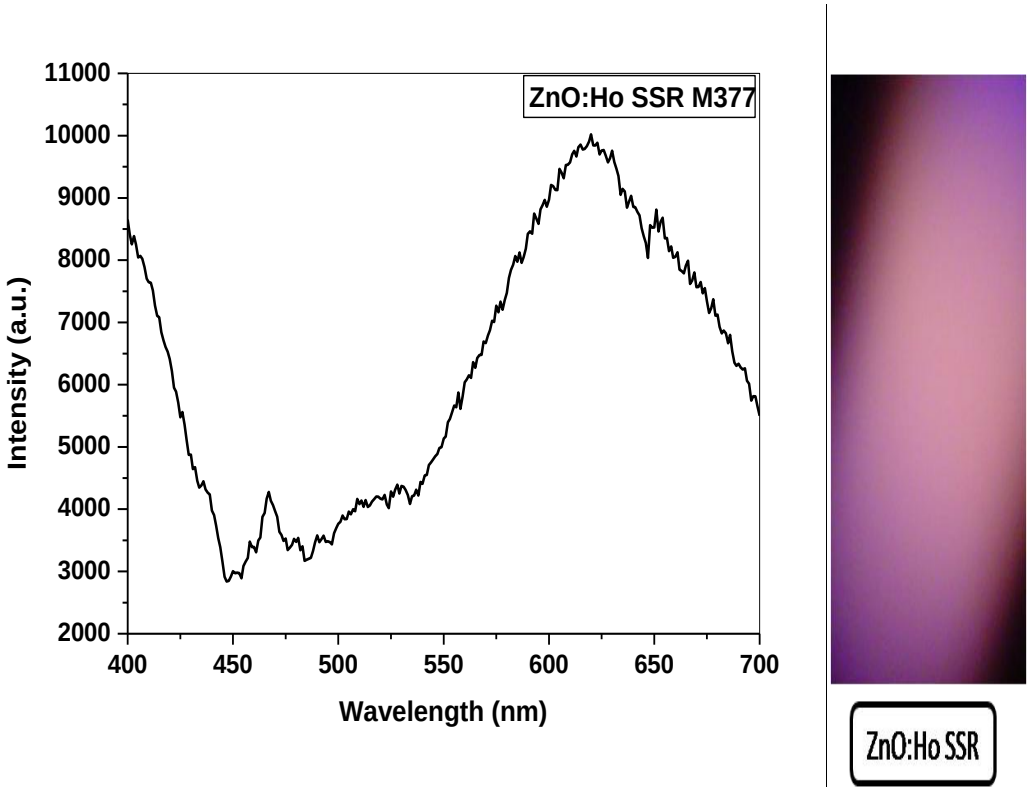

Fig 4.76: Emission spectra of ZnO:Ho by SSR at 377 nm.

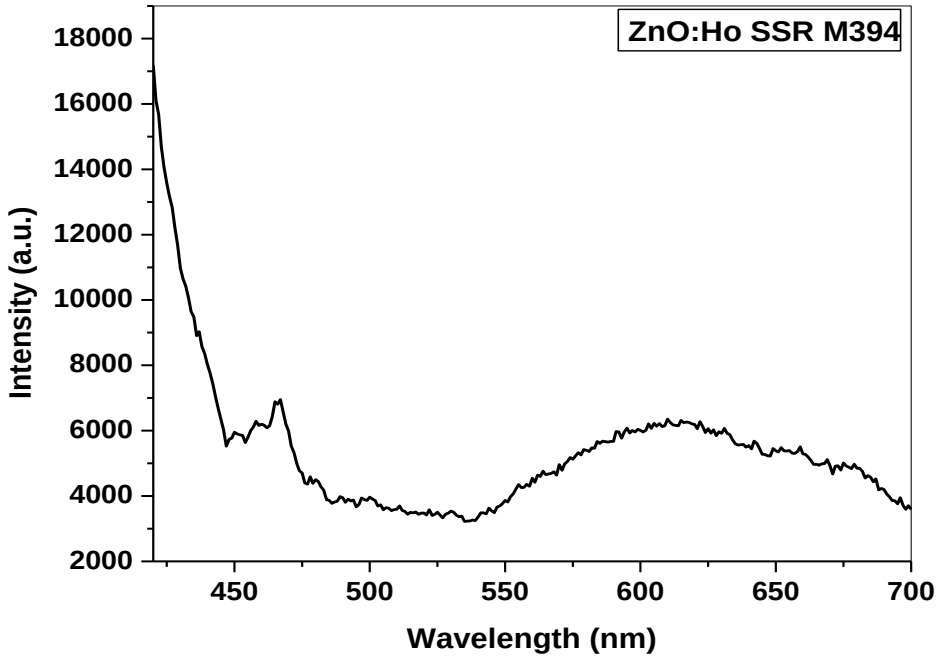

Fig 4.77: Emission spectra of ZnO:Ho by SSR at 394 nm.

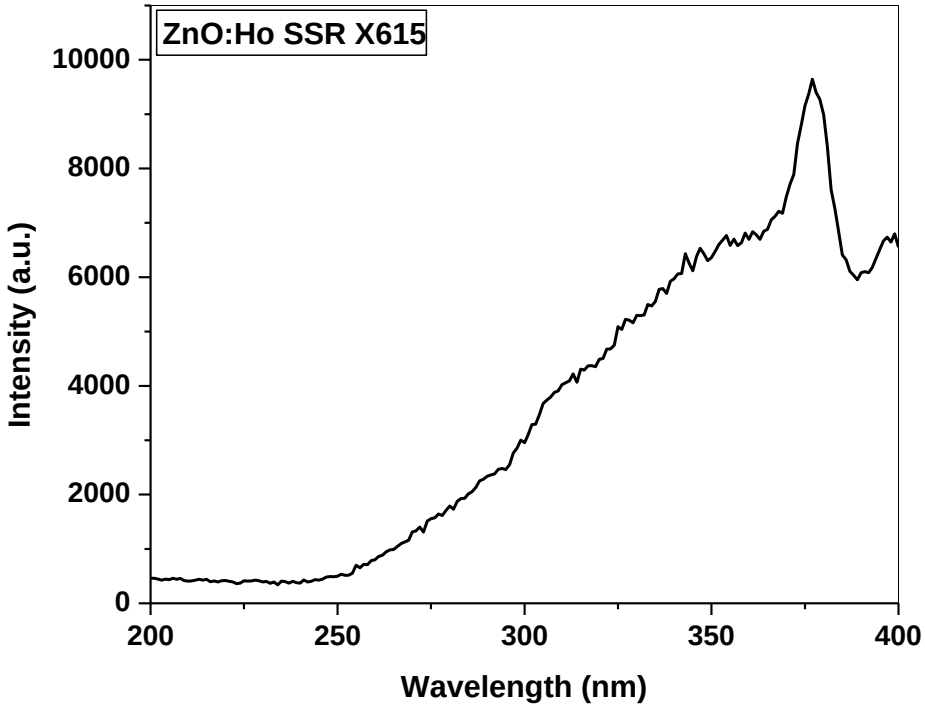

Fig 4.78: Excitation spectra of ZnO:Ho by SSR at 615 nm.

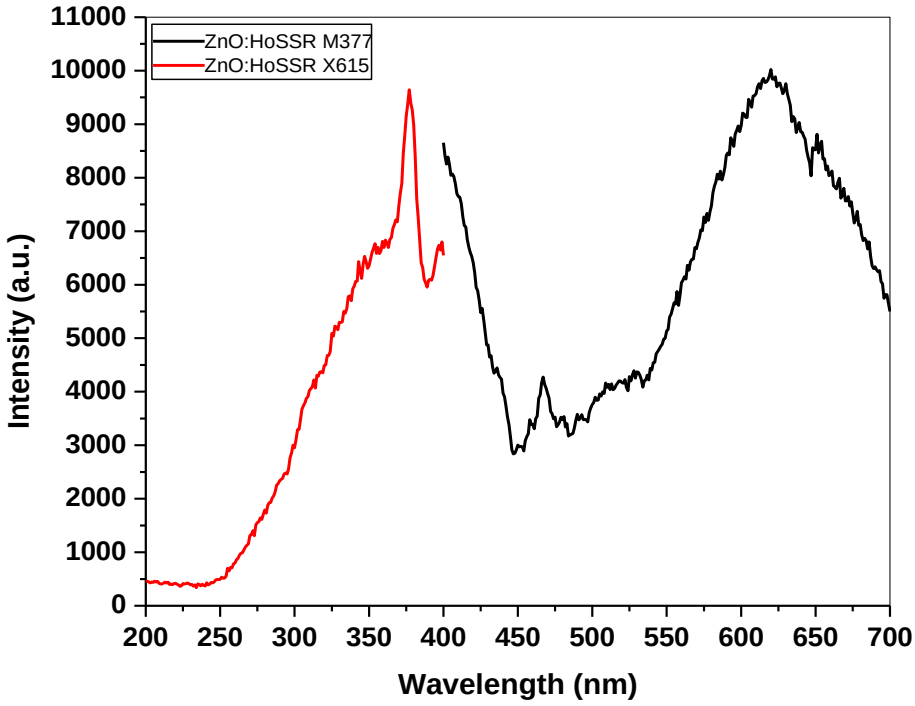

Fig 4.79: Excitation and Emission spectra of ZnO:Ho by SSR.

The emission and excitation spectra of ZnO:Ho(2%) prepared by SSR are shown in fig 4.76, 4.77, 4.78 and 4.79. For this sample red light was observed, which consists of the typical emission at 615 nm. The excitation spectra (λ_{em}=615 nm) have a broad excitation band around 377 nm. Fig 4.76 shows emission spectra at excitation wavelength of 377 nm which gives broad spectrum around 615 nm. In this spectrum broad band occurs in the region of red and orange but red region have more area thus its colour is more red than ZnO:Er(2%) by SSR. Here also colour is due to interstitial defects. Emitted colour is dependent on size of crystal (D) and both erbium and holmium have almost similar atomic radii.

10.ZnO:Ho(2%)Yb(10%) by SSR:

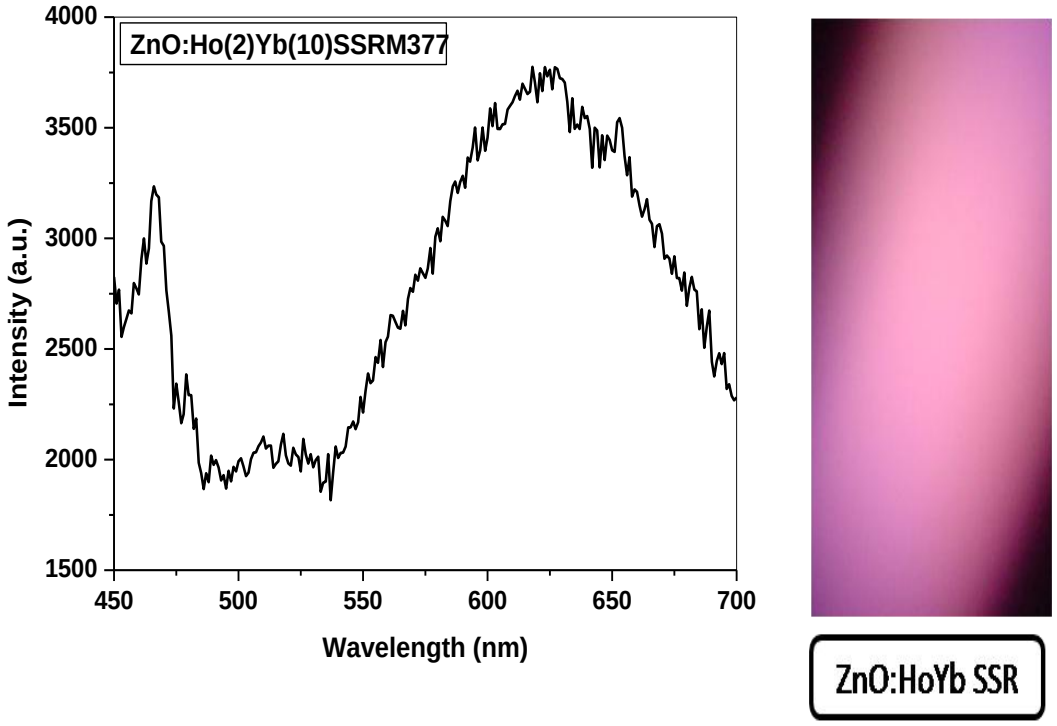

Fig 4.80: Emission spectra of ZnO:HoYb by SSR at 377 nm.

The emission and excitation spectra of ZnO:Ho(2%)Yb(10%) prepared by SSR are shown in fig 4.80, 4.81, 4.82 and 4.83. For this sample pink light (whitish red) was observed, which consists of the typical emission at 612 nm. The excitation spectra (λ_{em}=612 nm) have a narrow excitation band around 397 nm. Fig 4.80 shows emission spectra at excitation wavelength of 377 nm which gives broad spectrum around 612 nm.

In this spectrum only broad band occurs in the region of yellow and red thus colour of this sample is pink. PL emission spectrum is broad covering red region, in addition to a sharp peak in the blue part of the spectral region. Thus colour of this sample is pink rather than white.

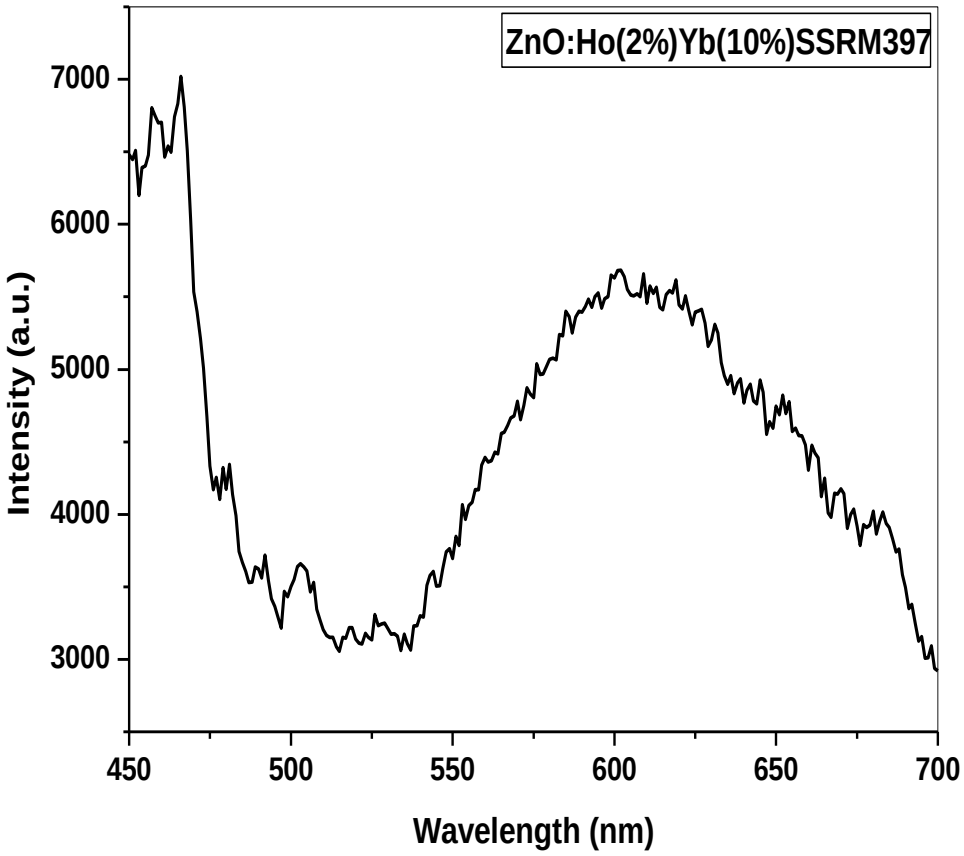

Fig 4.81: Emission spectra of ZnO:HoYb by SSR at 397 nm.

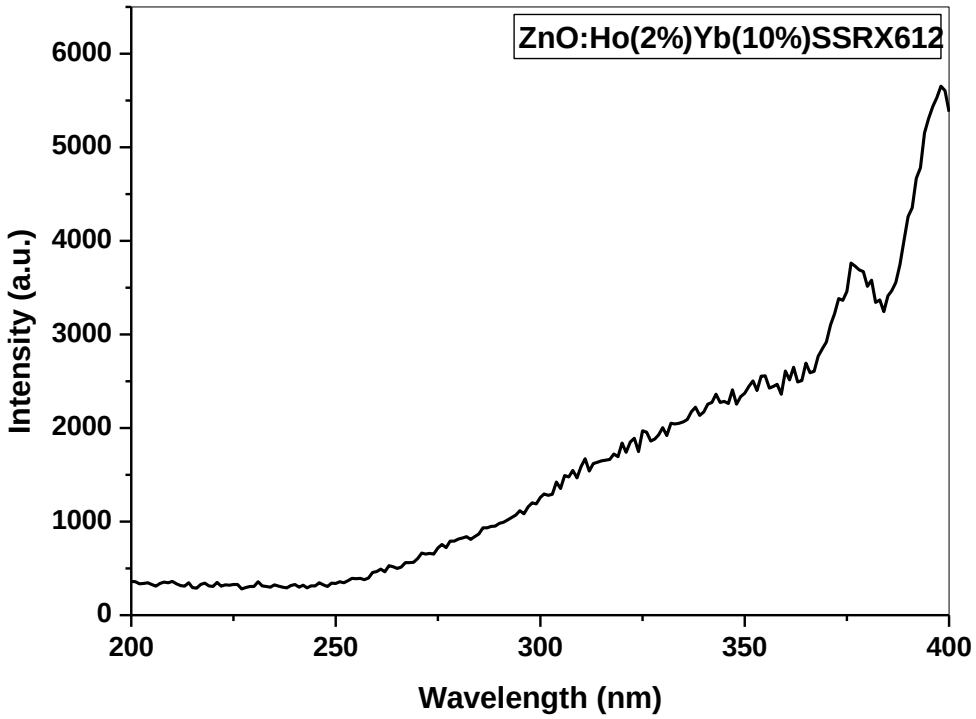

Fig 4.82: Excitation spectra of ZnO:HoYb by SSR at 612 nm.

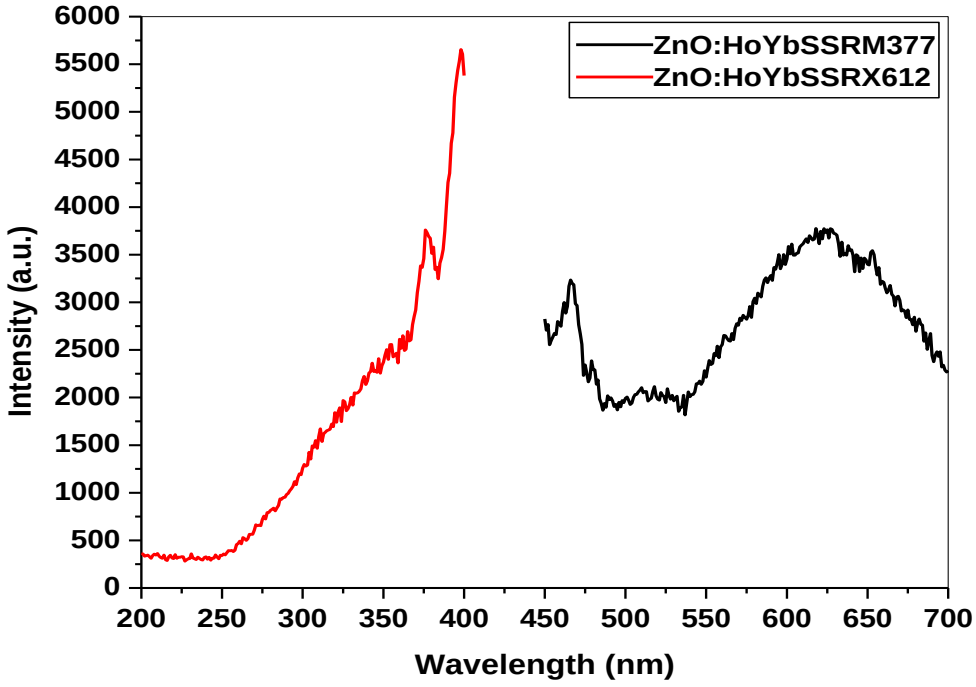

Fig 4.83: Excitation spectra of ZnO:HoYb by SSR at 612 nm.

4.4.2 Comparison of emitting light under UV excitation:

Photographs of synthesized phosphor powder under UV excitation as shown below indicates the change in emission colour due to incorporation of different dopants.

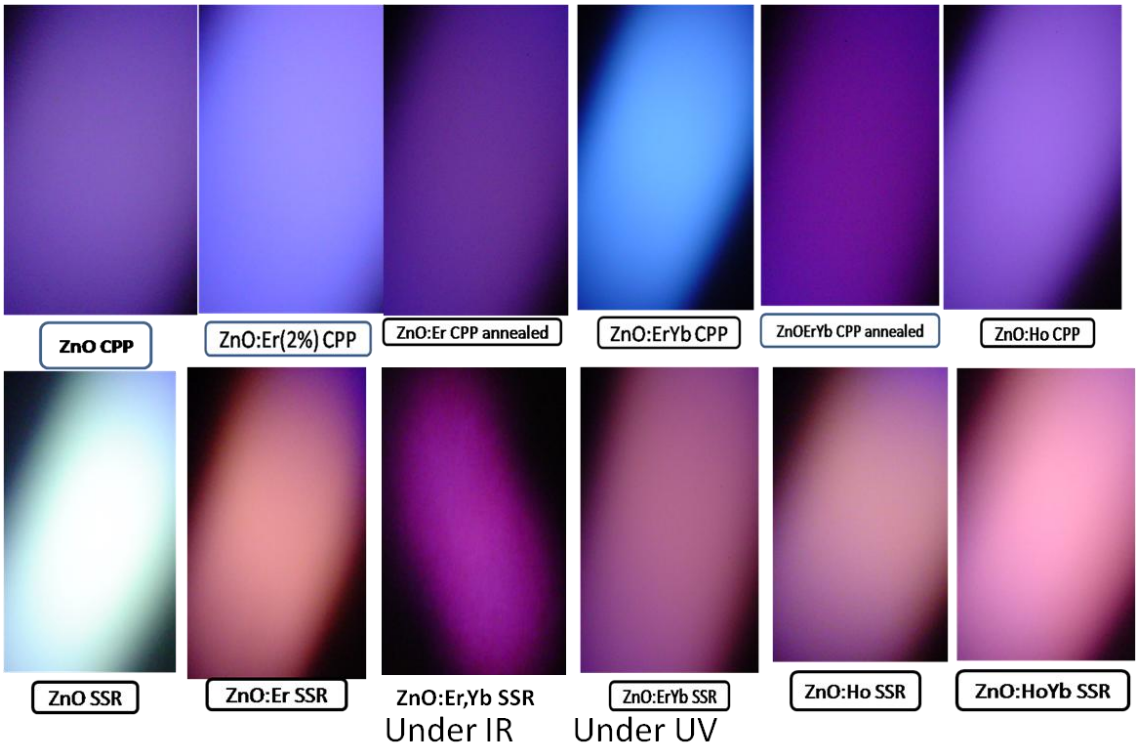

Fig 4.84: Actual photograph of synthesized nanophosphor powder under UV and IR excitation

The various photographs above show clearly how the emission colour changes due to change in various dopants. Colour also changes with the change of synthesis route and synthesis conditions such as aqueous environment or solid state diffusion at high temperature. Even with the same precursor in same stoichiometric proportion, emission colour changes in case of undoped ZnO and doped ZnO synthesized by solid state route and co-precipitation route.

4.4.3 Time resolved luminescence Decay:

Time resolved luminescence decay of undoped and ZnO doped with different rare earth ions. The decay is in microsecond range and the decay curves can be fitted into bi exponentials. The decay times are indicative of donor acceptor pair recombination. It can be noted that for ZnO:Ho prepared by CPP method shows the

fastest decay compared to ZnO:Ho prepared by SSR method. Decay rate of ZnO:Ho prepared by SSR is slowest.

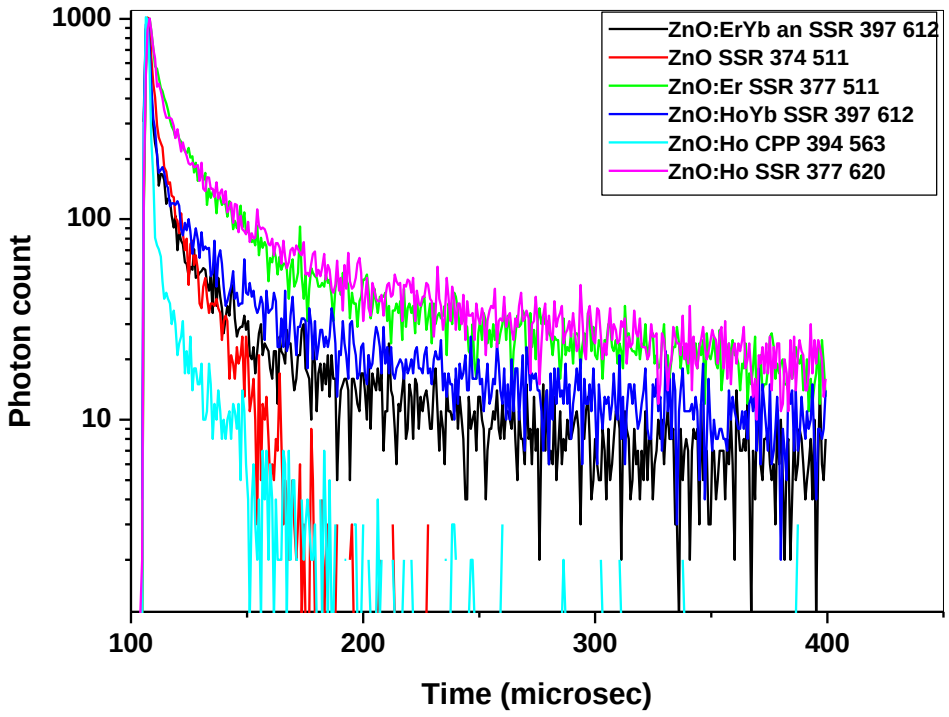

Fig 4.85: Time resolved decay of ZnO with different doping by SSR at 383 nm.

4.4.4 Up-Conversion:

1. ZnO:Er(2%) CPP:

Up conversion emission spectra of ZnO:Er under 980 nm diode laser excitation is shown in Fig.4.86. The emission enhances when Yb ions are simultaneously doped as sensitizer. Yb resonantly absorbs IR laser photons and transfer to ladder like energy levels of Er as shown in the energy level diagram (Fig.4.87). The emission takes place due to radiative transitions between different Er levels. Depending upon the concentration of Er and host, either green or red upconversion luminescence is usually observed from Er doped UC phosphor. Oxide semiconductors doped with Er mostly exhibit red UC luminescence. The ZnO:Er and ZnO:Er,Yb samples also exhibit red UC luminescence under 980 nm IR excitation. ZnO:Ho and ZnO:Ho,Yb show green UC luminescence under 980 nm laser light.

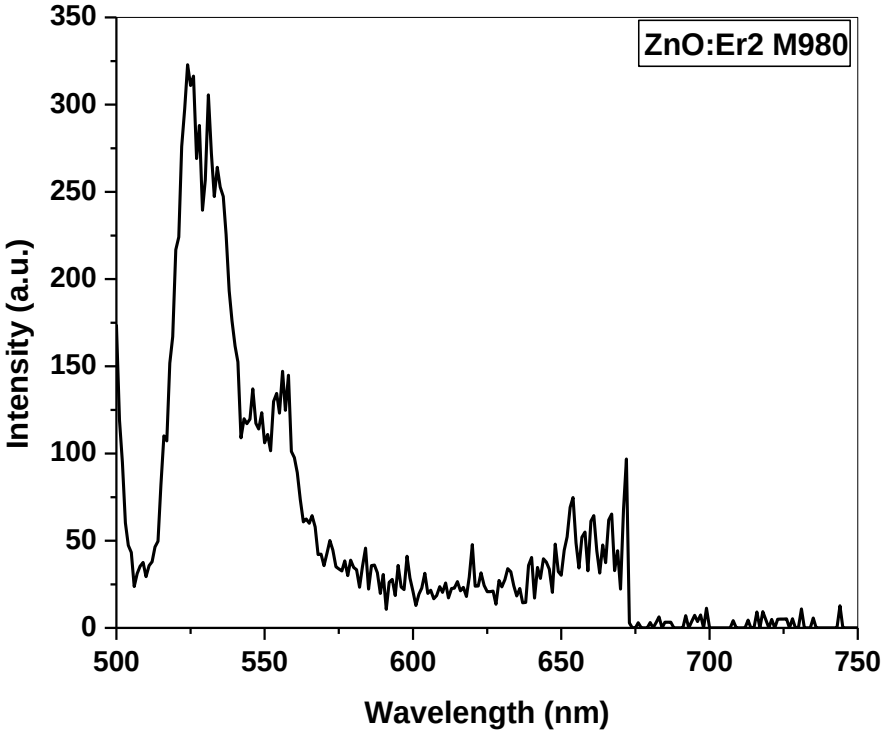

Fig 4.86: Emission spectra of ZnO:Er by CPP at 980 nm.

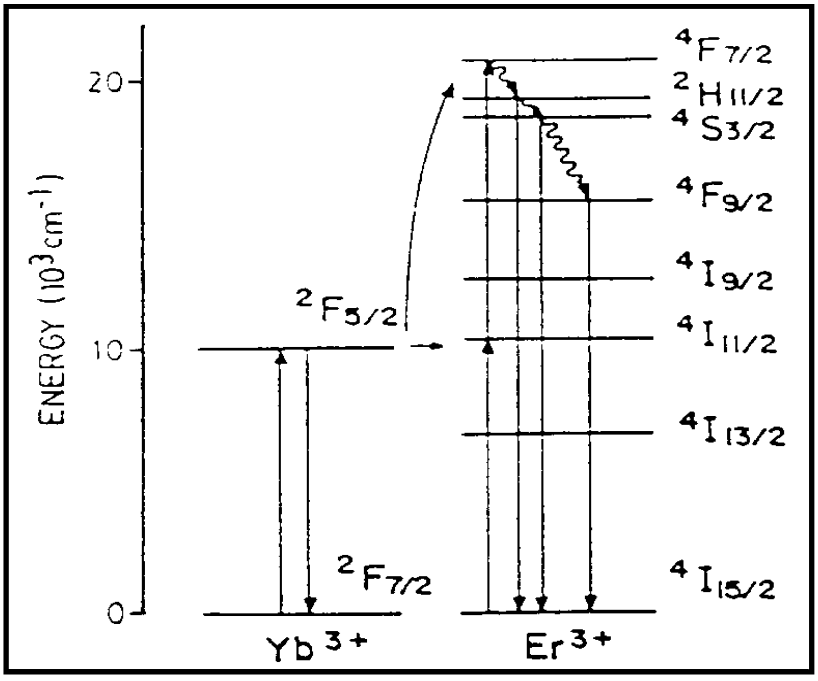

Fig 4.87: Energy level diagram showing absorption, energy transfer and emission giving UC emission

4.5 Dual mode luminescence

The down conversion and up conversion photoluminescence properties of rare earth doped ZnO nanoparticles described above clearly indicate that they exhibit dual mode luminescence characteristics. They are excitable by UV as well as IR light and the emission spectra also differ. The actual photograph of ZnO:Er (CPP annealed), ZnO:Er,Yb (SSR) and ZnO:Ho,Yb(ssr) powder sample under UV (370 nm) and IR (980nm) excitation is shown in Fig. 4.88, displaying dual excitation and dual emission characteristics.

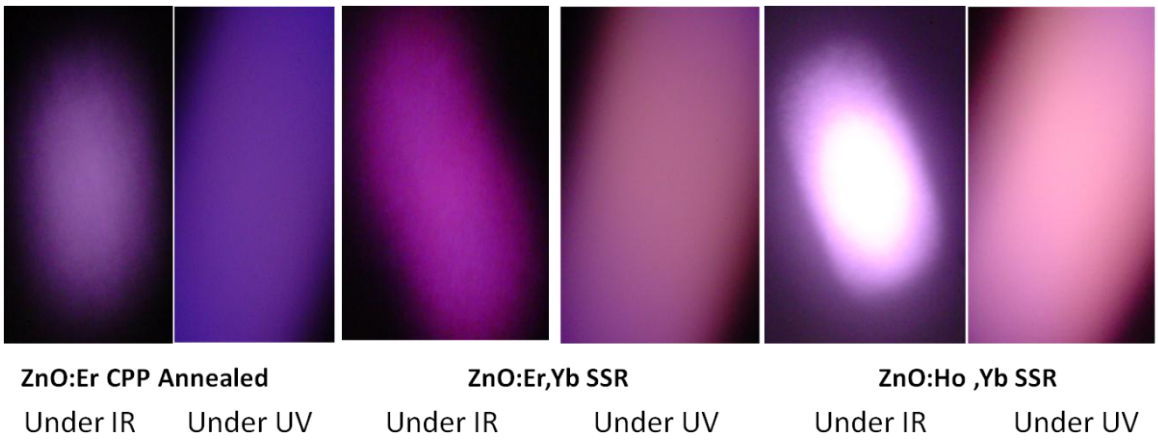

Fig 4.88: Dual mode luminescence in ZnO:Er (CPP annealed), ZnO:ErYb and ZnO:Ho,Yb prepared by SSR method.

CHAPTER 5

APPLICATIONS

5.1 Introduction

Over the past decades the demand for energy has increased substantially. The rate of energy consumption is projected to double in 2050 compared to worldwide energy consumption rates in 2001 [1]. The most commonly used energy sources are fossil fuels, but there are two problems with these energy sources. On one hand the resources of oil, coal and natural gas are depleted rapidly. On the other hand the use of fossil fuels has a large effect on the environment and climate by the emission of greenhouse gasses and other pollutants. Sustainable energy sources such as geothermal power, wind turbines and solar cells are already being used. From the various sustainable energy sources solar energy seems the most promising: the sun provides the earth with more energy in one hour (43 EJ) than the present energy consumption on the planet in one year (41 EJ) [1]. The production of sustainable energy by direct conversion of energy radiated from the sun into usable forms like heat or electricity is expected to gain importance because it may be the only renewable source capable of generating sufficient energy to meet the long-term worldwide energy demand [1, 2]. Utilization of solar energy requires effective means of capture and conversion of solar radiation, and storage of the acquired energy [1].

There are several ways to harvest energy from the sun. One of them is solar cells or photovoltaic cells. The capacity of photovoltaic cells to convert sunlight directly into electricity makes them prime candidates for the effective large-scale capture and conversion of solar energy. Solar cells are also useful in places where there is no electricity grid available and can be integrated into existing structures (e.g. on roofs of buildings and houses). At present the contribution of photovoltaic energy is limited due to its relatively high cost per kilowatt-hour [3]. A reduction in price may be achieved by either lowering the production cost or increasing the conversion efficiency.

5.2 Loss mechanisms in solar cells

State-of-the-art commercial single-junction crystalline and polycrystalline Si solar cells dominate the photovoltaic market [4, 5] and crystalline Si wafer cells typically have energy efficiencies around 15% [3]. Conventional solar cells consist of one layer of n-type and one layer of p-type semiconductor. Upon absorbing a photon above the energy band-gap (E_g) of the absorbing semiconductor material a single electron-hole (e-h) pair is generated. The electrons that are excited into the conduction band flow to the n-type side, and the holes in the valence band flow in the opposite direction, eventually resulting in an electrical current in the external circuit [6]. Fig. 5.1 is a schematic diagram showing the loss mechanisms that limit the efficiency of single-junction solar cells.

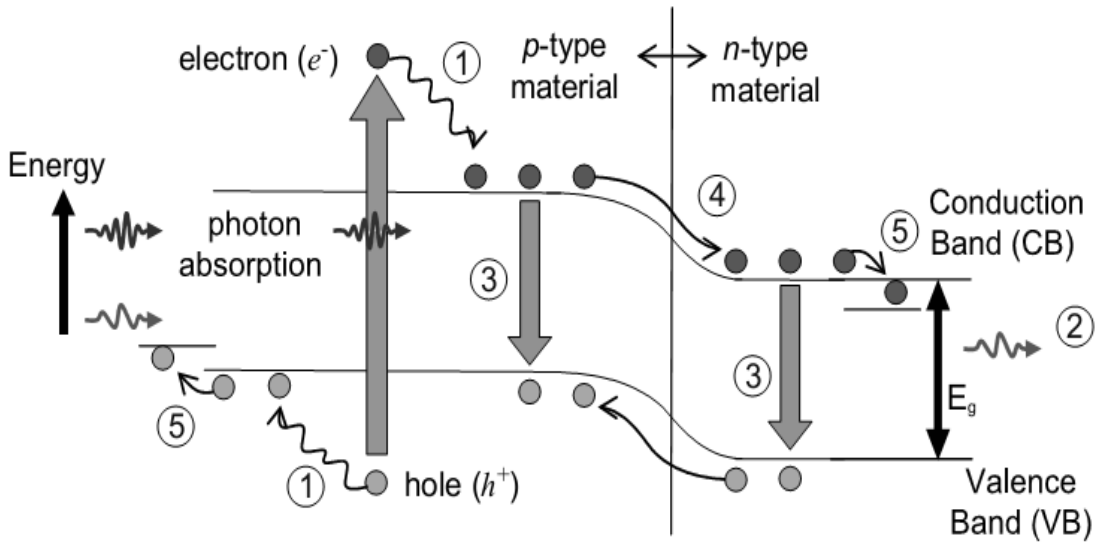

Fig 5.1: Loss processes in a single junction solar cell (1)- lattice thermalisation loss,(2)-transmission loss, (3)- recombination loss,(4)- junction loss and(5)- contact voltage loss. indicates the band gap of the solar cell).

The most significant loss mechanisms in solar cells are those due to relaxation of 'hot' charge carriers that are created upon absorption of a high energy photon [process (1)in Fig. 5.1] and transmission of photons with energies below the band gap of the semiconductor material [process (2)in Fig. 5.1]. The excess energy of high energy photons is rapidly dissipated as heat by thermalization of the electron and hole to the edges of the conduction band and valence band. These losses are known as

thermalization losses. Especially in solar cells based on semiconductors with a small band gap, these losses are substantial. The transmission losses arise from the fact that photons with energy smaller than the band-gap of silicon cannot be absorbed, and are therefore not converted to electricity. Transmission losses contribute especially to the losses for wider band gap solar cells, simply because a large part of the solar spectrum cannot be absorbed [7]. Process (3) shows recombination of e-h pairs, and this loss process can be minimized through maintaining high minority carrier lifetimes in the semiconductor material. The theoretical maximum efficiency of a silicon solar cell with a band-gap of 1.1 eV was calculated to be 30% by Shockley and Queasier [8].The largest part of the 70% energy loss is related to processes (1) and (2), and is known as the spectral mismatch. The detailed balance model used by Shockley and Queasier assumes that all recombination losses are radioactive (i.e., no non-radiative recombination losses), and includes the voltage drops across the contacts and p-n junction (depicted by (4)and (5) in Fig. 5.1).

There are two ways to reduce the losses that are caused by the spectral mismatch: adapt the solar cell to better use the solar spectrum or adapt the solar spectrum to better match the solar cell absorption. The first approach has been successfully applied in a-called multi-junction tandem solar cells for which efficiencies over 40% under concentrated solar light have been realized [10]. This is achieved by 'stacking' multiple solar cells made with different semiconductor materials having different band-gaps. Each of the cells will then absorb a different fraction of the solar spectrum [6, 11].With an infinite number of junctions the theoretical maximum efficiency becomes 68% [12]. Tandem solar cells are costly and are only now becoming cost-competitive for terrestrial concentrated solar cell applications [11].Other more recently proposed options for adapting solar cells to the solar spectrum include multiple exciton generation (MEG) and space-separated quantum cutting (SSQC). In both cases multiple e-h pairs are generated after absorption of one high energy photon by the solar cell.

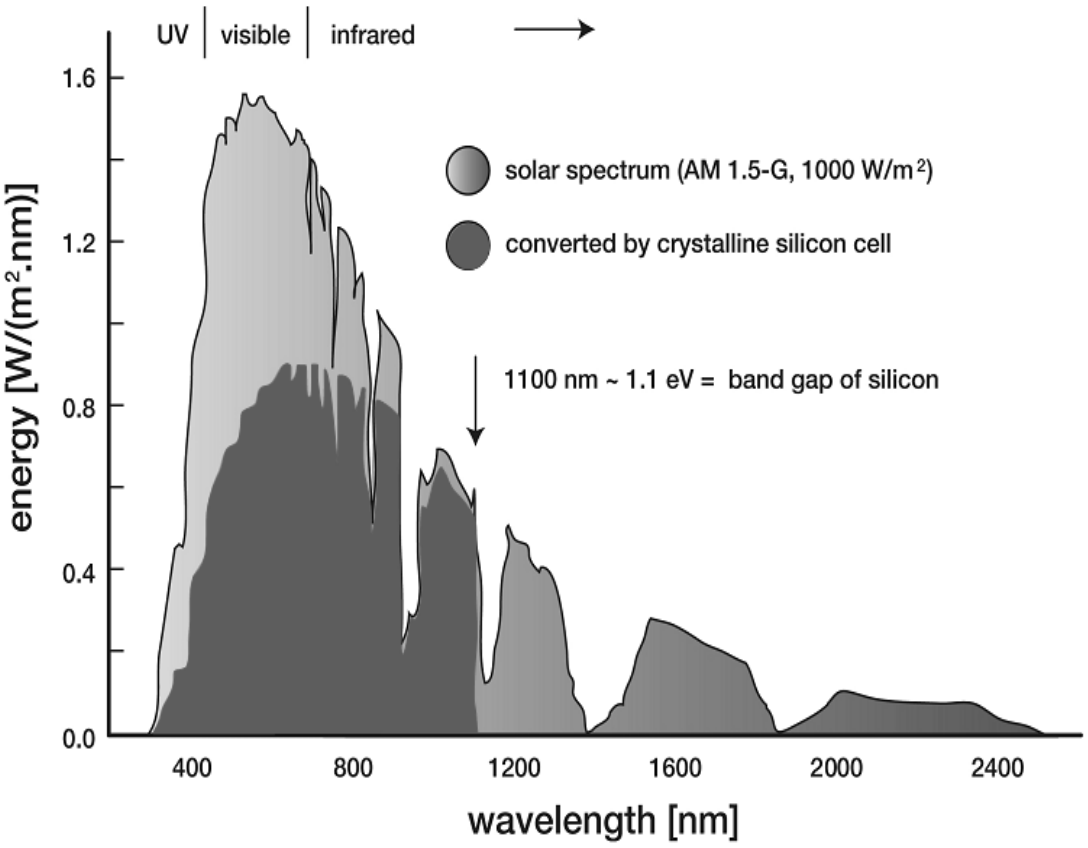

Fig 5.2: The AM1.5G terrestrial solar spectrum showing the fraction of terrestrial sunlight that is currently absorbed and effectively used by a thick crystalline silicon device [9].

From the picture above we may say that only a small portion (visible) of solar spectra has been used by conventional Si solar cells for generating e-h pairs. If any how we are able to use the side band of visible solar spectra i.e. UV and infrared region to generate extra e-h pair than it is obvious that the efficiency will increase. Theoretically the nano-phosphor prepared here can be used to down convert the solar spectrum i.e. a short wavelength photon is absorbed which belongs to UV region and emits two or more photon with larger wavelength laying in visible region which may be easily used by Si solar cell . Likewise there are more such phosphor which can be used to up convert the solar spectrum.

As discussed already the main energy loss in the conversion of solar energy to electricity is related to the so-called spectral mismatch: low energy photons are not absorbed by a solar cell while high energy photons are not used efficiently. To reduce the spectral mismatch losses both up conversion and down conversion are viable

options. In the case of up conversion two low energy infrared photons that cannot be absorbed by the solar cell, are added up to give one high energy photon that can be absorbed. In the case of down conversion one high energy photon is split into two lower energy photons that can both be absorbed by the solar cell. The rich and unique energy level structure arising from the 4fn inner shell configuration of the trivalent lanthanide ions gives a variety of options for efficient up- and down conversion.

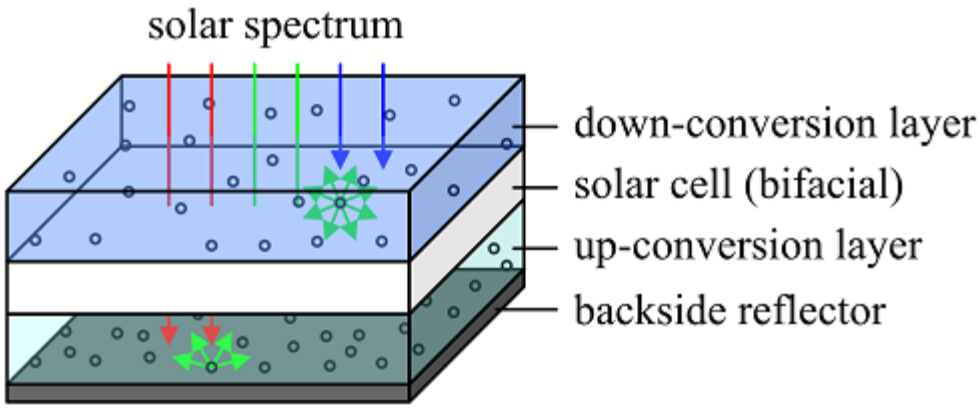

Fig 5.3: Bifacial solar cell with down- and up-converter.

Fig 5.3 shows a simple arrangement of the lanthanide ions in form of thin film around a Si solar cell to up convert and down convert the solar spectrum. These thin layer of phosphor material will use the UV & Infrared region of sun energy and provide the photovoltaic cell photons in visible region to generate e-h pairs by providing energy greater than band-gap of semiconducting material (i.e for Si=1.1eV).

5.3 References:

[1] N. Lewis and D. Nocera, Powering the planet: Chemical challenges in solar energy utilization,PNAS103, 15729 (2006).

[2] O. Morton,Solar energy: A new day dawning?: Silicon Valley sunrise, Nature 443, 19 (2006).

from III-V compound semiconductors, Physica Status Solidi(c) 3, 373 (2006). [3] B. van der Zwaan and A. Rabl,Prospects for PV: a learning curve analysis, Solar Energy 74, 19(2003).

[4] A. Goetzberger, C. Hebling, and H. Schock, Photovoltaic materials, history, status and outlook,Materials Science and Engineering: R: Reports40, 1 (2003).

[5] D. Bagnall and M. Boreland,Photovoltaic technologies, Energy Policy 36, 4390 (2008).

[6] M. Green, Photovoltaic principles, Physica E: Low-dimensional Systems and Nanostructures 14,11 (2002).

[7] B. Richards,Enhancing the performance of silicon solar cells via the application of passive lumi-nescence conversion layers, Sol. En. Mat. Sol. Cell. 90, 2329 2006).

[8] W. Shockley and H. Queisser, Detailed balance limit of efficiency of p-n unction solar cells, J.Appl. Phys.32, 510 (1961).

[9] http://www.vicphysics.org/documents/events/stav2005/spectrum.JPG.

[10] M. Green, K. Emery, Y. Hishikawa, and W. Warta, Solar cell efficiency tables (version 33), Prog.Photovolt: Res. Appl.17, 85 (2009).

[11] F. Dimroth,High-efficiency solar cells

CHAPTER 6

CONCLUSIONS

1. Doped Zinc Oxide (ZnO) nanoparticles were synthesized by two routes: a) Solid state reaction method b) Co-precipitation method.
2. In the experiments ZnO doped with different dopants i.e. Er^{3+}, Yb^{3+}, Ho^{3+} and Li^{+} were synthesized using co-precipitation method and solid state reaction method. The phase formation, structures, morphologies, and photoluminescence properties were studied in detail.
3. ZnO doped with the rare earths (RE) i.e. ZnO:Er^{3+}; ZnO:$Er^{3+}Yb^{3+}$; ZnO:Ho^{3+}; ZnO:$Ho^{3+}Yb^{3+}$; ZnO: Er^{3+} Li^{+} and undoped ZnO exhibit bright photoluminescence in the orange red region and green region.
4. Thin film of these nanophosphor powders can also be prepared by making a colloidal solution in ethanol using spin coating.
5. ZnO:Er^{3+} was prepared with SSR method as well as with co-precipitation method; the particle size is smaller in case of co-precipitation method than SSR method. The photoluminescence property with ZnO:Er^{3+} prepared with SSR method was better than ZnO:Er^{3+} prepared with co-precipitation method.
6. When ZnO:Er^{3+} is co-doped with Yb^{3+}, the photoluminescence property was improved and shows predominantly Yb^{3+} luminescence.
7. ZnO:$Er^{3+}Yb^{3+}$ nanoparticles produced the brightest luminescence emission.
8. When ZnO:Ho^{3+} is co-doped with Yb^{3+} the photoluminescence excitation spectrum becomes broader and excitation range increases.
9. UV absorbing and bright orange red and green emitting nanophosphor can act as spectrum modifiers for enhancement of solar cell efficiency.
10. Bifunctional fluorescent magnetic nanoparticles have immense application potential in biological applications like fluorescence tracing and targeted drug delivery.